Topology optimization using the lattice Boltzmann method and applications in flow channel designs considering thermal and two-phase fluid flows

Kentaro Yaji

2016

Table of contents

Chapter 1

General introduction

The study of design optimization under various specified conditions is an attractive area of research for engineers and mathematicians. Hence, there are many different kinds of optimization methods applied to various optimal design problems.

Among them, structural optimization is a popular methodology for obtaining an optimal configuration, based on physical and mathematical theories, whereas traditional design methods typically rely on the intuition and experience of designers. The structural optimization methods are categorized into three types, i.e., size, shape, and topology optimizations, according to the degree of design flexibility. Figure 1.1 shows the schematic diagram of the structural optimization methods, where the stiffness maximization problem for a cantilever is described. Sizing optimization, which is the oldest approach proposed in the 1960's [98], focuses on the size attributes of structural designs, such as length, width, and thickness. Shape optimization is also the one of well-studied approach in the 1970's [134], and its key idea is to optimize a performance by moving structural boundaries. Topology optimization, proposed in the 1980's [10], is the most flexible type of structural optimization method, since this allows the creation of new boundaries in the design domain. Such topological change during the optimization process is not allowed in the classical structural optimization methods.

The overall aim of this thesis is to construct topology optimization methods for fluid dynamics problems, whereas the majority of studies in topology optimization treat structural mechanics problems, e.g., stiffness maximization, stress minimization, and eigenvalue maximization. In the research field of structural optimization for fluids, Pironneau pioneered a shape optimization method for fluid dynamics problems and proposed the basic mathematical theory for obtaining minimum drag body profiles under Stokes flow [95] and Navier-Stokes

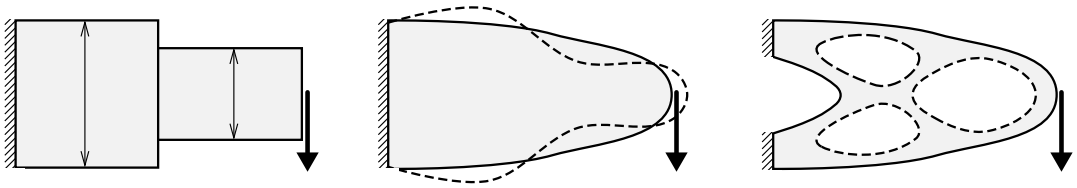

Fig. 1.1 Classification of structural optimization.

flow [96]. The reader is referred to a recent monograph by Mohammadi and Pironneau [79], in which a variety of shape optimization methods are discussed. As mentioned above, shape optimization, however, only allows changes in boundary shapes, so feasible design modifications are strictly limited. Thus, although shape optimization is suitable for slight modifications in the stage of detail design, it is difficult to be applied to the conceptual design by only utilizing the shape optimization methods. This limitation can be overcome by applying topology optimization, which allows the creation of new structural boundaries that correspond to the interface between fluid and solid domains in fluid problems. Borravall and Petersson [14] pioneered a fluid topology optimization method that aims to minimize the viscous dissipation energy for the design of an internal flow channel or a body profile in an external flow.

An advantage of topology optimization is that the optimal configuration can be derived by just setting the design domain, which is fulfilled with fluid. This means that an initial layout of fluid and solid domains, which need to be often determined after conducting many numerical experiments, is unnecessary for obtaining an optimal solution in topology optimization. Consequently, topology optimization is possible to derive a promising conceptual design, without relying on the intuition and experience of designers.

In previous research in fluid topology optimization problems, the finite element method (FEM) is generally used for discretizing the Navier-Stokes equations (NSE). The FEM is well established for the use of body-fitted meshes, but the accuracy and numerical robustness depend on the mesh quality, which is difficult to appropriately control during the optimization process. In generally, Eulerian coordinates system with an immersed boundary method is employed, due to its simplicity and robustness. Hence, it is naturally conceived that the finite difference method is well suited for topology optimization problems, but it has not yet been developed for fluid topology optimization problems. In my opinion, this is because that the

original concept of topology optimization was established by the specialists of structural mechanics.

As a radical numerical scheme based on the finite difference method, the lattice Boltzmann method (LBM) has recently been an attractive scheme in the research field of computational fluid dynamics [76, 110]. Comparison the coding used in LBM and the other schemes based on the NSE such as the finite element, and finite volume methods, the simplicity of the LBM algorithm and its scalability for complex flow problems such as porous, miscible, and immiscible fluid flow problems, are advantageous. In particular, the LBM enables one to avoid the numerical treatment of iterative computation for the correction of fluid velocity and pressure in the incompressible viscous fluid flow, whereas such numerical treatment is typically needed in the conventional schemes based on the NSE.

This thesis focuses on topology optimization using the LBM for various fluid flow optimization problems that can be promising ways for the conceptual design of flow channel devices. For the efficient optimization calculation, a sensitivity analysis based on the adjoint lattice Boltzmann method (ALBM), in which the adjoint problem is solved by using the discretization strategy in the LBM, is proposed. In addition, the presented method is applied to the standard flow resistance minimization problem and scalar transport problems where optimal design methodologies for a heat sink and an extraction microchannel are constructed.

This thesis is a summary of research done during my doctoral course. The outline of each chapter is as follows:

In Chapter 2, the basic idea of topology optimization is introduced, and the formulation of the density approach and the level set-based approach are explained. Various optimization schemes based on the gradient method are provided, and derivation strategies for design sensitivities are introduced. A brief history of topology optimization for fluid dynamics problems based on the NSE is provided, and the standard formulation of topology optimization problems for a minimum dissipation energy is explained. As an application of fluid topology optimization, a heat sink design problem is formulated based on the level set-based topology optimization method, and several numerical examples are provided to confirm the utility of the presented method for thermal-fluid problems.

In Chapter 3, a topology optimization method using the LBM is constructed. The proposed method is applied to the flow resistance minimization problem. In the sensitivity formulation, the discrete Boltzmann equation, which is defined by using the continuous space and time and the discrete particle velocity space, is employed to formulate the optimization

problem, so that the adjoint equation can be solved using the LBM and the accurate boundary conditions in the LBM can be incorporated. The derived adjoint sensitivity is compared with the numerical solution of direct method based on the finite difference approximation. Several numerical examples in two- and three dimensional problem are provided to confirm the validity and utility of the proposed method.

In Chapter 4, a topology optimization method for a scalar transport problem, in which the fluid velocity, the pressure, and the scalar corresponding to the temperature, is calculated by using the LBM. The optimization problem is formulated as the heat exchange maximization problem that is also treated in Chapter 2, where the FEM is employed to discretize the NSE. Additionally, a constraint to restrict the maximum pressure drop for the optimal flow channel is presented. The adjoint sensitivity analysis constructed in Chapter 3 is applied, and the adjoint sensitivity for the thermal-fluid problem is compared with the finite difference approximation for the validation of proposed method. Several numerical examples in a two-dimensional heat sink design problem are provided to confirm the effectiveness of the proposed method.

In Chapter 5, a topology optimization method for a scalar transport problem considering immiscible fluid flows is constructed, using the two-phase LBM with the same density. The optimization problem is formulated to maximize an efficiency of liquid-liquid extraction that is a separation operation using the microchannel device. The objective functional is defined as an error norm of the concentration in an observation domain with respect to a reference concentration. The key idea of this formulation is that the minimization of the error norm corresponds to the maximization of the extraction efficiency in a microchannel. In addition, the pressure drop constraint used in Chapter 4 is also introduced. Several numerical examples are provided to verify the effectiveness of the proposed method.

The last Chapter of this thesis is dedicated to summarize the obtained results.

Chapter 2

Topology optimization

2.1 Introduction

Topology optimization has been an attractive structural optimization method, after Bendsøe and Kikuchi [10] first proposed the so-called homogenization design method. The basic idea of topology optimization is the introduction of an extended design domain, the so-called fixed design domain, and the replacement of the optimization problem with a material distribution problem, using the characteristic function originally presented in the paper of Murat and Tartar [82]. A homogenization method is utilized to deal with the extreme discontinuity of the material distribution in the design domain, and to provide the material properties viewed in a global sense as homogenized properties. The homogenization design method [10, 114] has been applied to a variety of optimization problem, and density approach, also called the Solid Isotropic Material with Penalization (SIMP) method [11], is another currently used topology optimization method. In particular, the density approach is widely employed to solve topology optimization problems, due to its simple formulation. Recent developments in the field of topology optimization have been categorized in a review paper by Sigmund and Maute [105]. Around the same time, Deaton and Grandhi [24] presented a review for topology optimization of continuum structures from the year 2000 to 2012.

The level set method [99, 85] for structural optimization is an another popular approach[1] , since Osher and Sethian [86] constructed a fundamental methodology for tracking fronts and free boundaries. The novel aspect of the use of a level set method for structural optimization method is that the structural boundaries can split and merge during the optimization in an

[1] Note that this approach is essentially based on topology optimization rather than shape optimization, since the creation of new boundary is not allowed during the optimization process.

Eulerian coordinate system. Additionally, although this approach essentially does not allow the creation of new boundary in the design domain during the optimization process, the grayscale areas can be eliminated. The areas, which have intermediate material density and are generally meaningless from an engineering standpoint, can be eliminated by using the level set approaches, since the structural boundaries are expressed as the iso-surface of a scalar function called level set function. The level set function is evolved using an advection equation, the so-called Hamilton-Jacobi equation, during the optimization process. This equation is used to capture the structural boundaries, and the convection velocity is typically defined using the shape derivative. Seminal research pertaining to the level set method for structural optimization problems can be found in [100, 123, 4], and the reader is referred to a recent monograph by Van Dijk et al. [119]. In addition, since the structural boundaries can be exactly represented as the iso-surface of the level set function, the design-dependent boundary conditions, such as the pressure load [4], jump condition for different material [3], and surface effect in an electromagnetic problem [126] can be naturally imposed as Dirichlet boundary conditions, whereas it is fundamentally impossible to incorporate such conditions in the density-based topology optimization methods.

As a similar approach with the level set-based approach, the phase field method [17, 5] is also used for solving structural optimization problems [15, 116]. In this method, the phase filed function, used for representing different phases in multi-phase problems, is defined as the design variable in optimization problems. The phase field-based approach does not need to treat the advection equation for updating the design variable, and alternatively employs a reaction-diffusion equation for evolving the phase filed function during the optimization process.

In addition to the above approaches, a different type of method, the so-called the Evolutionary Structural Optimization (ESO) method [124], has been proposed. The basic idea of this approach is that unnecessary finite elements are gradually removed based on heuristic criteria so that the optimal configuration is obtained as an subset of initial design domain.

As mentioned above, many different kind of approaches have been proposed, and these methods have provided promising results in various optimization problems. Of course it is difficult to answer a question, "*Which is the best method?*", because it is fully imagine that superiority between each approach is dependent on optimization problems. We therefore should understand the utility of each approach, and appropriately chose an optimization approach. In this chapter, we focus on the most popular approaches, i.e., density and level

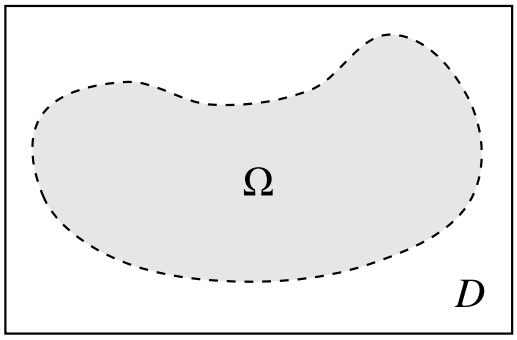

Fig. 2.1 Schematic figure of fixed design domain D and original domain $\Omega \subset D$.

set-based approach, and discuss their general formulations for solving optimization problems dealing with fluid dynamics problems.

2.2 Formulation of optimization problems

Consider a structural optimization problem to determine the boundary of a design domain, Ω, in which the objective function that expresses the intended performance of the target system is to minimized, or maximized, based on optimization theories. The basic concept of topology optimization is the introduction of a fixed design domain $D \subset \mathbb{R}^d$ that includes the original design domain, i.e., $\Omega \subset D$ (Fig. 2.1), and use of the characteristic function in order to replace the original structural optimization problem with a material distribution problem in the fixed design domain. Let χ be the characteristic function, defined as

$$\chi(\boldsymbol{x}) = \begin{cases} 1 & \text{if } \boldsymbol{x} \in \Omega \\ 0 & \text{if } \boldsymbol{x} \in D \setminus \Omega, \end{cases} \tag{2.1}$$

where $\boldsymbol{x}$ represents a position in the fixed design domain D.

Using the characteristic function $\chi(\boldsymbol{x})$ and a state variable $\boldsymbol{u}(\boldsymbol{x})$ given by solving a physical problem such as structural mechanics or fluid dynamics problems, we here consider the minimization problem with respect to the objective functional $J : \mathbb{R}^d \times \mathbb{R} \to \mathbb{R}$, as follows:

$$\inf_{\chi} \; J(\boldsymbol{u}, \chi) = \int_D j(\boldsymbol{u}, \chi) \mathrm{d}\Omega + \int_{\Gamma_N} k(\boldsymbol{u}) \mathrm{d}\Gamma, \tag{2.2}$$

where Γ_N represents a specific boundary of D, and $j, k : \mathbb{R}^d \to \mathbb{R}$ are smooth functions. Note that this abstract formation is not the unique representation for topology optimization problems.

Since the characteristic function can be highly discontinuous, some relaxation or regularization technique must be introduced for the numerical treatment. In the following, we briefly introduce two popular approaches.

2.2.1 Density approach

In the density approach, to avoid the discontinuous property of the original design variable χ, the characteristic function is replace by a continuous function, $\gamma : D \to \mathbb{R}$, which is the design variable in topology optimization problems. Here, we assume that the design variable γ, whose distribution corresponds to an admissible topology in D, belongs to the following set,

$$\mathfrak{X}_{\text{ad}} = \left\{ \gamma \in L^{\infty}(D) \,|\, 0 \leqslant \gamma \leqslant 1, \text{ a.e. in } D, |\Omega| \leqslant V \right\}, \tag{2.3}$$

where $|\Omega|$ represents the Lebesgue measure of Ω, and V that is the maximal fixed material volume in D given by $V_{\max} \int_D \mathrm{d}\Omega$ with $V_{\max} > 0$ is a parameter for determining the value of V. Noted that the inequality constraint with respect to $|\Omega|$ is an optional treatment, which should be originally used for the requirement of prescribed material volume. For instance, in the stiffness maximization problem for the design of industrial application such as automotive and aircraft, it is very important not only to maximize the stiffness but also to minimize or limit the maximum material volume, from an engineering standpoint. On the other hand, it is known that the use of volume constraint can help ones to stabilize the optimization computation. Consequently, many papers deal with the volume constraint in the optimization problem, even if it does not have the meaning of original subject for restricting the material volume.

The key idea of using the density approach for topology optimization is that a material property tensor $\boldsymbol{A}$ such as an elasticity tensor or permeability tensor, is represented using a density function $f(\gamma)$, as follows:

$$\boldsymbol{A} = f(\gamma)\boldsymbol{A}^0, \tag{2.4}$$

where $\boldsymbol{A}^0$ is the material property tensor of a given material in Ω. The density function is generally defined as a power function using a penalization parameter p, as follows [9, 11]:

$$f(\gamma) = \gamma^p. \tag{2.5}$$

This function is used for discriminating whether a material domain Ω or not.

Although the density approach is an useful methodology for topology optimization due to its simple formulation as mentioned above, it still has serious drawbacks. One particularly troublesome problem is that since the discontinuous design variable is replaced with the continuous variable to avoid the numerical instability, the density approach does essentially allow the existence of grayscale areas, where the density is an intermediate value between 0 and 1. Since the intermediate material property is hard to interpret and generally meaningless from an engineering standpoint, various scheme have been proposed to overcome this problem and provide grayscale-free optimal configurations. Such schemes can be categorized into two kind of treatments, i.e., geometric constraints, and filtering schemes. Reader is referred to a detailed reviews by Sigmund and Petersson [106] and Sigmund [104].

The optimal configuration, represented as the distribution of design variable $\gamma \in \mathfrak{X}_{\mathrm{ad}}$, is typically derived using a mathematical programming method such as Sequential Linear Programming (SLP), Sequential Quadratic Programming (SQP), Optimality Criteria (OC) method, a Convex Linearization (CONLIN) method, or the Method of Moving Asymptotes (MMA). In particular, the MMA is well-known to be very efficient for topology optimization problems, since its algorithm suited for nonlinear optimization problems with large number of design variables and few constraints.

2.2.2 Level set-based approach

Here, we discuss structural optimization based on the level set method, in which the boundary of material domain Ω is captured based on the Eulerian approach using the iso-surface of a scalar function, the so-called level set function, during the optimization process. This approach is essentially based on topology optimization rather than shape optimization, but the novel aspect of level set-based approach is that any part of the shape boundary is allowed to split or merge during the optimization process, whereas such topological changes are typically inhibited in classical shape optimization methods based on the Lagrangian approach. Although level set-based approaches do not enable the creation of new boundaries during

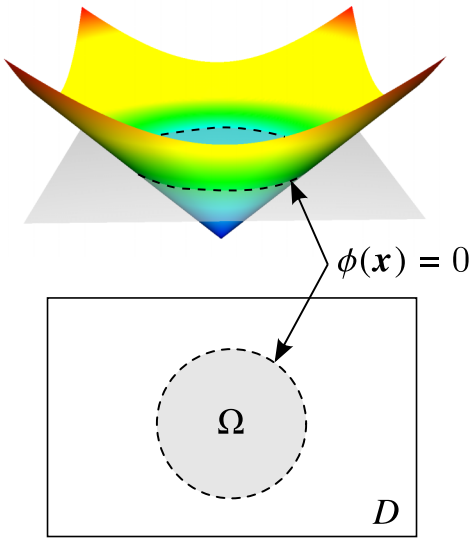

Fig. 2.2 Schematic figure of fixed design domain D and the level set function $\phi(\boldsymbol{x})$ based on the sign distance function.

the optimization process unless the bubble method is used [32], grayscales, i.e., areas with intermediate material density that are often meaningless from engineering standpoint, can be eliminated.

Standard level set-based approach

The basic idea of the level set method is to express a structural boundary, here, Γ, as the iso-surface of level set function $\phi : D \to \mathbb{R}$. As shown in Fig. 2.2, we define the level set function ϕ in D as follows:

$$\begin{cases} \phi(\boldsymbol{x}) = -d(\boldsymbol{x}, \partial\Omega) & \text{if } \boldsymbol{x} \in \Omega \setminus \partial\Omega \\ \phi(\boldsymbol{x}) = 0 & \text{if } \boldsymbol{x} \in \partial\Omega \\ \phi(\boldsymbol{x}) = d(\boldsymbol{x}, \partial\Omega) & \text{if } \boldsymbol{x} \in D \setminus \Omega, \end{cases} \tag{2.6}$$

where $\boldsymbol{x}$ is a point in the working domain[2] and $d(\cdot, \partial\Omega)$ is the Euclidean distance function to $\partial\Omega$.

[2] In level set-based approaches, D is called the working domain or reference domain, instead of the fixed design domain used in topology optimization. Note that the original definition of D is, however, identical, i.e., $\Omega \subset D$.

The material property is extended to the working domain D using the ersatz material approach. That is, we introduce an extended material property tensor $\boldsymbol{A}^*$, replacing the original tensor $\boldsymbol{A}$, as follows:

$$\boldsymbol{A}^* = H(\phi)\boldsymbol{A} \quad \text{with} \quad H(\phi) = \begin{cases} 1 & \text{if } \phi(\boldsymbol{x}) \leqslant 0 \\ \epsilon^* & \text{if } \phi(\boldsymbol{x}) > 0, \end{cases} \tag{2.7}$$

where $\epsilon^* > 0$ is a small value to avoid the singularity problem of the rigidity matrix. The Heaviside function $H(\phi)$ corresponds to the characteristic function χ in Eq. (2.1), and most of conventional level set-based approaches use interpolation treatments, in which the Heaviside function is replaced by a continuous smoothed function, e.g. [123],

$$\tilde{H}(\phi) = \begin{cases} 1 & \text{if } \phi(\boldsymbol{x}) \leqslant -h \\ \frac{3(1-\epsilon^*)}{4}\left(\frac{\phi}{h} - \frac{\phi^3}{3h^3}\right) + \frac{1+\epsilon^*}{2} & \text{if } -h < \phi(\boldsymbol{x}) \leqslant h \\ \epsilon^* & \text{if } \phi(\boldsymbol{x}) > h, \end{cases} \tag{2.8}$$

where $h > 0$ represents the parameter for determining the transition width of the smoothed Heaviside function $\tilde{H}(\phi)$. This approximation is necessary to stabilize the optimization computation, but the transition width h should be set as a small value because the use of this interpolation treatment means that the existence of grayscale is allowed in the vicinity of structural boundary. The structural boundary is, however, clear and expressed as the iso-surface of ϕ in level set-based approaches, even if an intermediate value of material property is allowed. Note that the use of transition width is just to stabilize the optimization computation and the discrete material property using the original Heaviside function is theoretically treated, whereas the standard density approach does essentially allows the existence of grayscales for topology optimization problems.

Using the pseudo-time $t \in [0, \infty)$, the boundary $\partial\Omega$ is evolved using the following advection equation:

$$\frac{\partial \phi}{\partial t} + \boldsymbol{V} \cdot \nabla \phi = 0, \tag{2.9}$$

where $\boldsymbol{V}$ represents the convection velocity defined as $\boldsymbol{V} = -v\boldsymbol{n}$, where v is a scaler function defined as shape sensitivity [4]. Since the unit normal is given by $\boldsymbol{n} = \nabla\phi/|\nabla\phi|$, Eq. (2.9) can

be reformulated as a Hamilton-Jacobi equation:

$$\frac{\partial \phi}{\partial t} - v|\nabla \phi| = 0. \tag{2.10}$$

An interesting feature of using the signed distance function is that we can ensure that the smoothness of the level set function is preserved, which is important when solving the advection equation with numerical schemes such as the finite element method and the finite difference method. In fact, since the property of the signed distance function, i.e., $|\nabla \phi| = 1$, is not retained by just solving Eq. (2.9) or (2.10), smooth solutions are not usually guaranteed during the optimization process. To avoid this numerical instability, the level set function must be reinitialized by periodically solving the following unsteady Eikonal equation:

$$\frac{\partial \phi}{\partial s} + \mathrm{sign}(\phi_0)(|\nabla \phi| - 1) = 0, \tag{2.11}$$

where $s \in [0, \infty)$ represents the pseudo-time for the reinitialization, and $\mathrm{sign}(\phi_0)$ represents the signed function with respect to the initial level set function at $s = 0$. Equation (2.11) provides as a stationary solution the signed distance to the initial interface, $\phi_0(\boldsymbol{x}) = 0$.

One of the main limitations of a conventional level set method is that the profile of the level set function must preserve the property of a signed distance function for the computation to remain stable, whereas classical shape optimization and topology optimization methods do not require additional calculations in the form of a reinitialization scheme. In practice, with conventional level set-based approaches, this can lead to a tradeoff between substantial numerical instability or massive computational cost to achieve an optimal shape.

In the level set-based approach, the optimal configuration that is represented as the iso-surface of ϕ is obtained when the value of objective functional is sufficiently converged during the optimization process that is updated by solving the Hamilton-Jacobi equation in Eq. (2.10). That is, the level set-based approach is based on the steepest descent method, due to the definition of the time evolution equation[3] .

Level set-based topology optimization

As a radical method that do without reinitialization treatments, new approach have been developed [125], where the regularization term is introduced in the objective functional to

[3] We can easily confirm that the discretized time evolution equation corresponds to a steepest descent method when using the upwind scheme with respect to the pseudo-time.

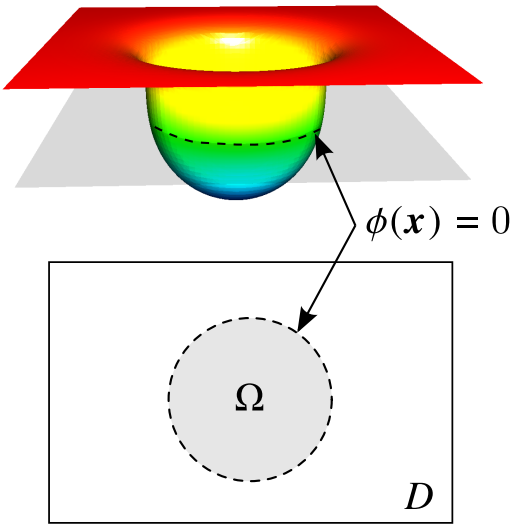

Fig. 2.3 Schematic figure of fixed design domain D and the level set function $\phi(\boldsymbol{x})$ based on the piecewise constant function.

preserve the smoothness of the level set function, redefined as a piecewise constant function that is originally based on the concept of the phase field method [17, 5]. In this method, the level set function is defined as follows:

$$\begin{cases} 0 > \phi(\boldsymbol{x}) \geqslant -1 & \text{if } \boldsymbol{x} \in \Omega \setminus \partial\Omega \\ \phi(\boldsymbol{x}) = 0 & \text{if } \boldsymbol{x} \in \partial\Omega \\ 1 \geqslant \phi(\boldsymbol{x}) > 0 & \text{if } \boldsymbol{x} \in D \setminus \Omega. \end{cases} \tag{2.12}$$

As shown in Fig. 2.3, the structural boundary $\partial\Omega$ is implicitly represented by the iso-surface of ϕ as with the conventional level set-based approach. The material property is also extended using the ersatz material approach in which the Heaviside function $H(\phi)$ is used as mentioned above.

While the standard level set method typically uses the Hamilton-Jacobi equation for updating the level set function during the optimization process, this method uses a different kind of time evolution equation, i.e., the reaction-diffusion equation, as follows:

$$\frac{\partial \phi}{\partial t} = -K(D_T J - \tau \nabla^2 \phi), \tag{2.13}$$

where $K > 0$ is a coefficient of proportionality. The key idea of this method is that the level set function is evolved using the topological derivative $D_T J : D \to \mathbb{R}$ so that the objective functional J is monotonically decreased. In addition, the second term in right side of Eq. (2.13) works to regularize the level set function so that it belongs to a smooth function space, i.e., $\phi \in H^1(D)$. The degree of regularization is controlled using the parameter $\tau > 0$ that is called the regularization coefficient and used for controlling the geometrical complexity of the optimal configuration. Otomori et al. [88] have recently provided the numerical code for the educational purpose.

In the following, a brief overview of the topological derivative is discussed. For a point $\boldsymbol{x}_0 \in \Omega$ and a model hole $\omega \subset \mathbb{R}^d$, the translated and rescaled hole is defined as

$$\omega_\epsilon = \boldsymbol{x}_0 + \epsilon\omega \quad \text{for } \forall\epsilon. \tag{2.14}$$

The perforated domain is given by

$$\Omega_\epsilon = \Omega \setminus \overline{\omega}_\epsilon. \tag{2.15}$$

The topological derivative is defined as the difference of objective functionals $J(\Omega_\epsilon)$ and $J(\Omega)$, as follows:

$$J(\Omega_\epsilon) = J(\Omega) + \epsilon^d D_T J(\boldsymbol{x}_0) + o(\epsilon^d), \tag{2.16}$$

where $D_T J(\boldsymbol{x}_0)$ is called the topological derivative at point $\boldsymbol{x}_0$. The topological derivative is essentially different from the density gradient used in the density approach because the topological derivative considers the perturbed hole that has an exact boundary everywhere in the fixed design domain, whereas the density approach only considers the material density[4] .

The level set-based topology optimization method is based on the steepest descent method due to the use of time evolution equation defined in Eq. (2.13). Otomori et al. [87] applied the mathematical programing to this approach, instead of the use of time evolution equation for updating the level set function.

[4] Since the density gradient does not include the information of topological change, the concept of density approach is originally related to that of sizing optimization where material densities at point $\boldsymbol{x}_0$ are optimized, respectively.

2.3 Optimization methods

As mentioned earlier, the mathematical programing is used for updating the design variable in the density approach, while the standard level set-based approach is typically based on the steepest decent method due to the use of time evolution equation for evolving the level set function. Although the Optimality Criteria (OC) method is the one of popular method for topology optimization problems, this approach is limited to optimization problems in which the sign of design sensitivities are always identical. Thus, the OC method is mainly applied to the stiffness maximization problem that is often treated as a benchmark to confirm the validity of topology optimization methodologies.

In the case dealing with plus and minus sensitivities, it is suitable to utilize the sequential linear programing, or sequential convex programing. Recently, a lot of papers dealing with density approach employ the Method of Moving Asymptotes (MMA)—a kind of sequential convex programing, due to its robustness and scalability in various topology optimization problems not only structural mechanics problems.

Here, we briefly discuss the basic concepts of each optimization method, where the design and state variables are respectively defined as $\boldsymbol{x} = [x_1, \ldots, x_n]^T$ and $\boldsymbol{x} \mapsto \boldsymbol{u}(\boldsymbol{x})$, an objective function and inequality constraint functions are respectively defined as $g_0, g_i : \mathbb{R}^n \times \mathbb{R}^n \to \mathbb{R}$, and we now consider the following optimization problem.

$$\begin{cases} \min\limits_{\boldsymbol{x}} g_0(\boldsymbol{x}, \boldsymbol{u}) \\ \text{subject to } g_i(\boldsymbol{x}, \boldsymbol{u}) \leqslant 0, \quad i = 1, \ldots, l \\ \boldsymbol{x} \in \mathscr{X} = \left\{ \boldsymbol{x} \in \mathbb{R}^n \,|\, x_j^{\min} \leqslant x_j \leqslant x_j^{\max}, j = 1, \ldots, n \right\}, \end{cases} \tag{2.17}$$

where $x_j^{\min}$ and $x_j^{\max}$ represent the upper and lower limits of the design variable $\boldsymbol{x}$, respectively.

To derive the optimality condition based on the Lagrange multiplier method, we introduce the Lagrangian $\mathscr{L} : \mathbb{R}^n \times \mathbb{R}^n \times \mathbb{R}^l \to \mathbb{R}$, as follows:

$$\mathscr{L}(\boldsymbol{x}, \boldsymbol{u}, \boldsymbol{\lambda}) = g_0(\boldsymbol{x}, \boldsymbol{u}) + \sum_{i=1}^{l} \lambda_i g_i(\boldsymbol{x}, \boldsymbol{u}). \tag{2.18}$$

where $\boldsymbol{\lambda} = [\lambda_1 ... \lambda_l]^{\mathrm{T}}$ represents the Lagrange multiplier. The Karush-Kuhn-Tucker (KKT) conditions are given by

$$\frac{\partial \mathscr{L}(\boldsymbol{x}, \boldsymbol{u}, \boldsymbol{\lambda})}{\partial x_j} \leqslant 0 \quad \text{if } x_j = x_j^{\max}, \tag{2.19}$$

$$\frac{\partial \mathscr{L}(\boldsymbol{x}, \boldsymbol{u}, \boldsymbol{\lambda})}{\partial x_j} = 0 \quad \text{if } x_j^{\min} < x_j < x_j^{\max}, \tag{2.20}$$

$$\frac{\partial \mathscr{L}(\boldsymbol{x}, \boldsymbol{u}, \boldsymbol{\lambda})}{\partial x_j} \geqslant 0 \quad \text{if } x_j = x_j^{\min},, \tag{2.21}$$

$$\lambda_i g_i(\boldsymbol{x}, \boldsymbol{u}) = 0, \tag{2.22}$$

$$g_i(\boldsymbol{x}, \boldsymbol{u}) \leqslant 0, \tag{2.23}$$

$$\lambda_i \geqslant 0, \tag{2.24}$$

$$\boldsymbol{x} \in \mathscr{X}, \tag{2.25}$$

for all $j = 1, \ldots, n$ and $i = 1, \ldots, l$.

Optimality Criteria (OC) method

The OC method is a classical approach for topology optimization, in order to find an optimal solution that satisfies the KKT conditions. Bendsøe and Kikuchi [10] and Suzuki and Kikuchi [114] used a simple heuristics as follows:

$$x_i^{(k+1)} = x_i^{(k)} \left(A_i^{(k)} \right)^{\eta}, \text{ with } A_i^{(k)} = \frac{\frac{\partial g_0}{\partial x_i^{(k)}}}{-\lambda_1 \frac{\partial g_1}{\partial x_i^{(k)}}}, \tag{2.26}$$

where superscript (k) represents the number of iterations carried out during the optimization process, and η is the parameter that is usually set to 0.75 so that $A_i^{(k)}$ monotonically converges to 1 in order to satisfy the KKT conditions. Here, only one constraint that is typically defined as the volume constraint in stiffness maximization problems is considered, but note that it is possible to extend this approach to multi-constraints problems.

Since this method can be easily implemented in an optimization algorithm, Sigmund [103], and Andreassen et al. [8] have provided numerical codes based on the density approach for the educational purpose.

Sequential Linear Programing (SLP)

In a SLP approximation of optimization problem defined as (2.17), the objective function and all constraint functions are linearized with respect to fixed design variable $\boldsymbol{x}_i^0$, as follows:

$$\begin{cases} \min\limits_{\boldsymbol{x}} g_0(\boldsymbol{x}^0) + \left.\frac{\partial g_0}{\partial x_i}\right|_{x_i=x_i^0}(x_i - x_i^0) \\ \text{subject to } g_i(\boldsymbol{x}^0) + \left.\frac{\partial g_i}{\partial x_i}\right|_{x_i=x_i^0}(x_i - x_i^0) \leqslant 0, \quad i = 1,\ldots,l \\ \boldsymbol{x} \in \mathscr{X} \\ -l_j^0 \leqslant x_j - x_j^0 \leqslant u_j^k, j = 1,\ldots,n. \end{cases} \tag{2.27}$$

Here, l_j^0 and u_j^0 are the so-called move limits that are used for restricting the feasible range of design variable in the vicinity of linearization point $\boldsymbol{x}^k$. The move limits are updated during the optimization process, according to some user-defined rule. Since the objective function and all constraints are affine functions with respect to $\boldsymbol{x}$, and they can be written on the form $\boldsymbol{a}^T\boldsymbol{x} + b$ where $\boldsymbol{a}$ and b are constants, i.e., they are convex. Thus, the above optimization problem is a convex problem, which can be efficiently solved by using the Simplex algorithm.

It is well-known that numerical stability of convergence in an optimization algorithm based on the SLP is poor, unless the move limits are appropriately set. This approach is suitable for solving an optimization problem in which the objective function is close to a linear equation.

Sequential Quadratic Programing (SQP)

The SQP approximation is based on the Taylor expansion up to a second order term of the objective function, as follows:

$$\begin{cases} \min\limits_{\boldsymbol{x}} g_0(\boldsymbol{x}^0) + \left.\frac{\partial g_0}{\partial x_i}\right|_{x_i=x_i^0}(x_i - x_i^0) + \frac{1}{2}(x_i - x_i^0)^T\boldsymbol{H}(\boldsymbol{x}^0)(x_i - x_i^0) \\ \text{subject to } g_i(\boldsymbol{x}^0) + \left.\frac{\partial g_i}{\partial x_i}\right|_{x_i=x_i^0}(x_i - x_i^0) \leqslant 0, \quad i = 1,\ldots,l \\ \boldsymbol{x} \in \mathscr{X}, \end{cases} \tag{2.28}$$

where $\boldsymbol{H}(\boldsymbol{x}^0)$ represents the Hessian of $g_0(\boldsymbol{x}^0)$. Since the objective function is given as a convex function, the SQP is a convex problem. The advantage of SQP compared with the SLP is that the need of move limits can be avoided due to the introduction of $\boldsymbol{H}(\boldsymbol{x}^0)$ that is

typically derived as the first order approximation of the Hessian of $g_0(\boldsymbol{x}^0)$, instead of the use of the actual Hessian.

SNOPT, proposed by Gill et al. [36], is an extended approach of SQP, and is suitable to large-scale optimization problems with linear and nonlinear constraints.

Sequential convex programming

The sequential convex programming consists of a) the convex approximation of objective and constraints functions; b) the separation of optimization problem with respect to a single design variable; and c) the application of dual approach to solve the subproblem.

In this approach, the objective function $g_0(\boldsymbol{x})$ and constraint functions $g_i(\boldsymbol{x})$, $i = 1,\ldots,l$, are expanded using the Taylor expansion, as follows:

$$g_i(\boldsymbol{x}) \approx g_i(\boldsymbol{x}^0) + \sum_{j=1}^{n} \frac{\partial g_i}{\partial x_j}\frac{\partial x_j}{\partial y_j}\bigg|_{x_j=x_j^0} (y_j(x_j) - y_j(x_j^0)), \tag{2.29}$$

where the intervening variable $x_i \mapsto y_i(x_i)$ is used for the convex approximation. In the Convex Linearization (CONLIN) developed by Fleury [34], $y_i(x_i)$ is defined as follows:

$$y_j(x_j) = \begin{cases} x_j & \text{if } \frac{\partial g_i}{\partial x_j} > 0 \\ \frac{1}{x_j} & \text{if } \frac{\partial g_i}{\partial x_j} \leqslant 0, \end{cases} \tag{2.30}$$

As a result, the approximation of g_i at $\boldsymbol{x}^0$ is given by

$$g_i(\boldsymbol{x}) \approx g_i(\boldsymbol{x}^0) + \sum_{j\in\Omega_+} \frac{\partial g_i}{\partial x_j}\bigg|_{x_j=x_j^0} (x_j - x_j^0) + \sum_{j\in\Omega_-} \frac{\partial g_i}{\partial x_j}\bigg|_{x_j=x_j^0} \frac{x_j^0(x_j - x_j^0)}{x_j}, \tag{2.31}$$

where $\Omega_+ = \{j : \partial g_i(\boldsymbol{x}^k)/\partial x_j > 0\}$ and $\Omega_- = \{j : \partial g_i(\boldsymbol{x}^k)/\partial x_j \leqslant 0\}$. That is, one linearizes using the direct variables if the corresponding components of the gradient is positive, and using the reciprocal variables otherwise. This approximation turns out to be the most conservative approximation.

As an expanded approach of the CONLIN, the Method of Moving Asymptotes (MMA) was developed by Svanberg [115]. This method has the flexibility to improve the numerical stability of convergence by introducing additional parameters in the CONLIN. In the MMA,

the intervening variable $y_i(x_i)$ is defined as follows:

$$y_j(x_j) = \begin{cases} \frac{1}{U_j - x_j} & \text{if } \frac{\partial g_i}{\partial x_j} > 0 \\ \frac{1}{x_j - L_j} & \text{if } \frac{\partial g_i}{\partial x_j} \leqslant 0, \end{cases} \tag{2.32}$$

where L_j and U_j are called moving asymptotes that are changed during the iterations (this is the source of the name of the algorithm), and satisfy $L_j < x_j^k < U_j^k$, for iteration k.

The novel aspect of the sequential convex programming is the use of separable and convex approximations. The subproblem of the sequential convex programming is constructed based on sensitivity information at the current iteration point. At each iteration point, the subproblem is solved using for instance a dual method or an interior point algorithm, and the solution of subproblem is used as the next design variable. According to the previous studies, it seems that sequential convex programming is very efficient and suitable for topology optimization.

The advantage of sequential convex programming can be found in the monograph by Bendsøe and Sigmund [11] in which the various topics of topology optimization are described and it is indicated that MMA may be a bit slower than the OC method in simple structural mechanics problems such as stiffness maximization problem, but for more complicated problems involving several constraints MMA stands for excellent convergence properties.

2.4 Sensitivity analysis

Sensitivity analysis is an important element in the optimization procedure to obtain the design sensitivity, whose accuracy affects the quality of the optimal solution. Although there are various methods employed in sensitivity analysis, these methods can be roughly divided into two categories, i.e., the direct, and adjoint methods [23].

Let us consider the derivatives of an objective function $J : D \to \mathbb{R}$ with respect to the design variable $\boldsymbol{x} \in \mathbb{R}^n$, in the case when $J(\boldsymbol{x}, \boldsymbol{u})$ depends on a function $\boldsymbol{x} \mapsto \boldsymbol{u}(\boldsymbol{x})$ that is the solution of a partial differential equation defined as $\boldsymbol{E}(\boldsymbol{x}, \boldsymbol{u}) = 0$. Thus, we here consider the

following minimization problem,

$$\begin{cases} \inf\limits_{\boldsymbol{x}} \ J(\boldsymbol{x}, \boldsymbol{u}) \\ \text{subject to } \boldsymbol{E}(\boldsymbol{x}, \boldsymbol{u}) = 0 \\ \boldsymbol{x} \in \mathbb{R}^n. \end{cases} \tag{2.33}$$

Although this optimization problem consists of an objective function with an equality constraint for simplifying the following explanation of each way of sensitivity analysis, an inequality constraint can be also imposed as with the equality constraint. Note that the relationship between the design variable and the state variable which depends on the design variable, $\boldsymbol{u}(\boldsymbol{x})$, is often seen as the typical situation in structural optimization problems.

2.4.1 Direct method

Finite difference method

The easiest method to obtain the design sensitivity is the finite difference method. For instance, the forward difference approximation of objective function J with respect to the design variable $\boldsymbol{x}$ is given by

$$\frac{\mathrm{d}J}{\mathrm{d}\boldsymbol{x}} \approx \frac{J(\boldsymbol{x} + \epsilon \boldsymbol{e}, \boldsymbol{u}(\boldsymbol{x} + \epsilon \boldsymbol{e})) - J(\boldsymbol{x}, \boldsymbol{u}(\boldsymbol{x}))}{\epsilon}, \tag{2.34}$$

where $\boldsymbol{e} \in \mathbb{R}^n$ is the unit vector, and $\epsilon > 0$ is a parameter for determining the perturbation of design variable. If $-\epsilon$ is substituted in Eq. (2.34), the equation is then defined as the backward difference method. In addition, if the design variable is perturbed in both directions, the sensitivity is given by

$$\frac{\mathrm{d}J}{\mathrm{d}\boldsymbol{x}} \approx \frac{J(\boldsymbol{x} + \epsilon \boldsymbol{e}, \boldsymbol{u}(\boldsymbol{x} + \epsilon \boldsymbol{e})) - J(\boldsymbol{x} - \epsilon \boldsymbol{e}, \boldsymbol{u}(\boldsymbol{x} - \epsilon \boldsymbol{e}))}{2\epsilon}, \tag{2.35}$$

which is the so-called central difference method. Although these methods are numerically robust and easy to implement, there are well-known difficulties [79]:

- the choice of perturbation ϵ;
- the round-off error due to the subtraction of nearly equal terms;
- a computing cost proportional to the size of the state space times the design space.

Complex variable method

To avoid the subtraction error in the finite difference method, we can use the complex variable method, which was first proposed by Lyness and Moler [71]. Like the finite difference method, this method is based on a Taylor series expansion of J around the point $\boldsymbol{x}$. But for a function of a complex variable, the gradient is easily accessible:

$$J(\boldsymbol{x}+i\epsilon\boldsymbol{e},\boldsymbol{u}(\boldsymbol{x}+i\epsilon\boldsymbol{e}))=J(\boldsymbol{x},\boldsymbol{u}(\boldsymbol{x}))+i\epsilon J'-\frac{\epsilon^2}{2}J''-i\frac{\epsilon^3}{6}J'''+o(\epsilon^3). \tag{2.36}$$

This equation implies

$$\frac{\mathrm{d}J}{\mathrm{d}\boldsymbol{x}}\approx\frac{\Im\mathrm{m}(J(\boldsymbol{x}+i\epsilon\boldsymbol{e},\boldsymbol{u}(\boldsymbol{x}+i\epsilon\boldsymbol{e})))}{\epsilon}. \tag{2.37}$$

We note that there is no more subtraction and the choice of ϵ is less critical. The computing cost is, however, promotional to the size of the state and design spaces as with the finite difference method. In addition, this method requires a redefinition in the numerical code of all variable and functions from real to complex.

2.4.2 Adjoint method

In order to obtain analytical expressions for $\mathrm{d}J/\mathrm{d}\boldsymbol{x}$, the chain rule is first applied in the adjoint method [31], as follows:

$$\frac{\mathrm{d}J(\boldsymbol{x},\boldsymbol{u}(\boldsymbol{x}))}{\mathrm{d}\boldsymbol{x}}=\frac{\partial J(\boldsymbol{x},\boldsymbol{u}(\boldsymbol{x}))}{\partial\boldsymbol{x}}+\frac{\partial J(\boldsymbol{x},\boldsymbol{u}(\boldsymbol{x}))}{\partial\boldsymbol{u}}\frac{\partial\boldsymbol{u}(\boldsymbol{x})}{\partial\boldsymbol{x}}, \tag{2.38}$$

where the partial derivatives, $\partial J(\boldsymbol{x},\boldsymbol{u}(\boldsymbol{x}))/\partial\boldsymbol{x}$ and $\partial J(\boldsymbol{x},\boldsymbol{u}(\boldsymbol{x}))/\partial\boldsymbol{u}$, are analytically obtained due to the definition of the objective function J, but $\partial\boldsymbol{u}(\boldsymbol{x})/\partial\boldsymbol{x}$ must be computed using for instance the finite difference method because the state variable $\boldsymbol{u}$ given by solving the PDE, $E(\boldsymbol{x},\boldsymbol{u})=0$, is implicitly dependent on the design variable $\boldsymbol{x}$. Thus, the computing cost problem as with the finite difference method remains proportional to the number of design variable times to dimension of $\boldsymbol{u}$.

To avoid the computing cost problem, the gradient of E with respect to $\boldsymbol{x}$ is introduced as follows:

$$\frac{\mathrm{d}E(\boldsymbol{x},\boldsymbol{u}(\boldsymbol{x}))}{\mathrm{d}\boldsymbol{x}}=\frac{\partial E(\boldsymbol{x},\boldsymbol{u}(\boldsymbol{x}))}{\partial\boldsymbol{x}}+\frac{\partial E(\boldsymbol{x},\boldsymbol{u}(\boldsymbol{x}))}{\partial\boldsymbol{u}}\frac{\partial\boldsymbol{u}(\boldsymbol{x})}{\partial\boldsymbol{x}}=0, \tag{2.39}$$

which is rewritten as

$$\frac{\partial \boldsymbol{u}(\boldsymbol{x})}{\partial \boldsymbol{x}} = -\left(\frac{\partial E(\boldsymbol{x}, \boldsymbol{u}(\boldsymbol{x}))}{\partial \boldsymbol{u}}\right)^{-1} \frac{\partial E(\boldsymbol{x}, \boldsymbol{u}(\boldsymbol{x}))}{\partial \boldsymbol{x}}. \tag{2.40}$$

Insertion of this into Eq. (2.38) yields

$$\begin{aligned}\frac{\mathrm{d}J(\boldsymbol{x}, \boldsymbol{u}(\boldsymbol{x}))}{\mathrm{d}\boldsymbol{x}} &= \frac{\partial J(\boldsymbol{x}, \boldsymbol{u}(\boldsymbol{x}))}{\partial \boldsymbol{x}} - \frac{\partial J(\boldsymbol{x}, \boldsymbol{u}(\boldsymbol{x}))}{\partial \boldsymbol{u}} \left(\left(\frac{\partial E(\boldsymbol{x}, \boldsymbol{u}(\boldsymbol{x}))}{\partial \boldsymbol{u}}\right)^{-1} \frac{\partial E(\boldsymbol{x}, \boldsymbol{u}(\boldsymbol{x}))}{\partial \boldsymbol{x}}\right) \\ &= \frac{\partial J(\boldsymbol{x}, \boldsymbol{u}(\boldsymbol{x}))}{\partial \boldsymbol{x}} - \left(\left(\frac{\partial E(\boldsymbol{x}, \boldsymbol{u}(\boldsymbol{x}))}{\partial \boldsymbol{u}}\right)^{-T} \frac{\partial J(\boldsymbol{x}, \boldsymbol{u}(\boldsymbol{x}))}{\partial \boldsymbol{u}}\right) \frac{\partial E(\boldsymbol{x}, \boldsymbol{u}(\boldsymbol{x}))}{\partial \boldsymbol{x}}.\end{aligned} \tag{2.41}$$

We then introduce a variable $\tilde{\boldsymbol{u}}(\boldsymbol{x})$, the so-called adjoint variable, such that

$$\left(\frac{\partial E(\boldsymbol{x}, \boldsymbol{u}(\boldsymbol{x}))}{\partial \boldsymbol{u}}\right)^{T} \tilde{\boldsymbol{u}}(\boldsymbol{x}) = \frac{\partial J(\boldsymbol{x}, \boldsymbol{u}(\boldsymbol{x}))}{\partial \boldsymbol{u}}, \tag{2.42}$$

which makes it possible to compute the gradient at a cost independent of the number of design variable, as only one solution of Eq. (2.42) is required:

$$\frac{\mathrm{d}J(\boldsymbol{x}, \boldsymbol{u}(\boldsymbol{x}))}{\mathrm{d}\boldsymbol{x}} = \frac{\partial J(\boldsymbol{x}, \boldsymbol{u}(\boldsymbol{x}))}{\partial \boldsymbol{x}} - \tilde{\boldsymbol{u}}^{\mathrm{T}}(\boldsymbol{x}) \frac{\partial E(\boldsymbol{x}, \boldsymbol{u}(\boldsymbol{x}))}{\partial \boldsymbol{x}}. \tag{2.43}$$

In structural optimization problems, Eq. (2.42) is solved for the objective function and each constraint function. We conclude that the adjoint method is to be preferred when there are fewer constraints than design variables, otherwise the direct method will be more efficient. Since a large number of design variables must be treated in general topology optimization problems, the adjoint method is the essential tool for efficiently solving optimization problems. In this thesis, the adjoint method is applied to topology optimization for fluid dynamics problems, in which a specific case of adjoint sensitivity analysis will be discussed in the later.

2.5 Topology optimization for fluid problems

2.5.1 Background

As mentioned earlier, structural optimization is a methodology to obtain an optimal solution using a numerical model based on mathematical optimization theory. Since this methodology can obtain high performance structures using structural optimization techniques, it is very attractive, even in the field of fluid mechanics. In 1973, Pironneau pioneered a structural

optimization method for fluid dynamics problems [95, 96]. Considerable research has been carried out since then and a number of structural optimization methods applicable to fluid dynamics problems have been proposed [79, 56, 80, 121, 54, 122, 109, 137, 132]. However, since the above research was based on shape optimization, the feasible design modifications only consisted in the adjustment of the boundaries of selected parts to the fluid domain.

Based on topology optimization, Borrvall and Petersson [14] first proposed a topology optimization method for minimum power dissipation in a Stokes flow problem, where the material distribution in the fixed design domain is expressed as either the presence of fluid or an impermeable solid domain. Since the feasible design modifications pertain to adjustments of the material porosity in the fixed design domain, the no-slip boundary condition along the fluid-solid interface can be implicitly satisfied. In research based on this methodology, Aage et al. [1] proposed a topology optimization method for large-scale Stokes flow problems. Olesen et al. [84] proposed a topology optimization method using the steady-state NSE for incompressible fluids, and introduced a numerical implementation scheme using commercial software. Deng et al. [27], and Kreissl et al. [64], proposed a topology optimization method using the unsteady NSE for incompressible fluids. On the other hand, Kondoh et al. [60] obtained optimal body shapes in NS flows for drag minimization and lift maximization problems by introducing a new types of objective function. Furthermore, using Borrvall and Petersson's methodology as a basis, considerable research has been carried out to develop engineering applications for fluidic devices [35, 7, 70, 68]. In addition, multiphysics topology optimization methods have been proposed to deal with fluid-structure [128], fluid-electric [37], fluid-thermal [89, 25, 75], and electro-fluid-thermal-compliant [129] problems.

All of the above-mentioned research encounters the problem of so-called grayscales, regions of intermediate density that are allowed to exist in the optimal configurations. In such cases, the no-slip boundary condition is incompletely satisfied, since a specific boundary along the solid-fluid interface does not exist in grayscale regions. Guest and Prévost [39] employed their nodal design variable method, a kind of penalization scheme, to eliminate grayscales in topology optimization for minimum power dissipation problems under Stokes flow.

Based on the level set-based approach, Challis and Guest [18] proposed a level set-based structural optimization method for minimum power dissipation problems under Stokes flow, and examined the same design problems as those treated in previous research using the density approach [14, 39]. Duan et al. [29], Zhou et al. [133], and Duan et al. [30] proposed

a level set-based structural optimization method for steady-state NS flow problems, and Deng et al. [28] extended it to unsteady NS flow optimization problems.

In structural optimization methods for fluid dynamics problems, reduction of flow field computational cost is a major factor when seeking to maintain practical total optimization times, since most numerical schemes for obtaining solutions to NSE for incompressible fluids include an iterative computation of a massive system of linear equations, which is related to the integration of the Poisson equation for the pressure field. That is, structural optimization methods for large-scale flow problems typically incur great computational cost to obtain optimal configurations. Similarly, since most previous research on structural optimization methods for fluid dynamics problems employ the FEM to obtain solutions of the incompressible NSE, the scale of feasible computational space has been very limited. Consequently, most numerical examples in previous research deal with two-dimensional cases, and those that do address three-dimensional cases have a relatively small number of finite elements. To deal with large-scale flow problems in structural optimization problems, these computational obstacles must be overcome.

As an alternative way for solving the flow field, the lattice Boltzmann method (LBM) has recently been an attractive scheme in the research field of computational fluid dynamics [76, 44, 20, 110]. Comparing the coding used in LBM and the conventional schemes based on the NSE, the simplicity of the LBM algorithm and its scalability for complex flow problems such as porous, miscible, and immiscible fluid flow problems, are advantageous. In addition, the LBM enables one to avoid the numerical treatment of iterative computation for the correction of fluid velocity and pressure in the incompressible viscous fluid flow. Topology optimization methods that use the LBM are therefore suitable for dealing with large-scale and complex flow optimization problems.

Pingen et al. [90] proposed a topology optimization using the LBM, and obtained optimal configurations similar to those using a conventional approach proposed by Borrvall and Petersson [14]. Based on this pioneering study using the LBM, Pingen et al. [94] and Kreissl et al. [66] proposed a level-set based structural optimization method using the LBM for a flow channel design problem. Pingen and Maute [93] dealt with non-Newtonian flows to represent the viscosity of blood in their design model of a flow channel. Kreissl et al. [65] proposed a topology optimization method for a fluid-structure interaction problem for micro-channel devices. In addition, Makhija et al. [74] proposed a topology optimization method using the LBM for a mixture efficiency maximization problem under multi-component flow.

In this thesis, the LBM is employed for solving fluid flow optimization problems, but the following in this chapter will introduce the basic formulation of the fluid flow topology optimization methods using the standard numerical scheme, e.g., the finite element method, for solving the NSE.

2.5.2 Topology optimization based on the Navier-Stokes formulation

We now discuss a brief summary of the fluid flow topology optimization that was first proposed by Borrvall and Petersson [14]. Although the original idea of the research focuses on Stokes flows, we extend it to NS flow optimization problems for formulating as general optimization problems of an incompressible viscous fluid. Let $\Omega \subset \mathbb{R}^d$ be filled with the fluid domain, and D be the fixed design domain that is a bounded open set of $\mathbb{R}^d$ and contains all admissible shapes of Ω. The fluid flow under the steady-state condition is governed by the continuity equation and NSE as follows:

$$\left.\begin{aligned} &\nabla \cdot \boldsymbol{u} = 0 \\ &\rho(\boldsymbol{u} \cdot \nabla)\boldsymbol{u} = -\nabla p + \mu \nabla^2 \boldsymbol{u} + \rho \boldsymbol{g} \end{aligned}\right\} \text{ in } \Omega, \tag{2.44}$$

where $\boldsymbol{u}(\boldsymbol{x})$, $p(\boldsymbol{x})$ and $\boldsymbol{g}(\boldsymbol{x})$ are the fluid velocity, pressure and a body force at the point $\boldsymbol{x}$, respectively. ρ and μ represents the fluid density and the viscosity of the fluid.

The key idea of fluid flow topology optimization is to consider the solid domain, $D \setminus \Omega$, as a porous medium governed by Darcy's law, which has been derived from the NSE via homogenization, given by

$$\boldsymbol{u} = -\frac{\kappa}{\mu}(\nabla p - \rho \boldsymbol{g}) \quad \text{in } D \setminus \Omega, \tag{2.45}$$

where κ is called the permeability. To discriminate the domains whether fluid or solid, the permeability is set so that $\kappa \ll 1$ in the solid domain. The NSE can be then formulated to represent the both fluid and solid domains, as follows:

$$\chi \rho(\boldsymbol{u} \cdot \nabla)\boldsymbol{u} = -\nabla p + \left(\chi \mu \nabla^2 - (1-\chi)\frac{\mu}{\kappa}\right)\boldsymbol{u} + \rho \boldsymbol{g} \quad \text{in } D, \tag{2.46}$$

where $\chi(\boldsymbol{x})$ represents the characteristic function defined as $\chi = 1$ in the fluid domain Ω, and $\chi = 0$ in the solid domain $D \setminus \Omega$. In fact, we can confirm that the NSE (2.44), and Darcy's law defined as Eq. (2.45) are derived when $\chi = 1$, and $\chi = 0$, respectively. The schematic figure is

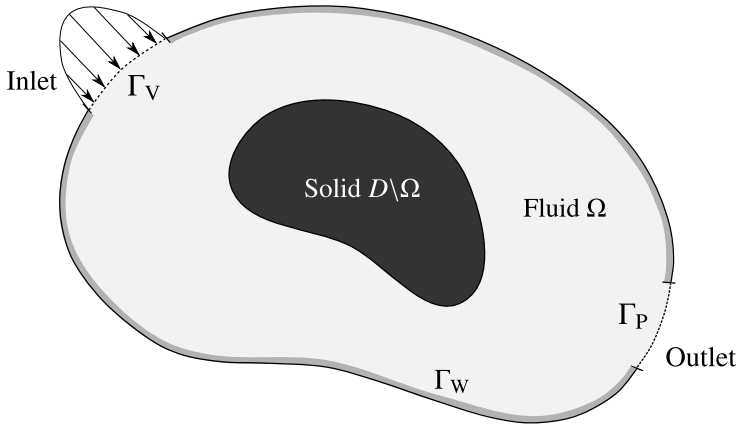

Fig. 2.4 The fixed design domain D and boundary conditions.

shown in Fig. 2.4, where the fixed design domain D is fulfilled with the porous medium in which the structural boundary $\partial\Omega$ between the fluid domain Ω and the solid domain $D \setminus \Omega$ is implicitly represented using the characteristic function χ. Here, let $(\Gamma_W \cup \Gamma_V) \subset \partial D$ denotes a Dirichlet boundary Γ_D, on which the velocity $\bar{\boldsymbol{u}}$ is prescribed, and a Neumann boundary Γ_N exists at $\Gamma_P \subset \partial D$ where a surface traction $\bar{\boldsymbol{t}}$ is applied, i.e.,

$$\boldsymbol{u} = \bar{\boldsymbol{u}} \quad \text{on } \Gamma_D, \tag{2.47}$$

$$\left(-p\boldsymbol{I} + \mu\nabla\boldsymbol{u}\right)\boldsymbol{n} = \bar{\boldsymbol{t}} \quad \text{on } \Gamma_N, \tag{2.48}$$

where $\boldsymbol{I}$ represents the identity matrix. We note that it is unnecessary to explicitly define a design-dependent boundary $\Gamma = \partial\Omega \subset (\Gamma_D \cup \Gamma_N)$ because the no-slip boundary condition, $\boldsymbol{u} = \boldsymbol{0}$ on Γ, is automatically satisfied.

In practice, the characteristic function is replaced with a continuous function, used in the density approach. Thus, a set of admissible design, $\mathfrak{X}_{\text{ad}}$, is chosen as follows:

$$\mathfrak{X}_{\text{ad}} = \left\{\gamma \in L^\infty(D) \,|\, 0 \leqslant \gamma \leqslant 1, \text{a.e. in } D, |\Omega| \leqslant V, \, (\Gamma_D \cup \Gamma_N) \subset \partial D\right\}. \tag{2.49}$$

Additionally, Eqs. (2.46) is typically simplified as

$$\left.\begin{aligned} &\nabla\cdot\boldsymbol{u} = 0 \\ &\rho(\boldsymbol{u}\cdot\nabla)\boldsymbol{u} = -\nabla p + \mu\nabla^2\boldsymbol{u} - \alpha(\gamma)\boldsymbol{u} + \rho\boldsymbol{g} \end{aligned}\right\} \text{ in } D, \tag{2.50}$$

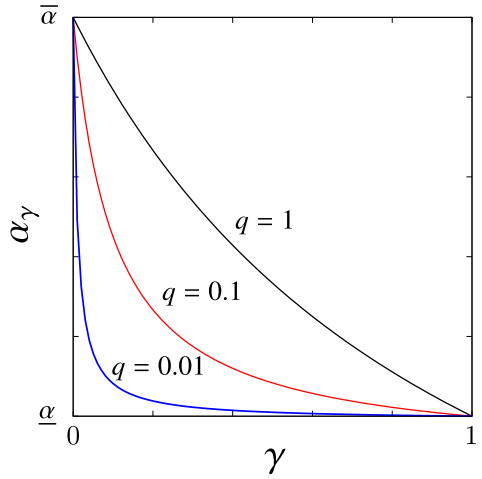

Fig. 2.5 The interpolation function $\alpha(\gamma)$ plotted for $q = 0.01$, 0.1, and 1.

where $\gamma \mapsto \alpha(\gamma)$ denotes the inverse permeability[5] , and is commonly defined using an interoperation function, as follows:

$$\alpha(\gamma) = \overline{\alpha} + (\underline{\alpha} - \overline{\alpha})\gamma \frac{1+q}{\gamma+q}, \tag{2.51}$$

which is defined as a strictly convex function as shown in Fig. 2.5, with a penalty control parameter $q > 0$. The inverse permeability $\alpha(\gamma)$ is assumed to vary between zero and infinity, i.e., $\underline{\alpha} = 0$ and $\overline{\alpha} \to +\infty$.

The introduction of penalty term, $-\alpha(\gamma)\boldsymbol{u}$, is an unique treatment for implicitly representing the structural boundaries between the fluid and solid domains, whereas different domains are discriminated by expanding the material property, which composes both of the different material properties, in other physical problems such as structure, thermal, or electromagnetic problem.

Equations (2.50) can be transformed into a non-dimensional form using non-dimensional variables, whose definitions are shown in Appendix A, as follows:

$$\left.\begin{aligned} &\nabla^* \cdot \boldsymbol{u}^* = 0 \\ &(\boldsymbol{u}^* \cdot \nabla^*)\boldsymbol{u}^* = -\nabla^* p^* + \tfrac{1}{Re}\nabla^{*2}\boldsymbol{u}^* - \alpha^*(\gamma)\boldsymbol{u}^* + \boldsymbol{g}^* \end{aligned}\right\} \text{ in } D, \tag{2.52}$$

[5] This interpretation is widely used, but somewhat simplified due to the definition of $\alpha = \mu/\kappa$.

where $\nabla^* = L\nabla$ represents the non-dimensional gradient operator, and Re is the Reynolds number defined as

$$Re = \frac{\mu UL}{\rho}. \tag{2.53}$$

Here, U and L are the reference speed and length, respectively. It is well-known that the non-dimensional form is useful to treat the fluid governing equations in the numerical analysis, since only the Reynolds number is the parameter that determines fluid characteristics. For brevity, we will henceforth drop the asterisk of the non-dimensional variables.

In the fluid flow topology optimization, the total potential energy is widely used as a standard objective functional. Let $J^A : D \to \mathbb{R}$ denote the potential power of the viscous flow:

$$J^A(\boldsymbol{u};\gamma) = \int_D \frac{1}{2Re}\nabla\boldsymbol{u} : \nabla\boldsymbol{u}\mathrm{d}\Omega - \int_D \boldsymbol{g}\cdot\boldsymbol{u}\mathrm{d}\Omega. \tag{2.54}$$

Let us further define the power dissipation $J^B : D \to \mathbb{R}\cup\{+\infty\}$

$$J^B(\boldsymbol{u},\gamma) = \int_D \frac{1}{2}\alpha(\gamma)\boldsymbol{u}\cdot\boldsymbol{u}\mathrm{d}\Omega. \tag{2.55}$$

Thus, the total potential energy J is given by

$$J(\boldsymbol{u},\gamma) = J^A(\boldsymbol{u};\gamma) + J^B(\boldsymbol{u},\gamma). \tag{2.56}$$

Note that the requirement, $\alpha(\gamma) \to +\infty \Rightarrow \boldsymbol{u} = \boldsymbol{0}$, is satisfied when $J^B(\boldsymbol{u},\gamma) < +\infty$

Consequently, the total potential energy minimization problem in a steady-state incompressible viscous fluid is formulated as follows:

$$\begin{cases} \inf\limits_{\gamma} \ J(\boldsymbol{u},\gamma) \\ \text{s.t. } \boldsymbol{u} \text{ and } p \text{ satisfy (2.52)} \\ \gamma \in \mathfrak{X}_{\text{ad}}. \end{cases} \tag{2.57}$$

We note that minimization of the total potential energy corresponds to minimize drag or average pressure drop across the domain when the prescribed velocity is uniform and normal to the boundary [84, 68]. A derivation procedures of the design sensitivity in this optimization problem can be referred in [27, 26].

2.5.3 Numerical implementation

For density-based approach

The optimization algorithm for Eq. (2.57) is structured as follows:

Step 1. The initial design is set in the fixed design domain.

Step 2. The governing equations are solved using the FEM.

Step 3. If the criteria of the objective functional and inequality constraint are satisfied, an optimal configuration is obtained and the optimization is finished, otherwise the adjoint equations are solved using the FEM and the procedure advances to Step 4.

Step 4. The design sensitivities are calculated using the current state and adjoint variables.

Step 5. The design variable is updated using MMA, after which the optimization procedure returns to Step 2 of the iterative loop.

For level set-based approach

We further construct an optimization algorithm for a thermal-fluid problem that will be introduced in the later Section. In this problem, the level set-based topology optimization [125] is applied. The algorithm is an iterative method based on the descent gradient method, and is structured as follows:

Step 1. The initial level set function is set in the fixed design domain.

Step 2. The governing equations are solved using the FEM.

Step 3. If the criteria of the objective functional and inequality constraint are satisfied, an optimal configuration is obtained and the optimization is finished, otherwise the adjoint equations are solved using the FEM and the procedure advances to Step 4.

Step 4. The design sensitivities are calculated using the current state and adjoint variables.

Step 5. The level set function is updated using the reaction-diffusion equation that is solved using the FEM, after which the optimization procedure returns to Step 2 of the iterative loop.

In level set-based topology optimization, the design sensitivity is defined as the topological derivative that is used for the reaction term in the reaction-diffusion equation. Although

several researchers [41, 6] revealed the topological derivative dealing with the NSE, it is hard to handle and limited to simple problems. This is because the topological derivative needs to deal with a fundamental solution of the state problem, in order to calculate a boundary integral of a perturbed small hole in the fixed design domain. To avoid this difficulty, we assume that the topological derivative can be approximated by the density gradient, which means that the boundary integral can be neglected due to its sufficiently small order compared with the other terms in the sensitivity. Note that this assumption is not always valid, but it seems that the boundary integral term is typically neglected in fluid problems because the no-slip boundary condition on the perturbed small hole is imposed.

Convergence criterion for objective functional

These procedures are iterated until the following criterion for the value of the objective functional is met:

$$\left| \frac{J^N - J^{N-1}}{J^N} \right| < \epsilon_{\mathrm{opt}}, \tag{2.58}$$

where superscript N represents the number of iterations carried out during the optimization process. The optimization procedures are iterated until the criterion $\epsilon_{\mathrm{opt}} > 0$ will be sufficiently small [6] .

2.6 Application to a thermal-fluid problem

2.6.1 Governing equations

Here we discuss flow channel problems that deal with an incompressible thermal-fluid flow in a steady-state. The formulation of the governing equations must therefore take into account the conservation of mass, momentum, and energy, as follows:

$$\left.\begin{aligned} &\nabla \cdot \boldsymbol{u} = 0 \\ &(\boldsymbol{u} \cdot \nabla)\boldsymbol{u} = -\nabla p + \tfrac{1}{Re}\nabla^2 \boldsymbol{u} \\ &Pr\,Re(\boldsymbol{u} \cdot \nabla)T = \nabla^2 T \end{aligned}\right\} \text{ in } \Omega, \tag{2.59}$$

[6] For detailed studies, the procedures should be stopped when necessary conditions of optimality, defined as the KKT conditions, are satisfied.

where Pr is the non-dimensional parameter, the so-called Prandtl number:

$$Pr = \frac{\mu c_p}{k_f}, \tag{2.60}$$

where c_p and k_f are the specific heat and the thermal conductivity of fluid, respectively.

As the general boundary conditions for T, we consider the following Dirichlet and Neumann boundary conditions:

$$T = \bar{T} \quad \text{on } \Gamma_D, \tag{2.61}$$

$$\boldsymbol{n} \cdot \nabla T = 0 \quad \text{on } \Gamma_N. \tag{2.62}$$

2.6.2 Expansion of governing equations

To construct a topology optimization method for the thermal-fluid flow problems, the formulation of the governing equations must be expanded to the fixed design domain D from the fluid domain $\Omega \subset D$. Based on the previous study [25, 75, 59], the governing equations in the coupled thermal-fluid problem are restated as

$$\left.\begin{aligned} &\nabla \cdot \boldsymbol{u} = 0 \\ &(\boldsymbol{u} \cdot \nabla)\boldsymbol{u} = -\nabla p + \tfrac{1}{Re}\nabla^2 \boldsymbol{u} - \alpha(\gamma)\boldsymbol{u} \\ &Pr\,Re(\boldsymbol{u} \cdot \nabla)T = \nabla^2 T + \beta(\gamma)(1-T) \end{aligned}\right\} \text{ in } D, \tag{2.63}$$

where $\gamma \mapsto \beta(\gamma)$ represents the non-dimensional parameter called the heat generation coefficient:

$$\beta(\gamma) = (1-\gamma)\bar{\beta} \quad \text{with } \bar{\beta} = \frac{hL^2}{k_s}, \tag{2.64}$$

where k_s is the thermal conductivity of the solid, and h is a dimensional coefficient that controls the heat generation according to the temperature difference. The use of the design variable γ allows us to assume that heat generation only arises in the solid domain.

2.6.3 Heat exchange maximization problem

In this thesis, the formulation of the optimization problem for a cooling device (such as a liquid-cooled heat sink) aims to maximize cooling performance, which can be evaluated according to the heat transfer between the flow channel and the heated structure. However, the

heat transfer is difficult to evaluate numerically during the optimization procedure, because its value may be different at each local point in the flow field. Therefore, to simplify the model used as the basis of our formulation, it is assumed that the heat transfer can be evaluated by considering the internal heat generation in the fixed design domain D. Note that the cooling performance can be qualitatively evaluated by the heat exchange defined according to this assumption and that, based on this assumption, previous research [75] has obtained appropriate solutions. However, since this assumption prevents representation of the actual heat transfer, it should be also noted that the present methodology must be developed based on heat transfer that is locally dependent on the flow field and evaluated quantitatively on the fluid-solid boundary.

Consequently, for the heat exchange maximization problem, the following objective functional $I : D \to \mathbb{R}$, defined as the heat generation in the fixed design domain D, is used:

$$I(T, \gamma) = \int_D \beta(\gamma)(1 - T)\mathrm{d}\Omega, \tag{2.65}$$

which represents the non-dimensional internal heat generation in the fixed design domain D, and is assumed to represent the heat exchange between the fluid and solid domains.

Based on the above objective functional, an optimization problem that aims to derive an optimal channel configuration, which indicates the maximum heat exchange amount in the fixed domain D, is formulated. The boundary conditions for p is considered as follows:

$$p = \Delta p \quad \text{on } \Gamma_{\text{in}}, \tag{2.66}$$

$$p = 0 \quad \text{on } \Gamma_{\text{out}}, \tag{2.67}$$

where Γ_{in}, and Γ_{out} represent the inlet, and outlet boundaries, respectively.

In this optimization problem, since the prescribed velocity is not set on Γ_{in}, the characteristic velocity, which is generally defined using the mean value of a prescribed velocity at the inlet boundary, is not able to be defined in order to obtain the Reynolds number. Thus, the characteristic velocity is defined as follows:

$$U = \sqrt{\frac{\Delta \bar{p}}{\rho}}, \tag{2.68}$$

where $\Delta \bar{p}$ represents the dimensional pressure difference between the pressures at the inlet and outlet. The characteristic velocity U in Eq. (2.68) is used, to formulate the non-

dimensional governing equation in Eq. (2.63). Here, it must be noted that the Reynolds number based on Eq. (2.68) has different meaning of the traditional Reynolds number used as an index for checking whether the observed flow is laminar or turbulent. To clarify the difference, a non-dimensional parameter θ using U in Eq. (2.68) is newly defined as follows:

$$\theta = \frac{\rho U L}{\mu} = \frac{\rho L}{\mu}\sqrt{\frac{\Delta \bar{p}}{\rho}}, \tag{2.69}$$

which is not the traditional Reynolds number but is used for formulating the non-dimensional governing equations. As a result, the physical meaning of using identical values of θ is equivalent to using identical settings for the dimensional pressure difference $\Delta \bar{p}$.

On the other hand, the traditional Reynolds number could be used when formulating the optimization problem using the inlet boundary condition based on the prescribed velocity, but this would require an additional constraint to prevent the occurrence of an infinite pressure loss between the inlet and outlet. Dede [25], and Koga et al. [59] proposed an optimization method that avoids the use of an additional constraint by using an objective functional composed of two objective functionals, the heat exchange and the dissipation energy, but weighting coefficients are a priori parameters that must be set to appropriate values by trial and error. To avoid the above complex formulation and to simplify the optimization problem, the fixed pressure difference condition and non-dimensional parameter θ are used in the presented method.

Consequently, since the maximization problem can be formulated as a minimization problem by changing sign of the objective functional, the optimization problem for the coupled thermal-fluid problem is formulated as follows:

$$\begin{cases} \inf\limits_{\gamma} \ -I(T,\gamma) \\ \text{s.t. } \boldsymbol{u}, p \text{ and } T \text{ satisfy (2.63)} \\ \gamma \in \mathfrak{X}_{\text{ad}}. \end{cases} \tag{2.70}$$

2.6.4 Numerical examples

Here, several numerical examples are provided to confirm the validity of the presented method. The level set-based topology optimization [125] is employed for obtaining optimal configurations that have clear boundaries.

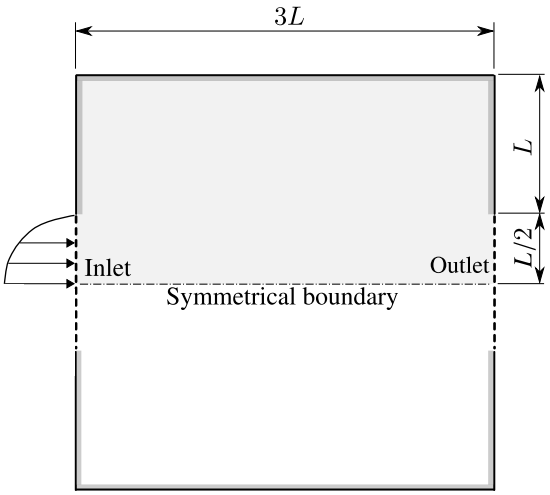

Fig. 2.6 Design model and fixed design domain D in the heat exchange maximization problem.

The design requirements are shown in Fig. 2.6, where the inlet pressure and temperature are respectively set to $\Delta p = 1$ and $T = 0$ on the inlet boundary Γ_{in}. Since the design model is symmetrical, the fixed design domain D is defined as the upper half of the model. The wall boundary conditions are defined as no-slip, i.e., $\boldsymbol{u} = \mathbf{0}$, and adiabatic, i.e., $\nabla T \cdot \boldsymbol{n} = 0$, and the outlet boundary condition is also defined as adiabatic.

In addition, the characteristic length is set to the inlet width L, and the characteristic velocity U is set based on Eq. (2.68). As noted previously, Note that the non-dimensional parameter θ is used in order to formulate the non-dimensional governing equations, instead of the traditional Reynolds number. However, to appreciate the flow information of each optimal configuration, the Reynolds numbers in each optimization result are respectively calculated using the mean value of the magnitude of the inlet velocity, $\hat{U}_{\text{in}}$, which is the non-dimensional value, normalized by the characteristic velocity U in Eq. (2.68), and obtained after the computation of flow field in each optimal configuration. That is, based on the definition of θ in Eq. (2.69), the Reynolds number, Re, can be derived from $Re = (\bar{U}_{\text{in}}/U)\theta = \hat{U}_{\text{in}}\theta$, where $\bar{U}_{\text{in}} (= U\hat{U}_{\text{in}})$ represents the dimensional mean value of the magnitude of the inlet velocity.

The parameters for the optimization problem are defined with $K = 1$, maximum fluid volume $V = 0.7$, transition width $w = 0.2$, and the time step for updating the level set function is set so that $\Delta\varsigma = 0.5$. In addition, the Prandtl number $Pr = 6.7$ (the standard value for water), and the initial level set function is set so that $\phi = 1$, which means that the initial configuration

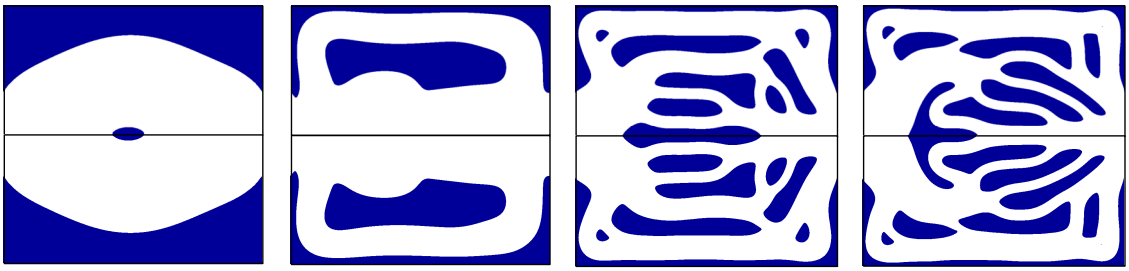

(a) $\theta = 1$ (b) $\theta = 100$ (c) $\theta = 300$ (d) $\theta = 500$

Fig. 2.7 θ dependency in heat exchange maximization problem (blue, solid domain; white, fluid domain). Reynolds numbers, Re, for each optimal configuration are (a) 1, (b) 70, (c) 170, and (d) 280.

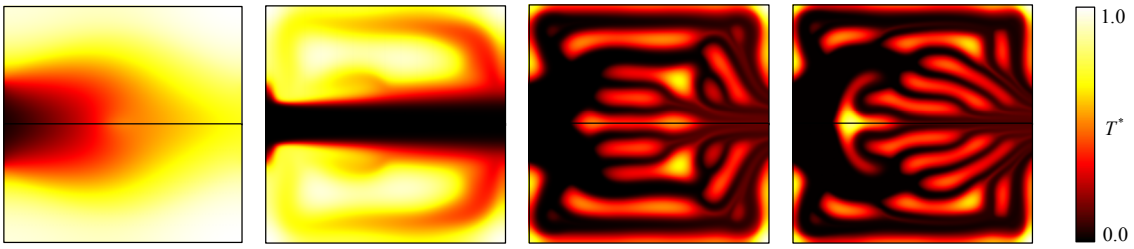

(a) $\theta = 1$ (b) $\theta = 100$ (c) $\theta = 300$ (d) $\theta = 500$

Fig. 2.8 Temperature distribution ($T^* = T/T_{\max}$ is the regularized temperature, where $T_{\max}$ is the maximum temperature in each optimal configuration, (a) $T_{\max} = 0.97$; (b) $T_{\max} = 0.61$; (c) $T_{\max} = 0.21$; (d) $T_{\max} = 0.16$).

Table 2.1 Value of objective functional with respect to each θ

θ	1	100	300	500
Objective	2.4	7.3	14.1	14.4

is filled with fluid. In this study, it is assumed that the heat generation coefficient $\bar{\beta}$ and the Nusselt number have a comparable order of magnitude, due to their definitional similarity. Since the Nusselt number of water is estimated to range from $1 \sim 10$ in internal channel flow problems, the heat generation coefficient is set to $\bar{\beta} = 10$ as an appropriate parameter value in all the numerical examples. In previous research [75], various optimal configurations obtained with values of $\bar{\beta} = 10 \sim 100$ were compared, and it was revealed that the structural complexity of the optimal configurations increased as $\bar{\beta}$ was increased. However, Note that

the dimensionless coefficient of heat generation cannot be set quantitatively to represent an actual thermal fluid.

The fixed design domain D is discretized using a structured mesh of unit length 1.6×10^{-3}, with quadrilateral quadratic elements for $\boldsymbol{u}$ and $\tilde{\boldsymbol{u}}$, and quadrilateral linear elements for p, $\tilde{p}$, T, $\tilde{T}$, and ϕ.

Dependency of optimal configurations on parameter θ

First, the dependency of the optimal configurations with respect to different value of θ is demonstrated. The physical meaning of using identical values of θ is equivalent to using identical settings for the dimensional pressure difference $\Delta\bar{p}$. Thus, Note that the increase of θ means the increase of pressure difference between inlet and outlet for transporting fluid flow in flow channels. For all numerical examples, the regularization parameter is set so that $\tau = 2.0\times10^{-4}$.

The obtained optimal configurations and corresponding temperature distributions are respectively shown in Figs. 2.7 and 2.8. In addition, the Reynolds numbers, Re, in each optimal configuration were (a) 1, (b) 70, (c) 170, and (d) 280, respectively. As shown in Fig. 2.7, the optimal configurations reveal an increasing number of thin and branched flow channels as the value of θ is increased. Here, since a symmetrical boundary condition cannot be imposed in the asymmetrical flow regimes that are often observed in high Reynolds number flows, we must verify whether or not transient phenomena appear in the high θ case examined here ($\theta = 500$), when the symmetrical boundary condition is not imposed. Figure 2.9 shows the calculation results for transient flow with respect to non-dimensional time $t = 0$ to $t = 30$ for the optimal configuration shown in Fig. 2.7(d), and the velocity distributions based on velocity magnitude $|\boldsymbol{u}|$ are shown at various time steps. Since transient phenomena do not appear, the use of a symmetrical boundary condition and the assumption of a steady-state condition are valid in the proposed method.

The temperature distributions shown Fig. 2.8 illustrate the effect of the different θ in these cases. It can be confirmed that in the low θ cases, Fig. 2.8(a) and (b), the fluid temperature is higher toward the upper and lower wall boundaries, while for the high θ cases, Fig. 2.8(c) and (d), the temperature gradient is minimal because the maximum temperature $T_{\max}$ is small. Thus, it appears that the cooling performance is best in the high θ cases, since the minimal temperature distributions in the optimal configurations indicate a high degree of cooling performance as the fluid flows through the channel.

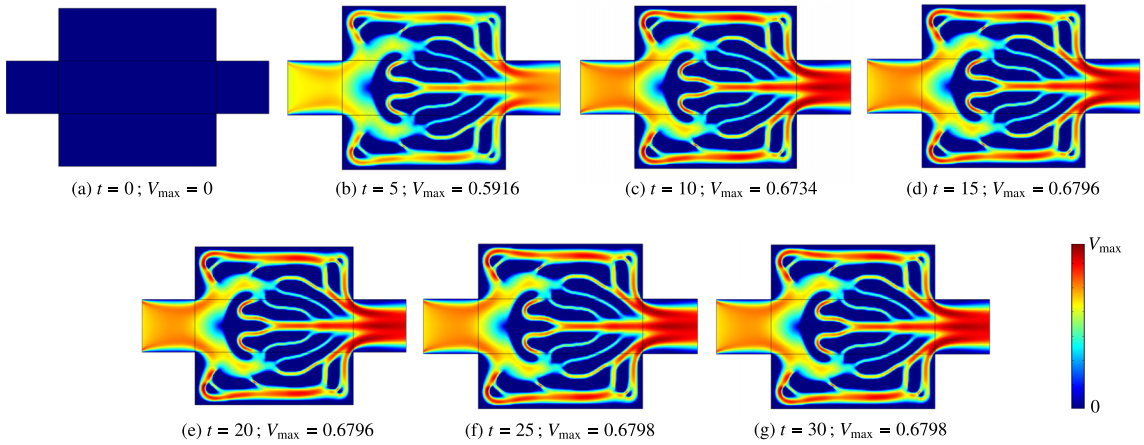

Fig. 2.9 Results of transient flow field calculations to verify that a symmetrical boundary condition and the assumption of a steady-state flow condition are appropriate. The velocity distributions in the optimal configuration for $\theta = 500$ are shown at each time step. $V_{\max}$ represents the maximum value of velocity magnitude $|\boldsymbol{u}|$.

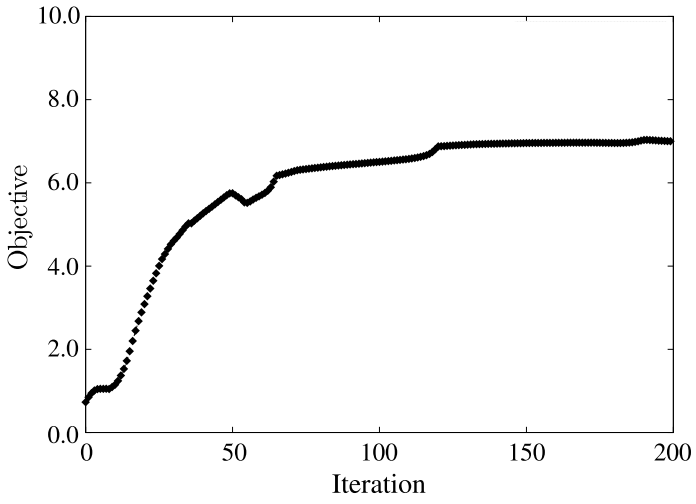

Fig. 2.10 Convergence history for objective functional I when setting $\theta = 100$ in the heat exchange maximization problem.

Figure 2.10 shows the convergence history of the value of the objective functional when $\theta = 100$. Since the value of the objective functional is converged so that volume constraint is satisfied, it can be confirmed that a valid optimal configuration is obtained. In addition, as shown in Table 4.1, the final value of objective functional I in Eq. (2.65) initially increases with increasing θ, but for high θ, e.g., $\theta = 300$, or 500, the values of the objective functional are almost the same. Note that, for this optimum design problem, $\theta = 300$ is sufficient, and

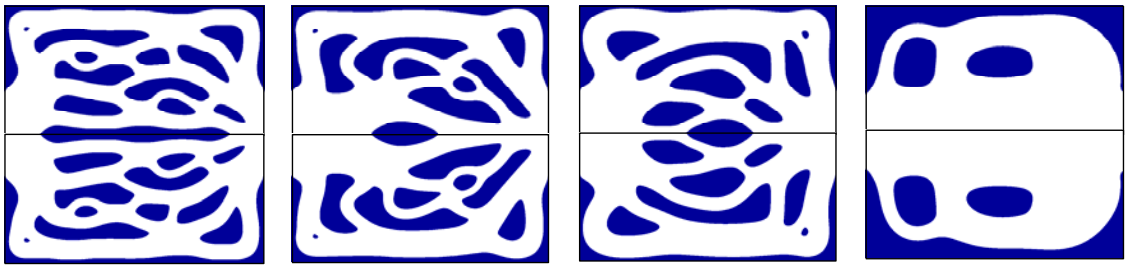

Fig. 2.11 Regularization parameter dependency in heat exchange maximization problem (blue, solid domain; white, fluid domain). Reynolds numbers, Re, for each optimal configuration are (a) 210, (b) 270, (c) 280, and (d) 800.

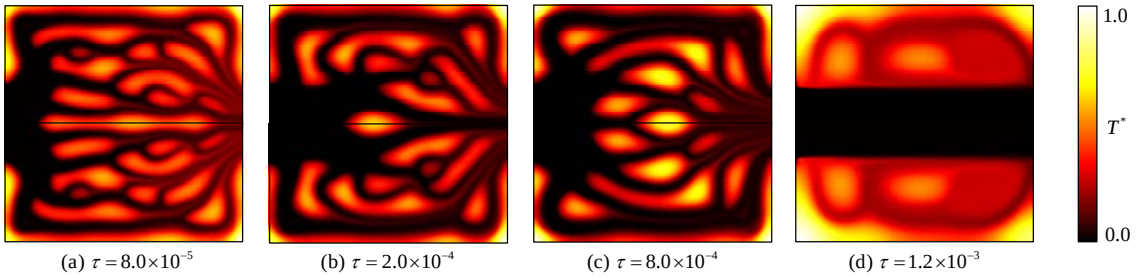

Fig. 2.12 Temperature distribution ($T^* = T/T_{\max}$ is the regularized temperature, where $T_{\max}$ is the maximum temperature in each optimal configuration, (a) $T_{\max} = 0.16$; (b) $T_{\max} = 0.19$; (c) $T_{\max} = 0.19$; (d) $T_{\max} = 0.62$).

Table 2.2 Value of objective functional with respect to each regularization parameter

τ ($\times10^{-4}$)	12.0	8.0	2.0	0.8
Objective	8.6	13.7	14.3	14.9

that higher θ, which means higher pressure difference, do not provide better results from an engineering standpoint.

Dependency of optimal configuration geometric complexity on regularization parameter settings

Next, it is explored that how different settings of the regularization parameter τ affect the geometrical complexity of obtained optimal configurations. As noted previously, the geometric complexity of optimized structures can be adjusted by setting different values of parameter τ. To confirm this behavior, the same fixed parameter values as for the previous case is used, is

set $\theta = 400$ that has qualitatively meaning of identical pressure difference condition, and is set different values of τ for four cases. The optimal configurations are shown in Fig. 2.11 and the corresponding thermal distributions are shown in Fig.2.12. In addition, the Reynolds numbers, Re, in each optimal configuration were (a) 210, (b) 270, (c) 280, and (d) 800, respectively.

The results shown in Fig. 2.11 allow us to confirm that optimal configurations with radically different geometric complexities can be obtained, depending on the set value of τ, and that increasingly complex structures are obtained as τ is set to smaller values. These radically different configurations are obtained despite the use of identical θ and pressure difference. This is because the parameter θ, which is based on the characteristic velocity U defined in Eq. (2.68), is used. Since the inlet velocity is not prescribed, this velocity qualitatively depends on the geometric complexity of the channel configuration. For the optimal configurations shown in Fig. 2.11, the mean values of the magnitude of the inlet velocity were respectively obtained as (a) 0.528, (b) 0.675, (c) 0.689, and (d) 1.992.

The objective functional values for these cases are listed in Table 5.2 and, based on cooling performance, the highest-performing configuration is that shown in Fig. 2.11(a). The data indicate that parameter τ should be set to as small a value as possible in order to derive a high-performance configuration, but the configuration shown in Fig. 2.11(a) would be difficult to fabricate. The optimal configurations shown in Fig. 2.11(b) or (c) would be better choices from an engineering standpoint, since the structures are less complex and the performances are not significantly degraded.

2.7 Summary

This chapter presented general formulations of topology optimization and its basic procedures to obtain the optimal result. As popular approaches in the filed of topology optimization, the basic ideas of the density approach and the level set-based approach were briefly explained. The typical optimization methods for updating design variables were introduced, and the strategies for getting design sensitivities were discussed. In addition, the standard methodology of topology optimization for fluid flow problems, where the objective functional is defined as the total potential energy, was introduced. As an application of the fluid flow topology optimization method, a level set-based topology optimization method for thermal-fluid

flow problems was proposed. In this method, the maximization of heat exchange efficiency was aimed for the design of cooling device such as heat sink.

Chapter 3

Topology optimization using the lattice Boltzmann method

3.1 Introduction

In structural optimization methods for fluid dynamics problems, reduction of flow field computational cost is a major factor when seeking to maintain practical total optimization times, since most numerical schemes for obtaining solutions to Navier-Stokes equations (NSE) for incompressible fluids include an iterative computation of a massive system of linear equations, which is related to the integration of the Poisson equation for the pressure field. That is, structural optimization methods for large-scale flow problems typically incur great computational cost to obtain optimal configurations. Similarly, since most previous research on structural optimization methods for fluid dynamics problems employ the finite element method (FEM) to obtain solutions of the incompressible NSE, the scale of feasible computational space has been very limited. Consequently, most numerical examples in previous research deal with two-dimensional cases, and those that do address three-dimensional cases have a relatively small number of finite elements, such as the 47,151 elements used for the design of a flow channel in Aage et al. [1]. To deal with large-scale flow problems in structural optimization problems, these computational obstacles must be overcome.

On the other hand, the lattice Boltzmann method (LBM) [76, 44, 43, 12, 20, 110, 2] has attracted attention as an alternative and promising numerical scheme for obtaining solutions to the NSE for incompressible fluids, without dealing with the Poisson equation

for the pressure field. In the LBM, the velocity distribution functions and a set of discrete fictitious particle velocities are explicitly computed, using the so-called lattice Boltzmann equation (LBE) that tracks the time evolution of the velocity distribution functions. The macroscopic variables such as the velocity and pressure are obtained by the moments of the velocity distribution functions, and satisfy the fluid dynamics conservation laws for mass, momentum, and energy. Considerable research has dealt with the construction of a mathematical theory that incorporates the above laws, such as the Chapman-Enskog expansion [20], the S-expansion of asymptotic theory [52, 50], and others [42, 55]. Because the LBM guarantees the conservation of mass, momentum, and energy, it can be applied to multiphase flows [101, 48, 131, 47] and the interface can be represented clearly, without any special treatments. Thus, with the LBM, the interface does not have to be explicitly tracked during the numerical computation. In addition, taking advantage of the fact that the algorithm is simple, computationally efficient, as well as highly scalable for parallel processing, many researchers have investigated complex and large-scale flows such as porous flows [111, 108, 40, 130] and turbulent flows [16, 45, 19, 67, 22], and an immersed boundary method based on the LBM [33, 102, 112, 113] has recently attracted attention in moving body problems.

The LBM is therefore extremely useful when working with complex and large-scale flow problems and can be successfully applied to structural optimization problems. In a pioneering study by Pingen et al. [90], a topology optimization methodology using the LBM was proposed and optimal configurations similar to those of a previous approach [14] proposed by Borrvall and Petersson using the FEM were obtained. Based on this pioneering study using the LBM, Pingen et al. [94] and Kreissl et al. [66] proposed a level-set based structural optimization method using the LBM for a flow channel design problem. Pingen and Maute [93] dealt with non-Newtonian flows to represent the viscosity of blood in their design model of a flow channel. Kreissl et al. [65] proposed a topology optimization method for a fluid-structure interaction problem for micro-channel devices. In addition, Makhija et al. [74] proposed a topology optimization method using the LBM for a mixture efficiency maximization problem under multi-component flow.

However, in the above-mentioned methodologies that employ the LBM, the design sensitivities cannot be treated precisely, since the LBE, which can be said to be an approximated equation, is used for the formulations of the optimization problems and the derivation of their adjoint equation. Furthermore, a large-scale asymmetric matrix must be dealt with

to obtain the design sensitivities in each iteration of the optimization process [91]. Thus, time-consuming numerical operations are required, and the advantages of the LBM, such as its algorithmic simplicity and computational efficiency, cannot be applied to the process of solving the adjoint equation.

To solve identification problems with the LBM, Tekitek et al. [117] proposed a methodology using the adjoint lattice Boltzmann equation (ALBE), and Krause et al. [62, 63] recently proposed the so-called adjoint lattice Boltzmann method (ALBM). The basic idea of these approaches is that both the state and adjoint fields are solved using the LBM, which can make use of highly efficient algorithms due to the similarity of the locality properties, and the design sensitivities can therefore be obtained without the use of matrix operations. Due to the different ways in which the adjoint sensitivity analysis is conducted, these approaches can be classified in two categories: 1) methods based on a discrete adjoint approach using the ALBE, in which the sensitivity analysis is conducted using discrete equations and the adjoint equation is therefore derived as a discrete equation, the so-called ALBE, and 2) the ALBM, which is based on a continuous adjoint approach in which the sensitivity analysis is conducted using the continuous Boltzmann equation with the Bhatnagar-Gross-Krook (BGK) approximation [13]. In the latter approach, the adjoint equation is therefore obtained as a continuous equation, whose formulation is similar to that of the Boltzmann equation, which is then discretized using the LBM. Krause et al. [62, 63] investigated the parallel performance of the ALBM and demonstrated that the ALBM is exceptionally useful for obtaining efficient parallel implementations, when compared with already well-established schemes.

In the research field of topology optimization, Liu et al. [69] recently applied the ALBE in a topology optimization method for a minimum power dissipation problem. Concerning an additional unique approach based on the LBM, Yonekura and Kanno [127] recently proposed a topology optimization method for a minimum power dissipation problem in which two computational steps, the gradient optimization algorithm and the lattice Boltzmann equation, are synchronized so that an optimal configuration is rapidly obtained.

In the ALBM [62, 63], the use of the continuous Boltzmann equation prevents the use of the high accuracy boundary conditions that are generally used in the LBM, since the LBM boundary conditions are formulated using discrete particle velocities. Liu et al. [69] recently asserted that most of the boundary conditions for the ALBE had to be defined *a posteriori*, due to the use of a discrete adjoint approach.

Although no-slip or periodic boundary conditions naturally influence the adjoint boundary conditions, their formulation is the same as those of the equations of the state problem, whereas other boundary conditions that are commonly used in fluid flow analysis, such as prescribed velocity or pressure boundary conditions (e.g., [136]), obviously require different formulations than those of the adjoint boundary conditions, due to the complex definition of these boundary conditions. Since various boundary conditions for the LBM [51, 72, 77] are provided, enabling analysis of diverse fluid flow problems, previous optimization methods employing the LBM must be expanded so that any desired boundary condition of the LBM can be treated in the optimization problem. In other words, the adjoint boundary conditions should be theoretically derived under the framework of sensitivity analysis based on the adjoint variable method.

To overcome the problem of how to incorporate the LBM boundary conditions in optimization problems, we propose a new sensitivity analysis based on the ALBM, in which we use the discrete velocity Boltzmann equation with the BGK approximation. Since the discrete velocity Boltzmann equation incorporates discrete particle velocities but continuous space and time, the various boundary conditions for the LBM can be easily introduced, and the adjoint equation can be analytically derived and discretized based on the strategy used in the ALBM [62, 63].

In this Chapter, we apply the proposed methodology to isothermal-fluid flow optimization problems in which prescribed flow velocity, and pressure are treated as representative boundary conditions in the LBM. Details of the sensitivity analysis dealing with these boundary conditions are provided to confirm the applicability of the proposed sensitivity analysis. Based on our new formulations, we construct a topology optimization method for the design of a flow channel in which the flow resistance minimization problem is formulated. In the following sections, the basic concept of the LBM is discussed first. Next, the topology optimization problem is formulated for the flow resistance minimization problem, and the procedures used in the sensitivity analysis based on the discrete velocity Boltzmann equation are described in detail. The numerical implementations and optimization algorithms are then explained and, finally, we introduce several numerical examples to confirm the utility of the proposed method.

3.2 Lattice Boltzmann method

3.2.1 Basic equation

We now discuss the concept of the LBM that will be applied here to an incompressible viscous fluid while considering the temperature field. The basic idea of the LBM is that the fluid regime is represented as an aggregation of fictitious particles, which makes it possible to obtain macroscopic variables such as the fluid velocity, pressure, and temperature, from the moments of the velocity distribution functions that express the distribution state of the particles. The concept of the LBM was originally constructed as a kinetic theory in which the distribution function is governed by the Boltzmann equation, and the LBM is a strategy for discretizing the Boltzmann equation in order to conduct a numerical simulation of macroscopic flow regimes. In kinetic theory, the velocity distribution function $f = f(\boldsymbol{x}, t, \boldsymbol{\xi})$, in which $\boldsymbol{x}$, t, and $\boldsymbol{\xi}$ represent the position, time, and particle velocity, respectively, is governed by the following Boltzmann equation,

$$\frac{\partial f}{\partial t} + \boldsymbol{\xi} \cdot \nabla f = Q(f), \tag{3.1}$$

where Q is a collision operator that expresses the effect of collisions among the fictitious particles. For simplicity, and without losing generality, we use the Bhatnagar-Gross-Krook (BGK) collision model [13], as follows:

$$Q(f) = -\frac{1}{\tau_c}(f - f^{\mathrm{eq}}), \tag{3.2}$$

where τ_c is the relaxation time that expresses the average time until the next collision, and f^{eq} is a Maxwell distribution as a local equilibrium solution of the Boltzmann equation, as follows:

$$f^{\mathrm{eq}} = \frac{\rho}{(2\pi RT)^{d/2}} \exp\left(-\frac{|\boldsymbol{\xi} - \boldsymbol{u}|^2}{2RT}\right), \tag{3.3}$$

where d, R, ρ, $\boldsymbol{u}$, and T represent the spacial dimension, gas constant, density, velocity, and temperature, respectively.

In the LBM, we consider a modeled fluid, which is composed of identical particles whose velocities are restricted to a finite set of q vectors, $\boldsymbol{c}_1, \boldsymbol{c}_2, \ldots, \boldsymbol{c}_q$, whereas the continuous particle velocity is used in the original Boltzmann equation. In the following, we briefly introduce the basic equations in the LBM, and use the non-dimensional variables defined in

Appendix A. If we use the BGK approximation [13] for collision terms, the behavior of the particles is described by the following discrete velocity Boltzmann equations:

$$Sh\frac{\partial f_i}{\partial t} + \boldsymbol{c}_i \cdot \nabla f_i = -\frac{1}{\varepsilon_f}(f_i - f_i^{\mathrm{eq}}), \tag{3.4}$$

where f_i is the velocity distribution function, f_i^{eq} is the local equilibrium distribution function given later, ε_f is a dimensionless parameter of the same order as the Knudsen number, and $Sh = U/c$ is the Strouhal number of $O(\varepsilon_f)$. Note that $1/\varepsilon_f$ in Eq. (3.4) corresponds to the frequency of the collision between the particles. Also, it should be noted that the Strouhal number appears in Eq. (3.4) because we have two scales for a characteristic speed: one is a particle speed c which is of the order of sound speed, and the other is a flow speed U which is of $O(1)$.

In the two-dimensional case, we employ the nine-velocity (D2Q9) model, which has the following velocity vectors:

$$\begin{aligned}&[\boldsymbol{c}_1, \boldsymbol{c}_2, \boldsymbol{c}_3, \boldsymbol{c}_4, \boldsymbol{c}_5, \boldsymbol{c}_6, \boldsymbol{c}_7, \boldsymbol{c}_8, \boldsymbol{c}_9] \\ &= \begin{bmatrix} 0 & 1 & 0 & -1 & 0 & 1 & -1 & -1 & 1 \\ 0 & 0 & 1 & 0 & -1 & 1 & 1 & -1 & -1 \end{bmatrix}.\end{aligned} \tag{3.5}$$

In the three-dimensional case, we employ the fifteen-velocity (D3Q15) model, which has the following velocity vectors:

$$\begin{aligned}&[\boldsymbol{c}_1, \boldsymbol{c}_2, \boldsymbol{c}_3, \boldsymbol{c}_4, \boldsymbol{c}_5, \boldsymbol{c}_6, \boldsymbol{c}_7, \boldsymbol{c}_8, \boldsymbol{c}_9, \boldsymbol{c}_{10}, \boldsymbol{c}_{11}, \boldsymbol{c}_{12}, \boldsymbol{c}_{13}, \boldsymbol{c}_{14}, \boldsymbol{c}_{15}] \\ &= \begin{bmatrix} 0 & 1 & 0 & -1 & 0 & 0 & 0 & 1 & -1 & -1 & 1 & 1 & -1 & -1 & 1 \\ 0 & 0 & 1 & 0 & -1 & 0 & 0 & 1 & 1 & -1 & -1 & 1 & 1 & -1 & -1 \\ 0 & 0 & 0 & 0 & 0 & 1 & -1 & 1 & 1 & 1 & 1 & -1 & -1 & -1 & -1 \end{bmatrix}.\end{aligned} \tag{3.6}$$

These velocity models are shown in Fig.3.1.

To formulate the LBE, the discrete velocity Boltzmann equation is discretized with respect to a position $\boldsymbol{x}$ and time t using a lattice spacing Δx and a time step Δt. Performing the same discretization as in [50], we obtain the following LBE for fluid flows:

$$f_i(\boldsymbol{x} + \boldsymbol{c}_i \Delta x, t + \Delta t) = f_i(\boldsymbol{x}, t) - \frac{1}{\tau_f}\{f_i(\boldsymbol{x}, t) - f_i^{\mathrm{eq}}(\boldsymbol{x}, t)\}, \tag{3.7}$$

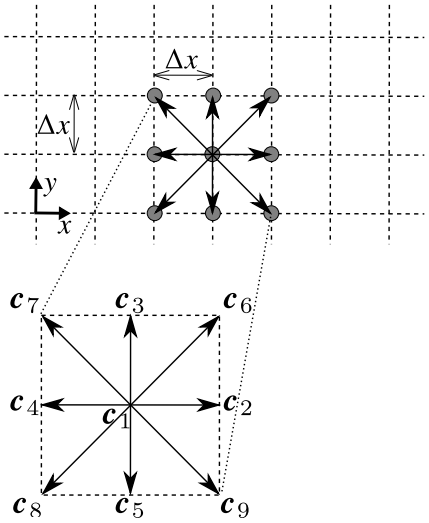

(a) D2Q9 model

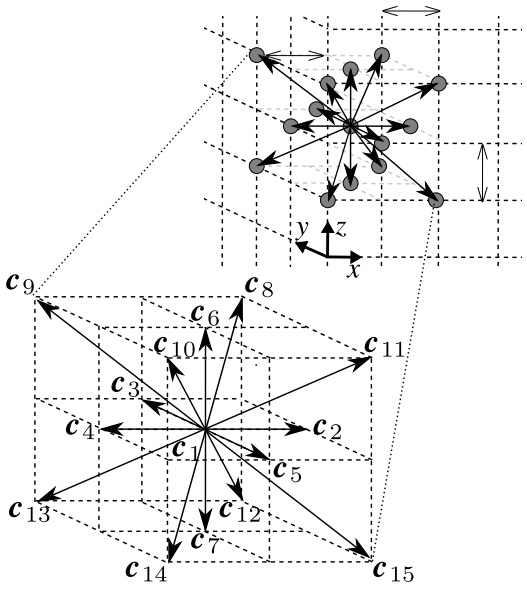

(b) D3Q15 model

Fig. 3.1 Particle velocity vectors $\boldsymbol{c}_i$ of (a) D2Q9 model and (b) D3Q15 model.

where $\tau_f = \varepsilon_f/\Delta x$ is the dimensionless relaxation time and of $O(1)$, which is related to the viscosity of the fluid given below. Note that the time step Δt is chosen so that the particles exactly travel the lattice spacing.

The discrete equilibrium distribution function f_i^{eq} is given by

$$f_i^{\mathrm{eq}} = E_i \rho \left\{ 1 + 3\boldsymbol{c}_i \cdot \boldsymbol{u} + \frac{9}{2}(\boldsymbol{c}_i \cdot \boldsymbol{u})^2 - \frac{3}{2}|\boldsymbol{u}|^2 \right\}. \tag{3.8}$$

For the D2Q9 model, the weight E_i is defined so that $E_1 = 4/9$, $E_2 = E_3 = E_4 = E_5 = 1/9$, $E_6 = E_7 = E_8 = E_9 = 1/36$, and for the D3Q15 model, the weight E_i is defined so that $E_1 = 2/9$, $E_2 = E_3 = \cdots = E_7 = 1/9$, $E_8 = E_9 = \cdots = E_{15} = 1/72$. The density ρ, and the fluid velocity $\boldsymbol{u}$ are obtained from the following moments of the velocity distribution functions:

$$\rho = \sum_{i=1}^{q} f_i, \tag{3.9}$$

$$\boldsymbol{u} = \frac{1}{\rho} \sum_{i=1}^{q} \boldsymbol{c}_i f_i. \tag{3.10}$$

In using the D2Q9 or D3Q15 models, the pressure p is represented as follows:

$$p = \frac{\rho}{3}. \tag{3.11}$$

Applying the asymptotic theory [107] to Eq. (3.7), Inamuro et al. [52] verified that the macroscopic variables in Eqs. (3.9)–(3.11) satisfy the following macroscopic equations, with relative errors of $O[(\Delta x)^2]$,

$$\nabla \cdot \boldsymbol{u} = 0, \tag{3.12}$$

$$Sh \frac{\partial \boldsymbol{u}}{\partial t} + (\boldsymbol{u} \cdot \nabla)\boldsymbol{u} = -\nabla p + \nu \nabla^2 \boldsymbol{u}, \tag{3.13}$$

which represent the continuity equation (3.12), and the NSE (3.13), respectively. The kinematic viscosity ν is given by

$$\nu = \frac{1}{3}\left(\tau_f - \frac{1}{2}\right)\Delta x. \tag{3.14}$$

When an external body force $\boldsymbol{F}(\boldsymbol{x}, t)$ is applied, the evolution equation in Eq. (3.7) can be computed in a stepwise fashion as follows:

Step 1. f_i is evolved without the body force, by the following equations:

$$f_i^*(\boldsymbol{x} + \boldsymbol{c}_i \Delta x, t + \Delta t) = f_i(\boldsymbol{x}, t) - \frac{1}{\tau_f}\{f_i(\boldsymbol{x}, t) - f_i^{\mathrm{eq}}(\boldsymbol{x}, t)\}, \tag{3.15}$$

Step 2. f_i is corrected as follows:

$$f_i(\boldsymbol{x}, t + \Delta t) = f_i^*(\boldsymbol{x}, t + \Delta t) + 3\Delta x \boldsymbol{E}_i \boldsymbol{c}_i \cdot \boldsymbol{F}(\boldsymbol{x}, t + \Delta t). \tag{3.16}$$

3.2.2 Initial and boundary conditions

Since problems formulated with the LBM include initial and boundary conditions, values for these conditions must be provided, to enable computation of the time evolution of the velocity distribution function. In this study, it is assumed that the initial values of the particle distribution functions are those of the equilibrium distribution functions, given initial values of $\rho(\boldsymbol{x}, 0)$, and $\boldsymbol{u}(\boldsymbol{x}, 0)$, as follows:

$$f_i(\boldsymbol{x}, 0) = f_i^{\mathrm{eq}}(\rho(\boldsymbol{x}, 0), \boldsymbol{u}(\boldsymbol{x}, 0)), \tag{3.17}$$

where the initial values of the macroscopic variables are set so that $\rho(\boldsymbol{x}, 0) = 1$, and $\boldsymbol{u}(\boldsymbol{x}, 0) = 0$ in this thesis.

On the other hand, the boundary conditions applied in the LBM are generally more complex than those in a conventional numerical scheme based on the NSE. Due to the characteristics of the particle propagations formulated in the lattice Boltzmann equations, the boundary values of the velocity distribution functions that satisfy $\boldsymbol{n} \cdot \boldsymbol{c}_i < 0$ (where $\boldsymbol{n}$ is the outward normal vector) are unknown, and must be specified so that boundary conditions for the macroscopic flow, such as no-slip, or prescribed velocity or pressure boundary conditions, are adequately represented.

For instance, in Fig. 3.1(a), if the x-y plane is defined so that $\boldsymbol{c}_1 = (0, 0)^{\mathrm{T}}$ is the origin of the coordinate axis and the fluid domain is defined such that $y > 0$, the velocity distribution functions f_3, f_6 and f_7 must be specified based on known values of f_1, f_2, f_4, f_5, f_8, and f_9. A no-slip boundary condition, which implies that $\boldsymbol{u} = \boldsymbol{0}$ on wall boundary Γ_{W}, can be

represented using the following simple exchange of the unknown f_i to the known f_i:

$$\left.\begin{aligned} f_3 &= f_5 \\ f_6 &= f_8 \\ f_7 &= f_9 \end{aligned}\right\} \text{ on } \Gamma_{\mathrm{W}}. \tag{3.18}$$

This is the so-called bounce back boundary condition [110], which is easy to implement in the LBM code and is often used to impose a no-slip boundary condition.

To treat the prescribed velocity boundary condition, Zhou and He [136] proposed the following boundary conditions:

$$\left.\begin{aligned} f_3 &= f_5 + \tfrac{2}{3}\rho v_0 \\ f_6 &= f_8 + \tfrac{1}{6}\rho v_0 - \tfrac{1}{2}(f_2 - f_4) \\ f_7 &= f_9 + \tfrac{1}{6}\rho v_0 + \tfrac{1}{2}(f_2 - f_4) \end{aligned}\right\} \text{ on } \Gamma_{\mathrm{V}}, \text{ and } \rho = \frac{f_1 + f_2 + f_4 + 2(f_5 + f_8 + f_9)}{1 - v_0}, \tag{3.19}$$

where v_0 represents the prescribed velocity in the y-direction on boundary Γ_{V}. Similarly, a prescribed density boundary condition, based on the pressure boundary condition arising from the relationship expressed in Eq. (4.9), can be introduced by using the following equations:

$$\left.\begin{aligned} f_3 &= f_5 + \tfrac{2}{3}\rho_0 v \\ f_6 &= f_8 + \tfrac{1}{6}\rho_0 v - \tfrac{1}{2}(f_2 - f_4) \\ f_7 &= f_9 + \tfrac{1}{6}\rho_0 v + \tfrac{1}{2}(f_2 - f_4) \end{aligned}\right\} \text{ on } \Gamma_{\mathrm{P}}, \text{ and } v = 1 - \frac{f_1 + f_2 + f_4 + 2(f_5 + f_8 + f_9)}{\rho_0}, \tag{3.20}$$

where ρ_0 represents the prescribed density on boundary Γ_{P}. Similarly, each boundary condition can be applied to three-dimensional cases [136].

3.3 Formulation of a topology optimization problem

Here, we formulate the flow resistance minimization problem for the design of a flow channel that can efficiently transport fluid between an inlet and an outlet in an internal flow system. A schematic diagram of this problem is shown in Fig. 2.4, where the completely fluid domain Ω is defined such that $\gamma = 1$ in the design variable, and the completely solid domain $D \setminus \Omega$ is defined as $\gamma = 0$. The inlet boundary condition is set to the prescribed velocity, i.e., $\boldsymbol{u} = \boldsymbol{u}_{\mathrm{in}}$ at Γ_{V}, and the outlet boundary condition is set to the prescribed pressure, i.e., $p = p_{\mathrm{out}}$ at

Γ_{P}. Here, to represent both fluid and solid domains, we employ the typical way proposed by Borravall and Petersson [14], in which the fixed design domain is defined as a porous medium, based on Darcy's law. Thus, we introduce the body force $\boldsymbol{F}$, as follows:

$$\boldsymbol{F} = -\alpha_\gamma \boldsymbol{u}, \tag{3.21}$$

where α_γ is defined as

$$\alpha_\gamma = \alpha_{\max} + (\alpha_{\min} - \alpha_{\max})\frac{\gamma(1+q)}{\gamma+q}, \tag{3.22}$$

where q is a tuning parameter to control the convexity of α_γ, and we set this parameter to $q = 0.1$. Since the material distribution of fluid and solid domains is represented using the porous model, α_γ is the so-called inverse permeability, as defined in Eq. (3.22). $\gamma = 0$ corresponds to a solid domain $D \setminus \Omega$ that is represented as having zero permeability, i.e., $\alpha_{\max} \to \infty$, and $\gamma = 1$ corresponds to a fluid domain Ω that is represented as having infinite permeability, i.e., $\alpha_{\min} = 0$. We note that a sufficiently large value must be chosen as $\alpha_{\max}$ in the numerical computation, to model the no-slip boundary condition in the fixed design domain D.

Based on the above formulation, the fluid flow in D is governed by the following problem concerning the initial and boundary values:

$$\left\{\begin{array}{l} \left.\begin{array}{l} \nabla\cdot\boldsymbol{u} = 0 \\ Sh\frac{\partial \boldsymbol{u}}{\partial t} + (\boldsymbol{u}\cdot\nabla)\boldsymbol{u} = -\nabla p + \nu\nabla^2\boldsymbol{u} - \alpha_\gamma\boldsymbol{u} \end{array}\right\} \text{Governing equations in } D \\ \left.\begin{array}{ll} \boldsymbol{u} = \boldsymbol{0} & \text{on } \Gamma_{\mathrm{W}} \\ \boldsymbol{u} = \boldsymbol{u}_{\mathrm{in}} & \text{on } \Gamma_{\mathrm{V}} \\ p = p_{\mathrm{out}} & \text{on } \Gamma_{\mathrm{P}} \end{array}\right\} \text{Boundary conditions} \quad \left.\begin{array}{l} \boldsymbol{u}(\boldsymbol{x},0) = \boldsymbol{u}^{\mathrm{ini}}(\boldsymbol{x}) \\ p(\boldsymbol{x},0) = p^{\mathrm{ini}}(\boldsymbol{x}) \end{array}\right\} \text{Initial conditions,} \end{array}\right. \tag{3.23}$$

where $\boldsymbol{u}^{\mathrm{ini}}(\boldsymbol{x})$ and $p^{\mathrm{ini}}(\boldsymbol{x})$ represent the initial values of the fluid velocity and pressure, respectively.

As a result, the flow resistance minimization problem can be formulated as follows:

$$\begin{cases} \inf\limits_{\gamma} & J_1 = \int_I \int_{\Gamma_V} p \, \mathrm{d}\Gamma \mathrm{d}t - \int_I \int_{\Gamma_P} p \, \mathrm{d}\Gamma \mathrm{d}t \\ \text{s.t.} & V = \int_D \gamma \, \mathrm{d}\Omega - V_{\max} \int_D \mathrm{d}\Omega \leqslant 0 \\ & \boldsymbol{u} \text{ and } p \text{ satisfy the initial-boundary value problem in Eq. (3.23),} \end{cases} \tag{3.24}$$

where J_1 represents the objective functional corresponding to the pressure difference between the inlet and the outlet, and V represents the volume constraint, where $V_{\max}$ is the volume ratio of fluid with respect to the volume of D. $I := [0, t_f]$ represents the observation time interval of the fluid flow, with the final time t_f that can be given as an arbitrary value. We note that the fluid velocity and pressure are calculated using the LBM in our study. That is, the initial-boundary value problem in Eq. (3.23) is solved using the LBM, whereas the FEM is typically used in previous studies dealing with the flow resistance minimization problem. We also note that the above optimization problem is formulated as a time-dependent problem, whereas in most previous studies, a steady-state condition is considered. This is because the LBM is used for computing the time-dependent fluid flow, so it is appropriate to formulate the optimization problem as a time-dependent problem. It should be noted that the above formulation can be used for solving not only time-dependent optimization problems, but also steady-state problems under sufficiently low Reynolds number conditions.

3.4 Sensitivity analysis based on the adjoint method

Based on the ALBM [62, 63], we now consider the strategy for deriving the design sensitivities for the optimization problems discussed in Section 3.3. The ALBM is based on the use of the LBM to compute the fluid flow in fluid optimization problems, and its key idea is that design sensitivities are derived using the adjoint variable method in which the Boltzmann equation is employed to formulate the Lagrangian. Based on the continuous adjoint approach, the adjoint equation is derived as an equation that closely resembles the Boltzmann equation, and is solved using the LBM. As a result, both the state and adjoint fields can be solved using the same efficient algorithm of the LBM, and the design sensitivities are obtained with a fully explicit calculation. The detailed formulation of the ALBM for fluid flow topology optimization problems is described in Appendix B.

Since boundary conditions when using the LBM are included in the equations for unknown velocity distribution functions, the ALBM, in which the Lagrangian is formulated using the Boltzmann equation, cannot be used because complex boundary conditions, such as the inlet and outlet boundary conditions in Eqs. (3.19) and (3.20), cannot be introduced. This means that boundary conditions for the adjoint equation, corresponding to the complex boundary conditions, cannot be imposed. Although simple inlet and outlet boundary conditions, such as $f = f^{\mathrm{eq}}$ at the inlet and outlet, can be used, these are rarely used in research dealing with the LBM due to the poor accuracy of the solutions of the NSE.

To overcome this restriction, in the method proposed here, we formulate the optimization problem using the discrete velocity Boltzmann equation in Eq. (3.4) that includes the position $\boldsymbol{x}$, time t, and discrete particle velocities $\boldsymbol{c}_i$. Since the discrete velocity Boltzmann equation is only discretized with respect to the particle velocities, the various boundary conditions required in the LBM can be easily introduced and the adjoint equation can be systematically derived and discretized based on the strategy used in the ALBM.

The design sensitivity we consider in this paper is the gradient of the objective functional, J_1, with respect to the design variable γ. the design sensitivity is defined as the Gâteaux derivative, $\langle J_1', \delta\gamma \rangle$, given by

$$\langle J_1', \delta\gamma \rangle = \frac{\mathrm{d}}{\mathrm{d}\varrho} J_1(\gamma + \varrho\delta\gamma)\bigg|_{\varrho=0}, \tag{3.25}$$

where ϱ represents a smooth function, and $\delta\gamma$ is a arbitrary function.

To clarify the difference between a conventional approach and the newly proposed method, the method proposed by Pingen et al. [90, 92] is briefly introduced for the formulation of the design sensitivities in an optimization problem using the LBE. We then discuss the approach in which the optimization problem is formulated using the discrete velocity Boltzmann equation.

3.4.1 Use of the steady-state lattice Boltzmann equation

In previous research by Pingen et al. [90, 92], the optimization problem was formulated under a steady-state flow condition. Since the standard LBM is an explicit time evolution scheme for computing time-dependent flows, the flow needs to be advanced in time until convergence to a steady-state condition is satisfied. Thus, the LBE for steady-state flow can

be represented as follows:

$$\boldsymbol{R}(\boldsymbol{f},\boldsymbol{p}) = \boldsymbol{M}(\boldsymbol{f},\boldsymbol{p}) - \boldsymbol{f} = \boldsymbol{0}, \tag{3.26}$$

where $\boldsymbol{R}$ represents the residual vector, and $\boldsymbol{f}$ and $\boldsymbol{p}$ represent the vectors of the velocity distribution functions and design variables, respectively. The operator $\boldsymbol{M}$ performs one collision and one propagation step according to the LBE in Eq. (3.7). Here, the collision and propagation steps respectively represent collision operator $\boldsymbol{C}$ and propagation operator $\boldsymbol{P}$, and we define $\boldsymbol{M} = \boldsymbol{P}(\boldsymbol{C}) : \boldsymbol{f}_t \rightarrow \boldsymbol{f}_{t+1}$, where index t represents the time step of the LBE.

Objective function $\mathscr{F} = \mathscr{F}(\boldsymbol{f},\boldsymbol{p})$ is now introduced in the optimization problem, and the design sensitivities that are the derivative of objective function $\mathscr{F}$ with respect to design variables $\boldsymbol{p}$ can be described as follows:

$$\frac{\mathrm{d}\mathscr{F}}{\mathrm{d}\boldsymbol{p}} = \frac{\partial\mathscr{F}}{\partial\boldsymbol{p}} + \frac{\partial\mathscr{F}^{\mathrm{T}}}{\partial\boldsymbol{f}}\frac{\mathrm{d}\boldsymbol{f}}{\mathrm{d}\boldsymbol{p}}, \tag{3.27}$$

where $\boldsymbol{f}$ is the velocity distribution function at the steady-state governed by the steady-state LBE in Eq. (3.26). Due to the large number of design variables, it would be computationally extravagant to compute the design sensitivities using the direct method by computing $\mathrm{d}\boldsymbol{f}/\mathrm{d}\boldsymbol{p}$ for every design variable. In this case, the gradients of $\mathscr{F}$ can be efficiently computed using the adjoint variable method.

First, we differentiate the residual $\boldsymbol{R}$ in Eq. (3.26) with respect to the design variables $\boldsymbol{p}$,

$$\frac{\partial\boldsymbol{R}}{\partial\boldsymbol{p}} + \frac{\partial\boldsymbol{R}}{\partial\boldsymbol{f}}\frac{\mathrm{d}\boldsymbol{f}}{\mathrm{d}\boldsymbol{p}} = 0. \tag{3.28}$$

Thus, the gradients of $\boldsymbol{f}$ are given by,

$$\frac{\mathrm{d}\boldsymbol{f}}{\mathrm{d}\boldsymbol{p}} = -\frac{\partial\boldsymbol{R}}{\partial\boldsymbol{f}}^{-1}\frac{\partial\boldsymbol{R}}{\partial\boldsymbol{p}}. \tag{3.29}$$

Substituting Eq. (3.29) into (3.27), the sensitivity formulation based on the adjoint variable method is obtained as follows:

$$\boldsymbol{J}^{\mathrm{T}}\boldsymbol{a} = \frac{\partial\mathscr{F}}{\partial\boldsymbol{f}}, \tag{3.30}$$

$$\frac{\mathrm{d}\mathscr{F}}{\mathrm{d}\boldsymbol{p}} = \frac{\partial\mathscr{F}}{\partial\boldsymbol{p}} - \boldsymbol{a}^{\mathrm{T}}\frac{\mathrm{d}\boldsymbol{R}}{\mathrm{d}\boldsymbol{p}}, \tag{3.31}$$

where $\boldsymbol{J} = \partial\boldsymbol{R}/\partial\boldsymbol{f}$ is the Jacobian, and $\boldsymbol{a}$ represents the adjoint variables.

Based on the above sensitivity formulations, we can obtain the design sensitivities without computing $\mathrm{d}\mathscr{F}/\mathrm{d}\boldsymbol{p}$ that incurs massive computational costs. However, in the above sensitivity formulations, the design sensitivities cannot be treated precisely, since the LBE, a so-called approximated equation, is used for the formulation of the optimization problems, and the derivation of their adjoint equation. Furthermore, even for the D2Q9 model, the Jacobian $\boldsymbol{J}$ is a sparse asymmetric square matrix of size $(N \times 9)^2$ where N is the number of lattice nodes. That is, time-consuming numerical operations are required to compute the Jacobian $\boldsymbol{J}$, and the advantages of the LBM, such as its algorithmic simplicity and computational efficiency, cannot be exploited in the adjoint equation.

3.4.2 Adjoint lattice Boltzmann method

We now discuss the sensitivity analysis for the flow resistance minimization problem. To conduct the sensitivity analysis based on the ALBM incorporating the discrete velocity Boltzmann equation, the adjoint variable, $\tilde{f}_i = \tilde{f}_i(\boldsymbol{x}, t)$, is introduced, and the expanded objective functional, $\bar{J}_1$, is defined as follows:

$$\bar{J}_1 = J_1 + R_1, \tag{3.32}$$

where R_1 is defined as

$$R_1 = \int_I \int_D \sum_{i=1}^{9} \tilde{f}_i \left\{ Sh \frac{\partial f_i}{\partial t} + \boldsymbol{c}_i \cdot \nabla f_i + \frac{1}{\varepsilon_f} \left(f_i - f_i^{\mathrm{eq}} \right) + 3\alpha_\gamma E_i \boldsymbol{c}_i \cdot \boldsymbol{u} \right\} \mathrm{d}\Omega \mathrm{d}t. \tag{3.33}$$

To introduce the initial and boundary conditions, Eq. (3.33) is rewritten as

$$\begin{aligned} R_1 = & \int_D \sum_{i=1}^{9} \left[Sh f_i \tilde{f}_i \right]_{t_0}^{t_1} \mathrm{d}\Omega + \int_I \int_\Gamma \sum_{i=1}^{9} (\boldsymbol{c}_i \cdot \boldsymbol{n}) f_i \tilde{f}_i \mathrm{d}\Gamma \mathrm{d}t \\ & + \int_I \int_D \sum_{i=1}^{9} f_i \left\{ -Sh \frac{\partial \tilde{f}_i}{\partial t} - \boldsymbol{c}_i \cdot \nabla \tilde{f}_i + \frac{1}{\varepsilon_f} \left(\tilde{f}_i - \tilde{f}_i^{\mathrm{eq}} \right) + 3\alpha_\gamma E_i \boldsymbol{c}_i \cdot \tilde{\boldsymbol{m}} \right\} \mathrm{d}\Omega \mathrm{d}t, \end{aligned} \tag{3.34}$$

where $\tilde{\boldsymbol{m}} = \sum_{i=1}^{9} \boldsymbol{E}_i \boldsymbol{c}_i \tilde{f}_i$. The Gâteaux derivative of $\bar{J}_1$ with respect to γ can be derived as

$$\begin{aligned}\langle \bar{J}_1', \delta\gamma \rangle = &\int_I \int_{\Gamma_\mathrm{V}} \sum_{i=1}^{9} \frac{1}{3} \delta f_i \mathrm{d}\Gamma \mathrm{d}t - \int_I \int_{\Gamma_\mathrm{P}} \sum_{i=1}^{9} \frac{1}{3} \delta f_i \mathrm{d}\Gamma \mathrm{d}t \\ &+ \int_D \sum_{i=1}^{9} Sh \delta f_i(t_1) \tilde{f}_i(t_1) \mathrm{d}\Omega + \int_I \int_{\Gamma} \sum_{i=1}^{9} (\boldsymbol{c}_i \cdot \boldsymbol{n}) \delta f_i^\mathrm{b} \tilde{f}_i \mathrm{d}\Gamma \mathrm{d}t \\ &+ \int_I \int_D \sum_{i=1}^{9} \delta f_i \left\{ -Sh \frac{\partial \tilde{f}_i}{\partial t} - \boldsymbol{c}_i \cdot \nabla \tilde{f}_i + \frac{1}{\varepsilon_f} \left(\tilde{f}_i - \tilde{f}_i^\mathrm{eq} \right) + 3\alpha_\gamma \boldsymbol{E}_i \boldsymbol{c}_i \cdot \tilde{\boldsymbol{m}} \right\} \mathrm{d}\Omega \mathrm{d}t \\ &+ \int_I \int_D \left(3\alpha_\gamma \boldsymbol{u} \cdot \tilde{\boldsymbol{m}} \right) \delta\gamma \mathrm{d}\Omega \mathrm{d}t, \end{aligned} \tag{3.35}$$

where $\delta f_i = (\partial f_i / \partial \gamma) \delta\gamma$, and $\tilde{f}_i^\mathrm{eq}$ is defined as

$$\tilde{f}_i^\mathrm{eq} = \tilde{\rho} + 3(\boldsymbol{c}_i - \boldsymbol{u}) \cdot \tilde{\boldsymbol{j}}, \tag{3.36}$$

where $\tilde{\rho}$, and $\tilde{\boldsymbol{j}}$ are defined as follows [120]:

$$\tilde{\rho} = \sum_{j=1}^{9} \boldsymbol{E}_j \tilde{f}_j \left(1 + 3\boldsymbol{c}_j \cdot \boldsymbol{u} + \frac{9}{2} \mathscr{H}_j^{(2)} : (\boldsymbol{u} \otimes \boldsymbol{u}) \right), \tag{3.37}$$

$$\tilde{\boldsymbol{j}} = \sum_{j=1}^{9} \boldsymbol{E}_j \tilde{f}_j \left(\boldsymbol{c}_j + 3\mathscr{H}_j^{(2)} \boldsymbol{u} \right), \tag{3.38}$$

where $\mathscr{H}_j^{(2)}$ represents the second Hermite polynomial in the discrete case, $\mathscr{H}_j^{(2)} = \boldsymbol{c}_j \otimes \boldsymbol{c}_j - 3\boldsymbol{\delta}$, with the Kronecker delta, $\boldsymbol{\delta}$. From the fifth term of the right-hand side in Eq. (3.35), the adjoint equation can be immediately derived as

$$-Sh \frac{\partial \tilde{f}_i}{\partial t} - \boldsymbol{c}_i \cdot \nabla \tilde{f}_i = -\frac{1}{\varepsilon_f} \left(\tilde{f}_i - \tilde{f}_i^\mathrm{eq} \right) - 3\alpha_\gamma \boldsymbol{E}_i \boldsymbol{c}_i \cdot \tilde{\boldsymbol{m}}. \tag{3.39}$$

In addition, the initial conditions can be obtained using the third term of the right-hand side in Eq. (3.35), as follows:

$$\tilde{f}_i(t_\mathrm{f}) = 0. \tag{3.40}$$

Next, the boundary conditions for the adjoint equation are derived using the first, second, and fourth terms in Eq. (3.35) for boundaries Γ_W, Γ_V, and Γ_P. The key point guiding the derivations of the boundary conditions is the handling of δf_i^b in the fourth term of the right-

hand side in Eq. (3.35), which represents the velocity distribution functions in the discrete particle velocity space at each boundaries, whereas the ALBM [63] deals with continuous particle velocity space. The use of discrete particle velocities enables systematic derivations of each adjoint boundary condition as shown in Appendix C, where the deriving the adjoint boundary conditions are described in detail. As a result, the adjoint boundary conditions are obtained as follows:

$$\left.\begin{aligned}\tilde{f}_5 &= \tilde{f}_3\\ \tilde{f}_8 &= \tilde{f}_6\\ \tilde{f}_9 &= \tilde{f}_7\end{aligned}\right\} \text{ on } \Gamma_{\mathrm{W}}. \tag{3.41}$$

$$\left.\begin{aligned}\tilde{f}_5 &= -\tfrac{2}{3(1-v_0)} + \tilde{f}_3 + \tfrac{v_0}{3(1-v_0)}\left(4\tilde{f}_3 + \tilde{f}_6 + \tilde{f}_7\right)\\ \tilde{f}_8 &= -\tfrac{2}{3(1-v_0)} + \tilde{f}_6 + \tfrac{v_0}{3(1-v_0)}\left(4\tilde{f}_3 + \tilde{f}_6 + \tilde{f}_7\right)\\ \tilde{f}_9 &= -\tfrac{2}{3(1-v_0)} + \tilde{f}_7 + \tfrac{v_0}{3(1-v_0)}\left(4\tilde{f}_3 + \tilde{f}_6 + \tilde{f}_7\right)\end{aligned}\right\} \text{ on } \Gamma_{\mathrm{V}}. \tag{3.42}$$

$$\left.\begin{aligned}\tilde{f}_5 &= \tilde{f}_3 - \tfrac{1}{3}\left(4\tilde{f}_3 + \tilde{f}_6 + \tilde{f}_7\right)\\ \tilde{f}_8 &= \tilde{f}_6 - \tfrac{1}{3}\left(4\tilde{f}_3 + \tilde{f}_6 + \tilde{f}_7\right)\\ \tilde{f}_9 &= \tilde{f}_7 - \tfrac{1}{3}\left(4\tilde{f}_3 + \tilde{f}_6 + \tilde{f}_7\right)\end{aligned}\right\} \text{ on } \Gamma_{\mathrm{P}}. \tag{3.43}$$

Consequently, the design sensitivity of this optimization problem is obtained from Eq. (3.35), as follows:

$$\langle \bar{J}_1', \delta\gamma \rangle = \int_I \int_D \left(3\alpha_\gamma' \boldsymbol{u}\cdot\tilde{\boldsymbol{m}}\right)\delta\gamma \mathrm{d}\Omega \mathrm{d}t, \tag{3.44}$$

with

$$\alpha' = (\alpha_{\min} - \alpha_{\max})\left(1 - \frac{\gamma}{\gamma+q}\right)\frac{1+q}{\gamma+q}, \tag{3.45}$$

where $\bar{J}_1' = \int_I 3\alpha_\gamma' \boldsymbol{u}\cdot\tilde{\boldsymbol{m}}\mathrm{d}t$, which is used for the gradient algorithm when updating the design variables so that the value of the objective functional is decreased during the optimization process.

3.5 Numerical implementation

3.5.1 Optimization algorithm

The optimization algorithm of the proposed method is now described.

Step 1. The initial design variable is set in the fixed design domain D.

Step 2. The lattice Boltzmann equations for the flow resistance minimization problem is calculated until a steady-state condition is satisfied.

Step 3. If the criteria of the objective functional and inequality constraint are satisfied, an optimal configuration is obtained and the optimization is finished, otherwise the adjoint equation is calculated and the procedure advances to Step 4.

Step 4. The design sensitivity $\bar{J}_1'$ is calculated using the current state and adjoint variables.

Step 5. The design variable is updated using the MMA, after which the optimization procedure returns to Step 2 of the iterative loop.

These procedures are iterated until the following criterion for the value of the objective functional is met:

$$\left| \frac{J_1^N - J_1^{N-1}}{J_1^N} \right| < \epsilon_{\mathrm{opt}}, \tag{3.46}$$

where superscript N represents the number of iterations carried out during the optimization process. The value of this criterion is set so that $\epsilon_{\mathrm{opt}} = 1.0 \times 10^{-4}$. In addition, the following criteria is used for judging the steady-state condition:

$$\left\| \frac{\boldsymbol{u}^N - \boldsymbol{u}^{N-1}}{\boldsymbol{u}^N} \right\|_{L^2(D)} < \epsilon_u, \tag{3.47}$$

where ϵ_u represents the judgment criteria for the steady-state condition of fluid velocity. The value of this criterion is set so that $\epsilon_u = 1.0 \times 10^{-4}$. Note that the criterion represented in Eq. (4.37) must be satisfied to obtain an optimal configuration in the flow resistance minimization problem.

Since the state variables must be recorded for all time steps when the LBE is used to solve the adjoint problem that includes state variables, memory requirements will be prohibitive in many practical engineering problems if data for all time steps are preserved. Fortunately, in steady-state problems, each converged state and adjoint value at each optimization step N can be used as an initial value when calculating the time evolution equations in next optimization step, $N + 1$. Since the state and adjoint equations are formulated as an explicit scheme, the calculations at each optimization step rapidly converge except for the first optimization step. Although the use of this numerical technique is only allowed in steady-state problems, the characteristics of the explicit scheme are highly advantageous and enable an optimal

configuration to be obtained quickly [69]. Similarly, the design sensitivities are calculated using only each converged value of the state and adjoint variables, whereas the time integral is contained in the original definition of the sensitivity in Eq. (3.44).

In addition, note that employing a filtering technique to preserve the smoothness of the design variables or design sensitivities during the optimization process is unnecessary here. This is because none of the design sensitivities given by Eq. (3.44) contain a derivative in its integrand. A filtering technique, e.g., [38] can, of course, be used to avoid the dependency of optimal configurations with respect to the mesh discretization of the design domain. However, it should be noted that such numerical treatment often causes difficulty in setting certain parameters.

3.5.2 Adjoint lattice Boltzmann equation

Due to the similarity between the configuration of the discrete Boltzmann equation and that of the adjoint equations represented in the previous Section, which is a consequence of the discretization strategy used in the LBM, the adjoint equation can also be discretized as simple time evolution equation, in the form of the so-called adjoint lattice Boltzmann equation (ALBE). That is, the adjoint problem based on the LBM in the flow resistance minimization problem can be formulated as follows:

$$\begin{cases} \tilde{f}_i^*(\boldsymbol{x}-\boldsymbol{c}_i\Delta x, t-\Delta t) = \tilde{f}_i(\boldsymbol{x},t) - \frac{1}{\tau_f}\{\tilde{f}_i(\boldsymbol{x},t) - \tilde{f}_i^{\mathrm{eq}}(\boldsymbol{x},t)\} \\ \tilde{f}_i(\boldsymbol{x}, t-\Delta t) = \tilde{f}_i^*(\boldsymbol{x}, t-\Delta t) - 3\Delta x \alpha_\gamma(\boldsymbol{x}) \boldsymbol{E}_i \boldsymbol{c}_i \cdot \tilde{\boldsymbol{m}}(\boldsymbol{x}, t-\Delta t) \\ \tilde{f}_i(\boldsymbol{x}, t_{\mathrm{f}}) = 0 \quad \text{(Initial condition)} \\ \tilde{f}_i(\boldsymbol{x}, t) = \tilde{f}_i^{\mathrm{b}}(\boldsymbol{x}, t) \quad \text{(Boundary condition)}, \end{cases} \tag{3.48}$$

where

$$\tilde{f}_{5,8,9}^{\mathrm{b}} = \begin{cases} \tilde{f}_{3,6,7} & \text{on } \Gamma_{\mathrm{W}} \\ \tilde{f}_{3,6,7} - \frac{2}{3(1-v_0)} + \frac{v_0}{3(1-v_0)}\left(4\tilde{f}_3 + \tilde{f}_6 + \tilde{f}_7\right) & \text{on } \Gamma_{\mathrm{V}} \\ \tilde{f}_{3,6,7} - \frac{1}{3}(4\tilde{f}_3 + \tilde{f}_6 + \tilde{f}_7) & \text{on } \Gamma_{\mathrm{P}}, \end{cases} \tag{3.49}$$

where $\tilde{f}_i^{\mathrm{b}}$ represents the boundary values based on Eqs. (3.41), (3.42), and (3.43) that express the boundary conditions for $\tilde{f}_i$ at $y = 0$ in Fig. 3.1(b), in which the analysis domain is located in $y \geqslant 0$ and the unknown values are $\tilde{f}_5$, $\tilde{f}_8$, and $\tilde{f}_9$. Note that the unknown values of

the adjoint problem at the $y = 0$ boundary are different from those of the state problem, in which the unknown values are f_3, f_6, and f_7. The unknown state values are in diametrically opposite locations with respect to those of the adjoint variables. For the other boundaries, e.g., the boundary at which $x = 0$ and the analysis domain is located in $x \geqslant 0$ in Fig. 3.1(a), the unknown values of the state variables are f_2, f_6, and f_9, and correspond to the unknown values of the adjoint variables f_4, f_8, and f_7, respectively. It should be noted that the boundary conditions for the adjoint equations at each boundary must be individually derived. We also note that the above discretized adjoint equation allows us to avoid having to deal with matrix operations when obtaining design sensitivities during the optimization process.

3.6 Numerical examples

In this Section, two- and three-dimensional numerical examples are provided. All numerical examples use the same parameters of MMA, and the initial design variable is set $\gamma = 1$ so that the fixed design domain D is filled with fluid. Since all numerical examples are treated as internal channel flow problems, the wall boundary of ∂D is set to a no-slip boundary condition by using the bounce back boundary condition. The inlet boundary is set as a prescribed velocity boundary based on Eq. (3.19), and the outlet boundary is set as a prescribed pressure boundary based on Eq. (3.20).

In addition, the Reynolds number Re is given by

$$Re = \frac{LU}{\nu}. \tag{3.50}$$

In this research, the non-dimensional values of reference length L and reference speed U, are set as the inlet width and mean value of the inlet speed, respectively.

3.6.1 Validation of adjoint sensitivity

To confirm the validity of the proposed method, the design sensitivities computed using the proposed sensitivity analysis were compared with the outcome of finite differences, as shown in Fig. 3.2. The evaluation nodes illustrated in this figure were selected in the design domain, in which a cylinder with a radius of $15\Delta x$ was placed at the center of the design domain, to magnify the variation of the sensitivities. The design variables were set so that $\gamma = 0.1$ for the cylinder and $\gamma = 0.9$ elsewhere.

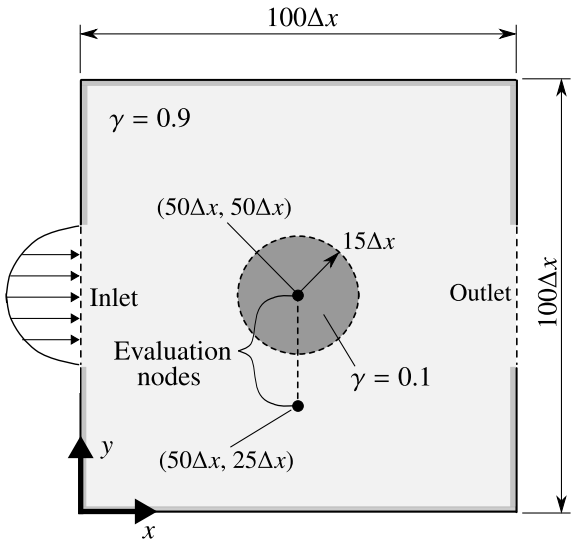

Fig. 3.2 Analysis domain for the validation of design sensitivity. The analysis domain was discretized using a $100\Delta x \times 100\Delta x$ grid, where a circle whose radius is set to $30\Delta x$ is put at the center of the domain. The design variables in the fluid and solid domains were set as $\gamma = 0.9$ and 0.1, respectively. The finite difference sensitivities were evaluated at the "evaluation nodes" that are composed of 25 nodes between $(x, y) = (50\Delta x, 25\Delta x)$ and $(x, y) = (50\Delta x, 50\Delta x)$

.

To confirm the relationship between the state and adjoint fields, Fig. 3.3 shows the sate field, the adjoint field, and the design sensitivity in the flow resistance minimization problem. To adapt previous research that discusses the adjoint field in fluid problems (e.g. [56]), the expanded objective functional is reformulated as $\bar{J}_1 = J_1 - R_1$. As shown in Fig. 3.3, it can be confirm that the adjoint variable $\tilde{\boldsymbol{m}}$ is the inverse vector of the fluid velocity. Note that this characteristic is also observed in the adjoint field dealing with NSE. The adjoint sensitivity J_1' that is defined using $\boldsymbol{u}$ and $\tilde{\boldsymbol{m}}$ were obtained as shown in Fig. 3.3(c), in which it is indicated that the objective functional is decreased by removing the vicinity of structural boundary.

Let confirm the validity of the above adjoint sensitivity by using the finite difference approximation. The finite difference, J'_{FD1}, is defined using the central difference scheme, as follows:

$$J'_{\mathrm{FD1}} = \frac{J_1(\gamma+\epsilon) - J_1(\gamma-\epsilon)}{2\epsilon}, \tag{3.51}$$

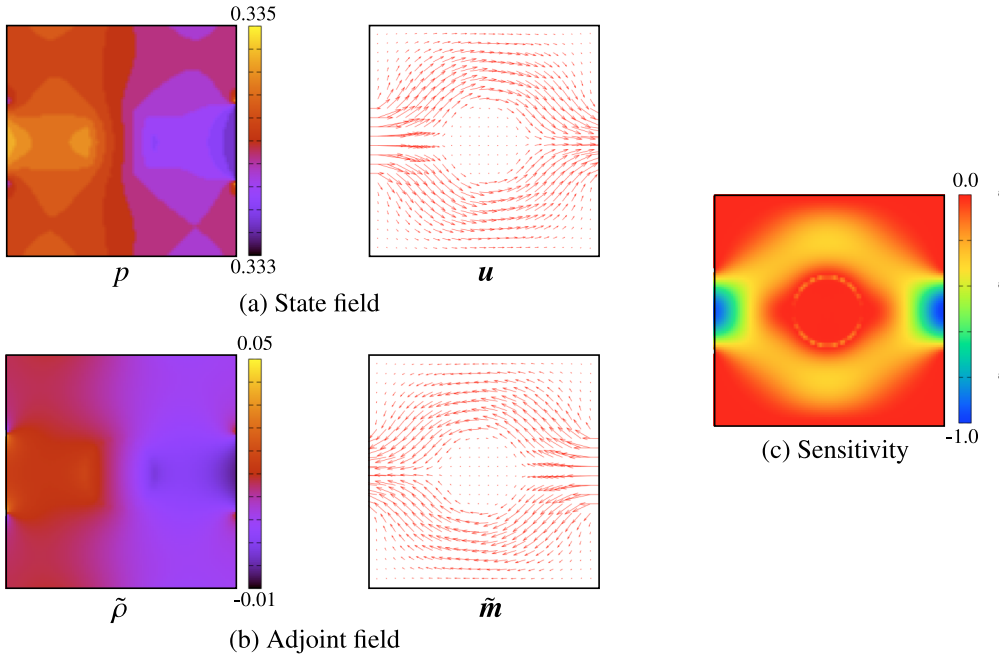

Fig. 3.3 State field (p, $\boldsymbol{u}$), adjoint field (ρ, $\tilde{\boldsymbol{m}}$), and the distribution of adjoint sensitivity in the flow resistance minimization problem using the LBM.

where ϵ is an small positive value. We can validate the adjoint model if and only if the adjoint sensitivity in Eq. (3.44) and finite difference sensitivity in Eq. (3.51) are equal.

Figure 3.4 illustrates that the proposed method computes sensitivities which are in agreement with the finite differences except the case of $\epsilon = 1.0 \times 10^{-6}$. The evaluation index is introduced for the relative error of the finite difference sensitivity with respect to the adjoint sensitivity, as follows:

$$E_{L^2}(\boldsymbol{x}) = \sqrt{\left(\frac{J_1'(\boldsymbol{x})}{\max\{J_1'(\boldsymbol{x})\}} - \frac{J_{\mathrm{FD1}}'(\boldsymbol{x})}{\max\{J_{\mathrm{FD1}}'(\boldsymbol{x})\}} \right)^2}, \tag{3.52}$$

where both sensitivities are normalized using each maximum value. As shown in Fig. 3.5, the relative error $E_{L^2}(\boldsymbol{x})$ was approximately obtained as $10^{-7} \sim 10^{-2}$, whereas the numerical instability was observed when setting $\epsilon = 1.0 \times 10^{-6}$ due to the machine precision errors. Consequently, it can be confirmed that certain values of the adjoint sensitivity were obtained.

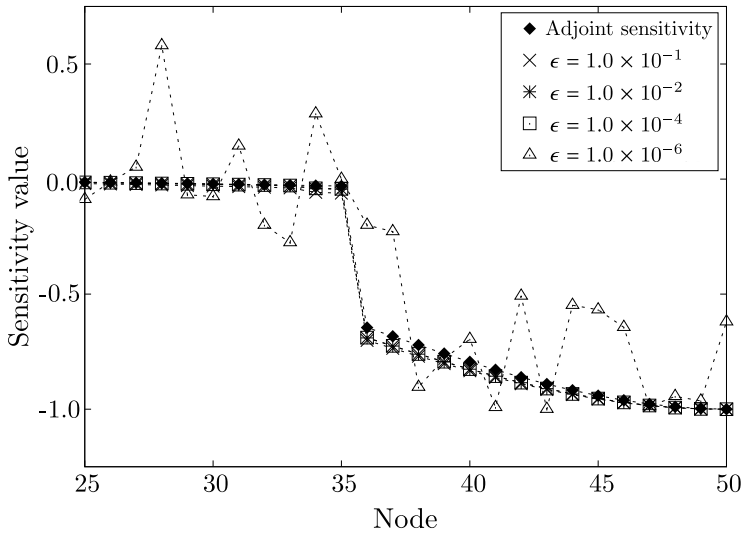

Fig. 3.4 Comparison of the finite differences with respect to the adjoint sensitivities in flow resistance minimization problem. The node in the horizontal axis corresponds to each evaluation node in the analysis domain as shown in Fig. 3.2.

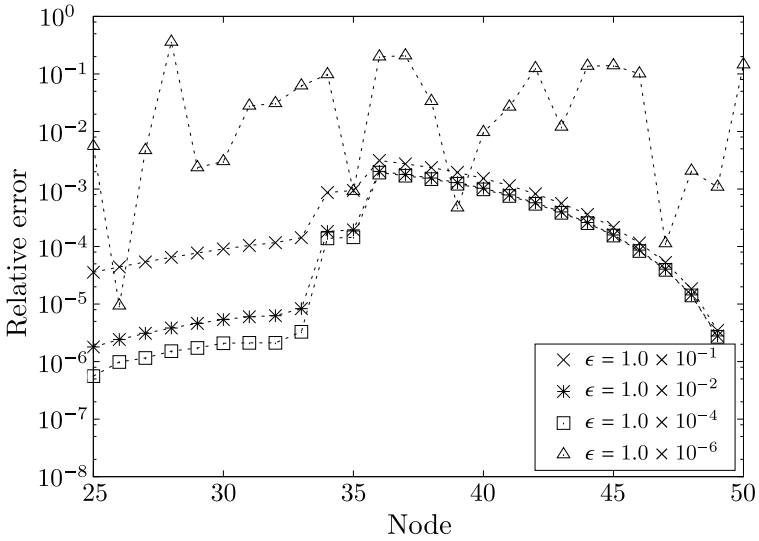

Fig. 3.5 Relative errors of the finite difference approximation with respect to the adjoint sensitivity in the flow resistance minimization problem.

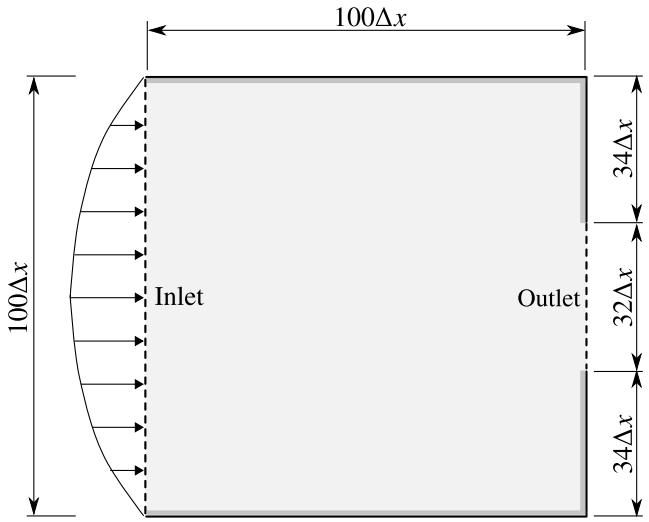

Fig. 3.6 Design settings in the diffuser problem using the LBM.

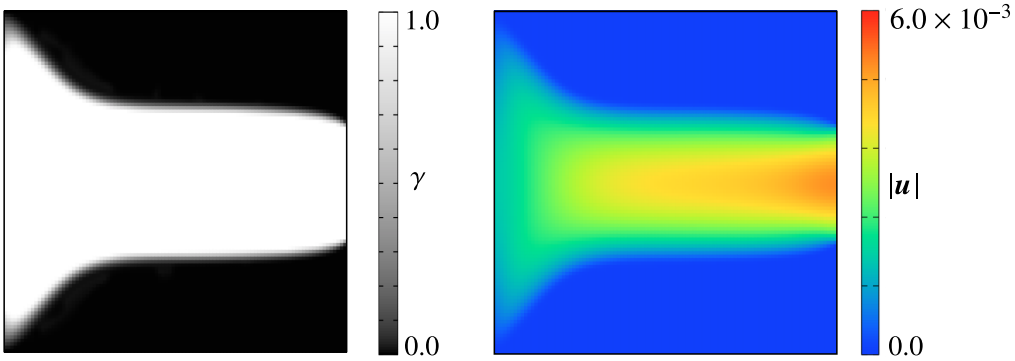

(a) Optimal configuration (b) Velocity magnitude

Fig. 3.7 Optimal configuration (black: fluid, white: solid) and the velocity magnitude in the diffuser problem using the LBM.

3.6.2 Diffuser

Here, we confirm the validity of our proposed method by applying it to the diffuser problem shown in Fig. 3.4, which is often treated in fluid flow topology optimization research [14, 39, 90, 18, 69, 127]. As shown in Fig. 3.6, the analysis domain is discretized using a $100\Delta x \times 100\Delta x$ grid, and the volume constraint is set so that $V_{\max} = 0.5$. Since previous research on this diffuser problem constructed methodologies for Stokes flow, or very low Reynolds number flow, we set our fluidic system to a low Reynolds number flow to enable a

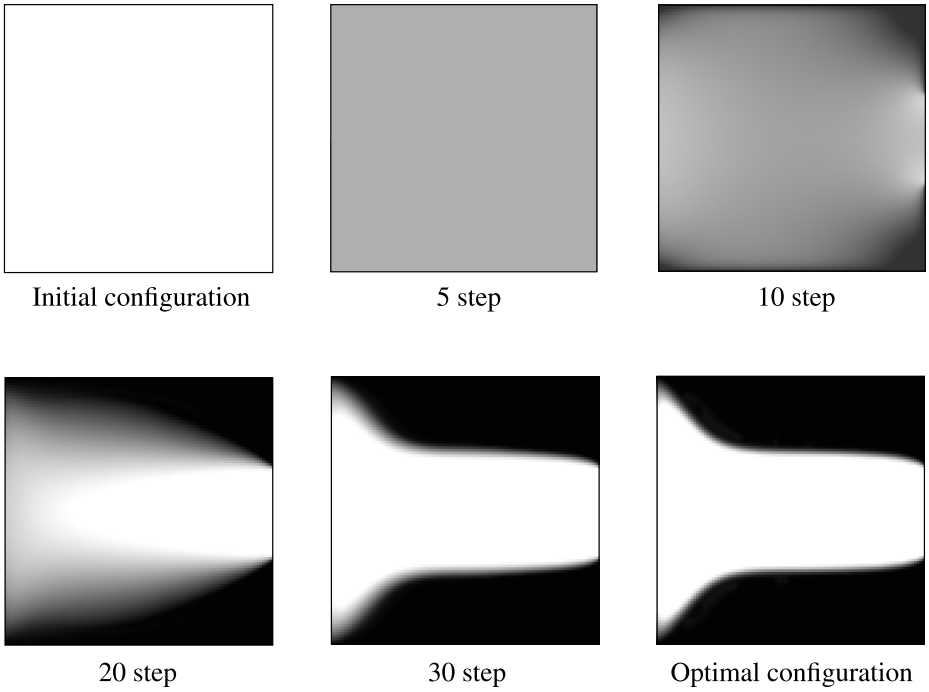

Fig. 3.8 Optimization history of design variable for the diffuser problem using the LBM.

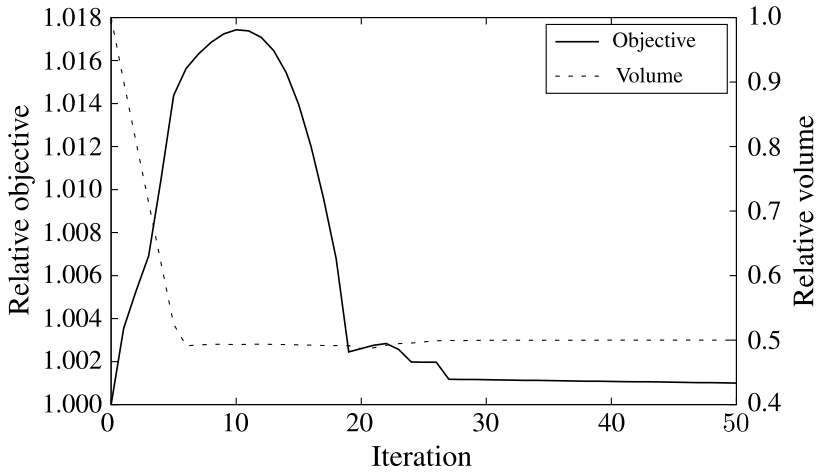

Fig. 3.9 Convergence histories of the relative objective functional and fluid volume. The relative objective functional is defined as $\hat{J}_1 = J_1/J_1^{\text{init}}$, with J_1^{init} representing the initial value of the objective functional. The relative fluid volume is defined as $\hat{V} = \int_D \gamma \mathrm{d}\Omega / \int_D \mathrm{d}\Omega$. The maximum fluid volume is set to $V_{\max} = 0.5$.

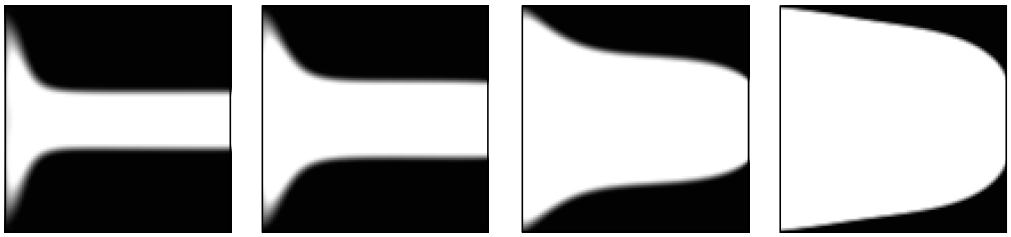

(a) $V_{\max} = 0.3$ (b) $V_{\max} = 0.4$ (c) $V_{\max} = 0.6$ (d) $V_{\max} = 0.8$

Fig. 3.10 Effect of parameter $V_{\max}$ settings on optimal configurations: (a) $V_{\max} = 0.3$, (b) $V_{\max} = 0.4$, (c) $V_{\max} = 0.6$, (d) $V_{\max} = 0.8$.

valid comparison. Here, $Re = 1$ in Eq. (3.50), and the following settings are used: $L = 100\Delta x$, $U = 1.0 \times 10^{-3}$, and $\tau_f = 0.8$. The prescribed pressure at the outlet boundary was set to $p_0 = \rho_0/3$ where $\rho_0 = 1.0$.

Figure 3.7 shows the optimal configuration obtained with the proposed method, and its close similarity to the configuration obtained by Borrvall and Petersson [14] confirms that it can obtain appropriate results. Although the dissipation energy is generally used for the objective functional when formulating a fluid flow optimization problem, it is noted that the pressure drop that corresponds to the flow resistance is essentially equivalent to the dissipation energy [84, 68] under low Reynolds number flows, where the loss of dynamic pressure and the effect of body force can be safely ignored [90]. The convergence histories of the objective functional and the volume fraction are shown in Fig. 3.9, in which both values are monotonically converged by approximately the 40th step.

From the physical viewpoint, the squeezed shape near the outlet in Fig. 3.7(a) is difficult to understand why this is valid as the optimal shape. The reason why such shape is obtained that the magnitude of the fluid velocity near both end of the outlet boundary is almost zero. This means that the design sensitivity is almost zero in the vicinity of both end of the outlet boundary. That is, in this case, the outlet shape of the optimal configuration does not practically affect the performance of flow channel that aims to minimize the flow resistance. Since it is expected that such unimportant shape is changed when changing the volume constraint of the fluid, Fig. 3.10 shows the effect of parameter $V_{\max}$ on optimal configuration in the flow resistance minimization problem. In fact, the optimal configuration has a straight channel as shown in Fig. 3.10(a) and (b).

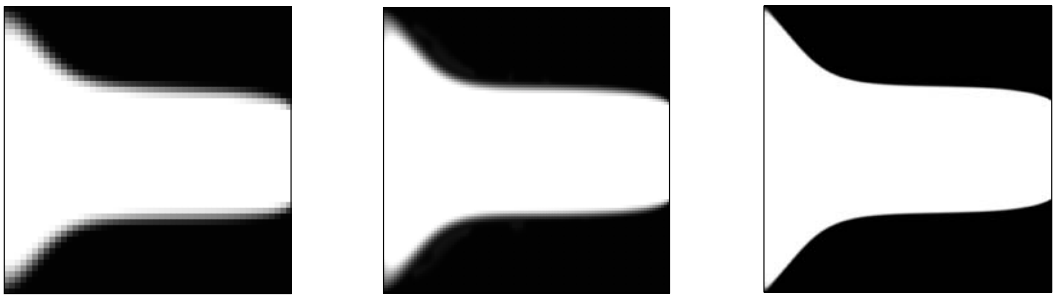

(a) $50\Delta x \times 50\Delta x$ (b) $100\Delta x \times 100\Delta x$ (c) $1000\Delta x \times 1000\Delta x$

Fig. 3.11 Dependency of optimal configurations on grid size in the diffuser problem using the LBM: (a) $50\Delta x \times 50\Delta x$, (b) $100\Delta x \times 100\Delta x$, (c) $1000\Delta x \times 1000\Delta x$.

Table 3.1 Values of relative objective functional in different settings of grid size in the diffuser problem using the LBM.

Grid	$50\Delta x \times 50\Delta x$	$100\Delta x \times 100\Delta x$	$1000\Delta x \times 1000\Delta x$
Relative objective	1.003	1.001	1.001

Table 3.2 Values of relative objective functional in different settings of Reynolds number in the pipe bend problem using the LBM.

Re	1	100	250
Relative objective	0.199	6.92	64.3

3.6.3 Effect of grid size

Next, it is examined the dependency of the optimal configurations with respect to the grid size, using the design model shown in Fig. 3.4. Here, three cases are treated, using grid sizes of $50\Delta x \times 50\Delta x$, $100\Delta x \times 100\Delta x$ and $1000\Delta x \times 1000\Delta x$ under the same volume constraint condition.

The Reynolds number is set as $Re = 1$ in order to ensure that the Reynolds number condition is the same in both cases that use different grid sizes.

The similarity of the optimal configurations in Fig. 3.11 indicates that dependency with respect to grid size is low. The final values of objective functional are shown in Table 3.1, where it can be confirmed that the obtained values are almost same.

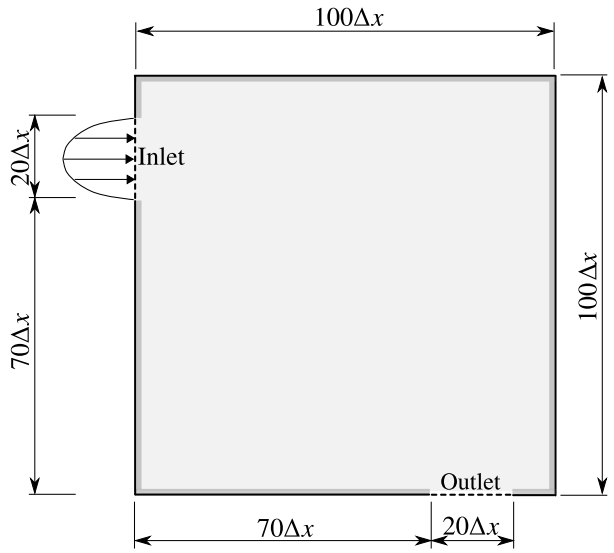

Fig. 3.12 Design settings in the pipe bend problem using the LBM.

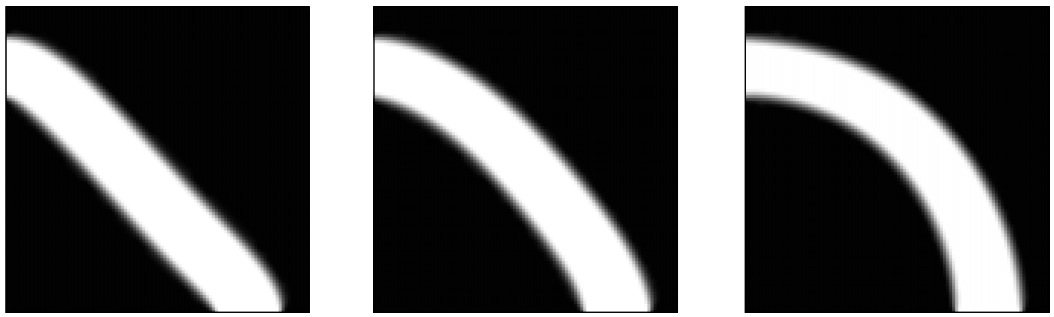

(a) $Re = 1$ (b) $Re = 100$ (c) $Re = 250$

Fig. 3.13 Dependency of optimal configurations on the value of Reynolds number in the pipe bend problem using the LBM: (a) $Re = 1$, (b) $Re = 100$, (c) $Re = 250$.

3.6.4 Pipe bend

Next, the pipe bend problem shown in Fig. 3.12 is addressed to confirm the dependency of the optimal configurations with respect to the Reynolds number. The analysis domain is discretized using a $100\Delta x \times 100\Delta x$ grid, and the volume constraint is set so that $V_{\max} = 0.25$. Here, the following settings are used: $L = 40\Delta x$, $\tau_f = 0.8$, $p_0 = \rho_0/3$ where $\rho_0 = 1.0$. The Reynolds number is controlled by setting the inlet speed U.

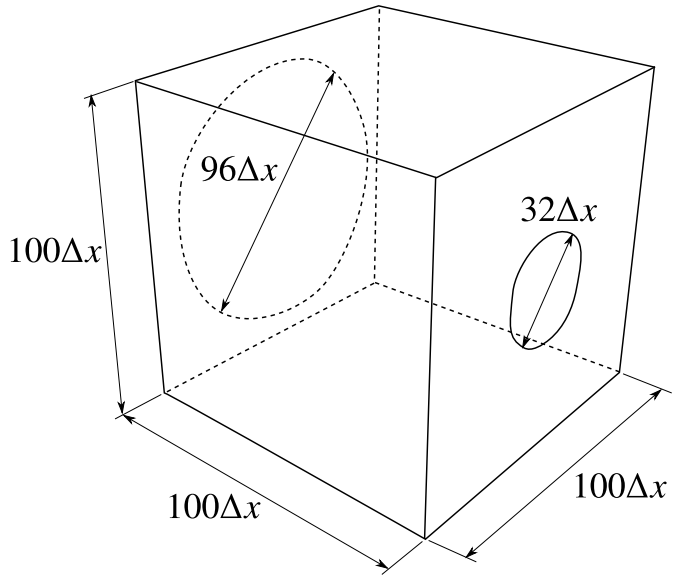

Fig. 3.14 Design settings for the three-dimensional diffuser problem. The analysis domain is discretized using a $100\Delta x \times 100\Delta x \times 100\Delta x$ grid.

Figure 3.13 shows the optimal configurations for the pipe bend problem and it is noted that they are radically different for the three Reynolds number values used, (a) $Re = 0.1$, (b) $Re = 50$, and (c) $Re = 200$. The values of the objective functional in each result are shown in Table 3.2. The differences in the optimal configurations indicate that the value of the Reynolds number affects the curvature of the obtained channel configuration. That is, under the high Reynolds number flow regime, the optimal configuration is noticeably curved, whereas under the low Reynolds number flow regime, the configuration is almost straight. This dependency on the Reynolds number is a characteristic noted in previous research [69], and can be appreciated as a natural outcome of physical phenomena that would cause a large flow resistance due to a large inertial force if the straight channel configuration were used under high Reynolds number flow. Thus, we can confirm that our proposed method is applicable to fluid flow topology optimization and that the form of the obtained optimal configurations changes when different Reynolds numbers are employed.

3.6.5 Three-dimensional problems

Here, we discuss the three-dimensional problem in the flow resistance minimization problem.

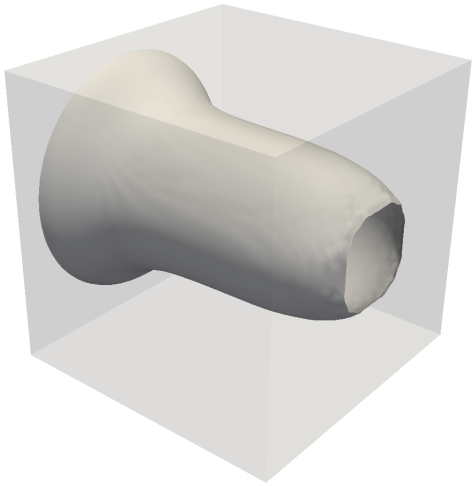

(a) $50\Delta x \times 50\Delta x \times 50\Delta x$

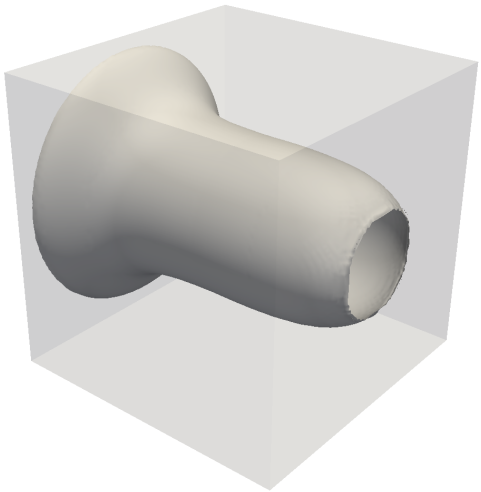

(b) $100\Delta x \times 100\Delta x \times 100\Delta x$

Fig. 3.15 Optimal configurations of the three-dimensional diffuser problem in different grid size: (a) $50\Delta x \times 50\Delta x \times 50\Delta x$, (b) $100\Delta x \times 100\Delta x \times 100\Delta x$. The iso-surface of $\gamma = 0.5$ is shown as the optimal configuration. The volume constraint is set to $V_{\max} = 0.25$.

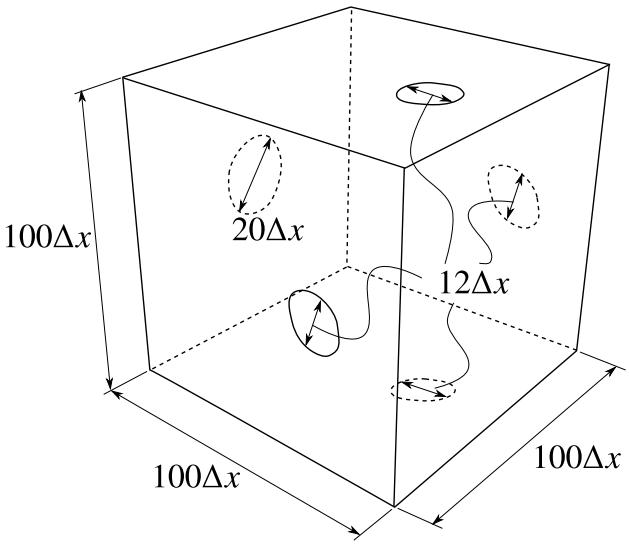

Fig. 3.16 Design settings in the three-dimensional multi-outlets problem. The analysis domain is discretized using a $100\Delta x \times 100\Delta x \times 100\Delta x$ grid.

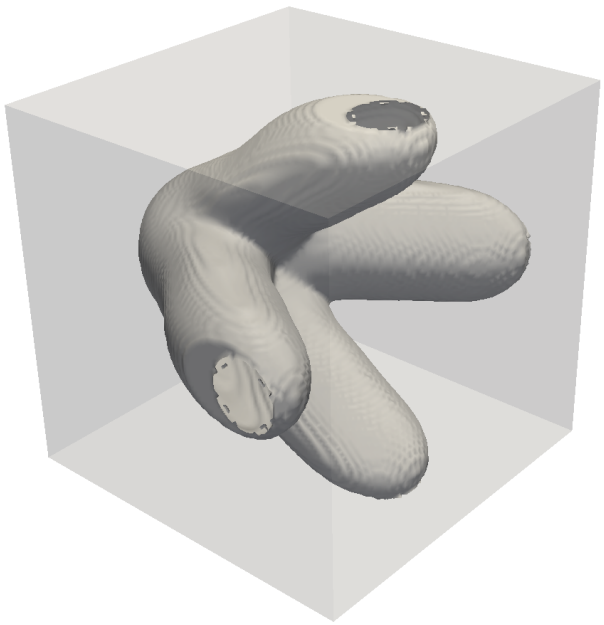

Fig. 3.17 Optimal configurations of the three-dimensional multi-outlets problem, in which the analysis domain is discretized using a $100\Delta x \times 100\Delta x \times 100\Delta x$ grid. The iso-surface of $\gamma = 0.5$ is shown as the optimal configuration. The volume constraint is set to $V_{\max} = 0.25$.

First, we consider the three-dimensional diffuser problem shown in Fig. 3.14, in which the volume constraint is set to $V_{\max} = 0.25$, and the analysis domain is discretized using two cases: (a) $50\Delta x \times 50\Delta x \times 50\Delta x$, and (b) $100\Delta x \times 100\Delta x \times 100\Delta x$ lattices. Since the reference length in this problem is the diameter of the inlet, the Reynolds number is set as $Re = 1$. Figure 3.15 shows the optimal configuration in the three-dimensional diffuser problem, where the iso-surface of $\gamma = 0.5$ is shown, and it is found that the optimal configurations are almost independent of the resolution in the analysis domain.

In the second numerical example for a three-dimensional case, we consider a problem with a single inlet and four outlets, as shown in Fig. 3.16. In this problem, the volume constraint, and Reynolds number are respectively set as $V_{\max} = 0.25$, and $Re = 1$. The analysis domain is discretized using $100\Delta x \times 100\Delta x \times 100\Delta x$ lattices. Figure 3.17 shows the optimal configuration for the three-dimensional multi-outlet problem.

These optimal configurations indicate that the proposed method can derive a valid optimal structure in a three-dimensional case.

3.7 Summary

This chapter presented a topology optimization method using the LBM incorporating a new sensitivity analysis based on the discrete Boltzmann equation. The presented method was applied to the flow resistance minimization problem. We achieved the following:

(1) A topology optimization problem was formulated for flow resistance minimization problem. The design sensitivity for the optimization problem was derived based on the ALBM, and we newly introduces a discrete velocity Boltzmann equation to formulate the Lagrangian, whereas the Boltzmann equation is used in the original ALBM. As a result, the accurate boundary conditions generally used in the LBM could be incorporated in the optimization problem formulations, and derivation of adjoint systems in which the adjoint boundary conditions reflect the boundary conditions of the LBM was enabled.

(2) An optimization algorithm was constructed based on the formulations of the optimization problem. The use of the LBM discretization strategy allowed discretization of the adjoint equation as simple time evolution equation, in the same manner as that used for the LBE. Additionally, the converged state variable values and adjoint variable

values at each optimization step were used as initial values when calculating the time evolution equation in the next optimization step, which greatly reduced computational cost.

(3) Several numerical examples for both two- and three-dimensional problems were provided to confirm the validity and utility of the presented method, for a flow resistance minimization problem. It is demonstrated that the presented method obtains an optimal configuration similar to that when using an FEM-based method. Based on the obtained results, we confirmed that the presented method obtains optimal configurations that show minimal dependency upon the mesh size. In addition, it was also found that the optimal configurations show dependency with respect to Reynolds number settings.

Chapter 4

Thermal-fluid flow channel design

4.1 Introduction

Multiphysics optimization problems that combine fluid behavior formulations with those of other physical phenomena are especially challenging, and the development of particularly useful optimal configurations based on designer intuition is extremely difficult.

One example of a typical multiphysics optimization problem for an engineering application is a thermal device used for cooling mechanical or electronic systems, i.e., a heat sink. Since the physical phenomena active in a heat sink are mainly governed by thermal and fluid dynamic interactions, optimal cooling performance can be obtained by maximizing the exchange of heat. Among various heat sink designs, the liquid-cooled type [118, 78] has recently attracted much attention as a high-performance cooling device. This basic design has been implemented in a variety of sizes, including compact designs for micro-scale thermal devices used in microelectromechanical system (MEMS) applications. Many researchers have investigated the relationship between the performance of heat sinks and the geometrical configuration of their channels, using experimental [81], analytical [57], and numerical [97, 61] approaches.

However, as mentioned above, the intuition of designers is usually ineffective when the goal is to develop optimal configurations for such devices, since their performance must satisfy multiple demands, such as maximal heat exchange with minimal pressure drop or pumping power. Thus, given the utility of mathematical optimization approaches for the design of these devices, several optimization methods for the design of high-performance devices have been proposed [118, 58, 46]. However, most previous research has been based

on size optimization that only allows changes in sizes, such as length, height, and depth, with respect to the geometry of the device. Therefore, the initial channel configuration setting for the optimization is crucially important to the realization of a high-performance device, and the optimal solution strongly depends on this initial setting. Although size optimization methods are useful at the detailed design stage of a heat sink design problem, the low degree of design freedom is an obstacle to achieving dramatic improvements in heat sink performance during the conceptual design stage. As a conceptual design optimization method, topology optimization is a particularly useful approach for obtaining optimal configurations based on mathematical and physical laws.

In this chapter, a topology optimization method for a thermal-fluid engineering application is presented, to derive a highly efficient cooling device. The optimization problem is formulated as a heat exchange maximization problem in which the fluid velocity, pressure and temperature are computed using the LBM. In addition, the design sensitivity is derived using the adjoint sensitivity analysis constructed in Chapter 3. Several numerical examples are provided to confirm the applicability of the proposed method.

4.2 Lattice Boltzmann method for a thermal-fluid flow

4.2.1 Basic equation

Here, the following lattice Boltzmann equation (LBE) proposed by Inamuro et al. [50] is employed, to compute the incompressible viscous fluid flow while considering the scalar transport:

$$f_i(\boldsymbol{x}+\boldsymbol{c}_i\Delta x, t+\Delta t) = f_i(\boldsymbol{x},t) - \frac{1}{\tau_f}\{f_i(\boldsymbol{x},t) - f_i^{\mathrm{eq}}(\boldsymbol{x},t)\}, \tag{4.1}$$

$$g_i(\boldsymbol{x}+\boldsymbol{c}_i\Delta x, t+\Delta t) = g_i(\boldsymbol{x},t) - \frac{1}{\tau_g}\{g_i(\boldsymbol{x},t) - g_i^{\mathrm{eq}}(\boldsymbol{x},t)\}, \tag{4.2}$$

where τ_f and τ_g are the non-dimensional relaxation times of f_i and g_i, respectively. Although Inamuro et al. proposed their method to introduce a buoyancy force, based on the Boussinesq approximation, it is note that this buoyancy force is not treated in our study. The equilibrium

distribution functions, f_i^{eq} and g_i^{eq}, are given by

$$f_i^{\mathrm{eq}} = E_i \rho \left\{ 1 + 3\boldsymbol{c}_i \cdot \boldsymbol{u} + \frac{9}{2}(\boldsymbol{c}_i \cdot \boldsymbol{u})^2 - \frac{3}{2}|\boldsymbol{u}|^2 \right\}, \tag{4.3}$$

$$g_i^{\mathrm{eq}} = E_i T (1 + 3\boldsymbol{c}_i \cdot \boldsymbol{u}). \tag{4.4}$$

Density ρ, fluid velocity $\boldsymbol{u}$, temperature T, and heat flux $\boldsymbol{q}_T$ are obtained from the moments of the velocity distribution functions, as follows:

$$\rho = \sum_{i=1}^{9} f_i, \tag{4.5}$$

$$\boldsymbol{u} = \frac{1}{\rho} \sum_{i=1}^{9} \boldsymbol{c}_i f_i, \tag{4.6}$$

$$T = \sum_{i=1}^{9} g_i, \tag{4.7}$$

$$\boldsymbol{q}_T = \sum_{i=1}^{9} \boldsymbol{c}_i g_i - T\boldsymbol{u}. \tag{4.8}$$

The pressure p is given by

$$p = \frac{\rho}{3}. \tag{4.9}$$

Applying the asymptotic theory [107] to Eqs. (4.1) and (4.2), Inamuro et al. [50] verified that the macroscopic variable in Eqs. (4.5)–(4.7) and (4.9) satisfy the following macroscopic equation, with relative errors of $O[(\Delta x)^2]$,

$$\nabla \cdot \boldsymbol{u} = 0, \tag{4.10}$$

$$Sh \frac{\partial \boldsymbol{u}}{\partial t} + (\boldsymbol{u} \cdot \nabla)\boldsymbol{u} = -\nabla p + \nu \nabla^2 \boldsymbol{u}, \tag{4.11}$$

$$Sh \frac{\partial T}{\partial t} + (\boldsymbol{u} \cdot \nabla) T = \alpha_T \nabla^2 T, \tag{4.12}$$

which represent the continuity equation (4.10), the NSE (4.11), and the convection-diffusion equation (4.12) for the temperature, respectively. The kinematic viscosity ν and the thermal

diffusivity α_T of the fluid are given by

$$\nu = \frac{1}{3}\left(\tau_f - \frac{1}{2}\right)\Delta x, \tag{4.13}$$

$$\alpha_T = \frac{1}{3}\left(\tau_g - \frac{1}{2}\right)\Delta x. \tag{4.14}$$

When a heat source $\boldsymbol{Q}_T(\boldsymbol{x},t)$ is applied, the evolution equations in Eq. (4.2) can be computed in a stepwise fashion as follows:

Step 1. g_i is evolved without the heat source, by the following equations:

$$g_i^*(\boldsymbol{x}+\boldsymbol{c}_i\Delta x, t+\Delta t) = g_i(\boldsymbol{x},t) - \frac{1}{\tau_g}\{g_i(\boldsymbol{x},t) - g_i^{\mathrm{eq}}(\boldsymbol{x},t)\}. \tag{4.15}$$

Step 2. g_i is corrected as follows:

$$g_i(\boldsymbol{x},t+\Delta t) = g_i^*(\boldsymbol{x},t+\Delta t) + \Delta x E_i \boldsymbol{Q}_T(\boldsymbol{x},t+\Delta t). \tag{4.16}$$

4.2.2 Initial and boundary conditions

As with the setting of initial value of f_i in Eq. (3.17), it is assumed that the initial value of the particle distribution function g_i is that of the equilibrium distribution function, given initial values of $\boldsymbol{u}(\boldsymbol{x},0)$, and $T(\boldsymbol{x},0)$, as follows:

$$g_i(\boldsymbol{x},0) = g_i^{\mathrm{eq}}(T(\boldsymbol{x},0), \boldsymbol{u}(\boldsymbol{x},0)), \tag{4.17}$$

where the initial values of the macroscopic variables are set so that $\boldsymbol{u}(\boldsymbol{x},0) = 0$, and $T(\boldsymbol{x},0) = 1$ in this study.

For the boundary conditions of g_i, Inamuro et al. [50], and Yoshino and Inamuro [130] proposed an adiabatic boundary condition, as follows:

$$\left.\begin{aligned} g_3 &= \tfrac{1}{9}T(1+3v) \\ g_6 &= \tfrac{1}{36}T(1+3v) \\ g_7 &= \tfrac{1}{36}T(1+3v) \end{aligned}\right\} \text{ on } \Gamma_{\mathrm{A}}, \text{ and } T = \frac{6(g_5+g_8+g_9)}{1-3v}. \tag{4.18}$$

Likewise, a prescribed temperature boundary condition can be introduced by using the following equations:

$$\left.\begin{aligned} g_3 &= \tfrac{1}{9}T(1+3v) \\ g_6 &= \tfrac{1}{36}T(1+3v) \\ g_7 &= \tfrac{1}{36}T(1+3v) \end{aligned}\right\} \text{ on } \Gamma_{\mathrm{T}}, \text{ and } T = \frac{6\{T_0 - (g_1+g_2+g_4+g_5+g_8+g_9)\}}{1+3v}, \tag{4.19}$$

where T_0 represents the prescribed temperature.

4.3 Formulation of a topology optimization problem

4.3.1 Heat exchange maximization problem

The second problem we formulate is to maximize heat exchange for a flow channel design that can be applied for cooling devices such as a heat sink. Here, we consider the design domain shown in Fig. 2.4. A heat source Q_T is defined in the solid domain $D\backslash\Omega$ and the aim is to find an optimal configuration of the flow channel so that the coolant flow removes a maximal amount of heat input through an area of the solid domain. The boundary conditions for $\boldsymbol{u}$ and p are same as those applied in the pressure drop minimization problem. Additionally, the adiabatic boundary condition, $\boldsymbol{n}\cdot\nabla T = 0$, and the prescribed temperature condition, $T = T_{\mathrm{in}}$, are imposed at $\Gamma_{\mathrm{W}}\cup\Gamma_{\mathrm{P}}$, and Γ_{V}, respectively.

Based on previous research dealing with heat exchange maximization problems [75], the heat generation coefficient β_γ, which is dependent on design variable γ, is introduced as follows:

$$Q_T = \beta_\gamma(1-T), \tag{4.20}$$

where $\beta_\gamma(\boldsymbol{x})$ is defined as

$$\beta_\gamma = \beta_{\max} + (\beta_{\min} - \beta_{\max})\frac{\gamma(1+q)}{\gamma+q}, \tag{4.21}$$

We note that since the dimensionless temperature T is normalized according to the value of the reference temperature T_{ref}, the heat source Q_T restricts the maximum value of dimensional temperature so that $T \approx T_{\mathrm{ref}}$, which corresponds to a maximum value for dimensionless temperature of $T = 1$. Due to the definition of β_γ in Eq. (4.21), the maximum value of heat

generation coefficient $\beta_{\max}$ is given in the solid domain corresponding to $\gamma = 0$, while the minimum value of heat generation coefficient $\beta_{\min}$ is given in the fluid domain corresponding to $\gamma = 1$. In this study, the minimum value of heat generation coefficient is set to $\beta_{\min} = 0$.

Based on the above formulation, the thermal-fluid flow in D is governed by the following problem concerning the initial and boundary values:

$$\left\{\begin{array}{l}
\left.\begin{array}{l}
\nabla\cdot\boldsymbol{u} = 0 \\
Sh\frac{\partial \boldsymbol{u}}{\partial t} + (\boldsymbol{u}\cdot\nabla)\boldsymbol{u} = -\nabla p + \nu\nabla^2\boldsymbol{u} - \alpha_\gamma \boldsymbol{u} \\
Sh\frac{\partial T}{\partial t} + (\boldsymbol{u}\cdot\nabla)T = \alpha_T\nabla^2 T + \beta_\gamma(1-T)
\end{array}\right\} \text{ Governing equations in } D \\
\left.\begin{array}{ll}
\boldsymbol{u} = \boldsymbol{0} & \text{on } \Gamma_{\mathrm{W}} \\
\boldsymbol{u} = \boldsymbol{u}_{\mathrm{in}} & \text{on } \Gamma_{\mathrm{V}} \\
p = p_{\mathrm{out}} & \text{on } \Gamma_{\mathrm{P}} \\
\boldsymbol{n}\cdot\nabla T = 0 & \text{on } \Gamma_{\mathrm{W}}\cup\Gamma_{\mathrm{P}} \\
T = T_{\mathrm{in}} & \text{on } \Gamma_{\mathrm{V}}
\end{array}\right\} \text{ Boundary conditions} \quad
\left.\begin{array}{l}
\boldsymbol{u}(\boldsymbol{x},0) = \boldsymbol{u}^{\mathrm{ini}}(\boldsymbol{x}) \\
p(\boldsymbol{x},0) = p^{\mathrm{ini}}(\boldsymbol{x}) \\
T(\boldsymbol{x},0) = T^{\mathrm{ini}}(\boldsymbol{x})
\end{array}\right\} \text{ Initial conditions,}
\end{array}\right. \tag{4.22}$$

where $T^{\mathrm{ini}}(\boldsymbol{x})$ represents the initial temperature value.

Based on a previous study [75], the heat exchange maximization problem can be formulated as

$$\left\{\begin{array}{ll}
\inf\limits_{\gamma} & J_2 = -\int_I\int_D \beta_\gamma(1-T)\mathrm{d}\Omega\mathrm{d}t \\
\text{s.t.} & P = \int_I\int_{\Gamma_{\mathrm{V}}} p\,\mathrm{d}\Gamma\mathrm{d}t - \int_I\int_{\Gamma_{\mathrm{P}}} p\,\mathrm{d}\Gamma\mathrm{d}t - \eta_{\max}\Delta p^{\mathrm{init}} \leqslant 0 \\
 & \boldsymbol{u}, p, \text{ and } T \text{ satisfy the initial-boundary value problem in Eq. (4.22),}
\end{array}\right. \tag{4.23}$$

where J_2 is the objective functional that corresponds to the total amount of heat exchanged in the fixed design domain and P is an inequality constraint that limits the maximum pressure drop based on the value of an initial pressure drop, Δp^{init}, obtained after computing the first optimization step. The parameter $\eta_{\max}$ is used for determining the maximum pressure drop in the fluidic system. In this optimization problem, we note that P is an essential constraint that prevents optimal configurations from having channels with infinitesimal widths, which would be allowed in the absence of a pressure drop constraint, due to the occurrence of infinite pressure drops [7, 74, 73].

As with the above pressure drop minimization problem, the fluid velocity, pressure and temperature are calculated using the LBM. That is, the initial-boundary value problem in Eq. (4.22) is solved using the LBM in this study.

4.3.2 Sensitivity analysis

Next, we discuss the sensitivity analysis for the heat exchange maximization problem. The basic procedure for conducting the sensitivity analysis is similar to that used in the above pressure drop minimization problem, but the Lagrangian with respect to J_2 is formulated here using the augmented Lagrange multiplier method (e.g. [53]), which enables the inequality constraint P to be precisely imposed on the optimization problem. We use the Lagrange multipliers $\tilde{g}_i = \tilde{g}_i(\boldsymbol{x}, t)$ and $\mu > 0$, and a penalty parameter $\sigma > 0$. Consequently, the Lagrangian, $\bar{J}_2$, is defined as follows:

$$\bar{J}_2 = J_2 + R_1 + R_2 + \frac{1}{2\sigma}\left\{\left(\max\left\{0, \mu + \sigma P\right\}\right)^2 - \mu^2\right\}, \tag{4.24}$$

where R_1 is as defined in Eq. (3.33) above, and R_2 is defined as

$$R_2 = \int_I \int_D \sum_{i=1}^{9} \tilde{g}_i \left\{ Sh \frac{\partial g_i}{\partial t} + \boldsymbol{c}_i \cdot \nabla g_i + \frac{1}{\varepsilon_g}\left(g_i - g_i^{\mathrm{eq}}\right) - \beta_\gamma (1 + \tilde{T}) \right\} \mathrm{d}\Omega \mathrm{d}t. \tag{4.25}$$

In this study, we set the value of penalty parameter to $\sigma = 1.0 \times 10^{-2}$. Since the design sensitivity of $\bar{J}_2$ is derived using $\langle \bar{J}_2', \delta\gamma \rangle$ in the same manner as for $\langle \bar{J}_1', \delta\gamma \rangle$, the adjoint equation for $\tilde{g}_i$ can be derived as follows:

$$-Sh \frac{\partial \tilde{g}_i}{\partial t} - \boldsymbol{c}_i \cdot \nabla \tilde{g}_i = -\frac{1}{\varepsilon_g}\left(\tilde{g}_i - \tilde{g}_i^{\mathrm{eq}}\right) + \beta_\gamma (1 + \tilde{T}), \tag{4.26}$$

where $\tilde{g}_i^{\mathrm{eq}}$ is defined as

$$\tilde{g}_i^{\mathrm{eq}} = \tilde{T} + 3\boldsymbol{u} \cdot \tilde{\boldsymbol{q}}, \tag{4.27}$$

where $\tilde{T}$ and $\tilde{\boldsymbol{q}}$ are defined as follows:

$$\tilde{T} = \sum_{i=1}^{9} E_i \tilde{g}_i, \tag{4.28}$$

$$\tilde{\boldsymbol{q}} = \sum_{i=1}^{9} E_i \boldsymbol{c}_i \tilde{g}_i. \tag{4.29}$$

On the other hand, based on Eq. (3.39), the adjoint equation for $\tilde{f}_i$ is defined as follows:

$$-Sh\frac{\partial \tilde{f}_i}{\partial t} - \boldsymbol{c}_i \cdot \nabla \tilde{f}_i = -\frac{1}{\varepsilon_f}\left(\tilde{f}_i - \tilde{f}_i^{\mathrm{eq}}\right) - 3\alpha_\gamma E_i \boldsymbol{c}_i \cdot \tilde{\boldsymbol{m}} + G_i^f, \tag{4.30}$$

where G_i^f is derived from the derivative of $\boldsymbol{E}_2$ with respect to f_i, and is defined as

$$G_i^f = \frac{3T}{\rho \varepsilon_g}(\boldsymbol{c}_i - \boldsymbol{u}) \cdot \tilde{\boldsymbol{q}}. \tag{4.31}$$

In addition, the initial conditions applied in Eq. (4.26) are defined as follows:

$$\tilde{g}_i(t_{\mathrm{f}}) = 0. \tag{4.32}$$

Based on the derivation strategy for the boundary conditions discussed in Appendix C, the boundary conditions corresponding to Eqs. (4.18) and (4.19) can be derived as follows:

$$\left.\begin{aligned} \tilde{g}_5 &= \tfrac{1+3v}{6(1-3v)}(4\tilde{g}_3 + \tilde{g}_6 + \tilde{g}_7) \\ \tilde{g}_8 &= \tfrac{1+3v}{6(1-3v)}(4\tilde{g}_3 + \tilde{g}_6 + \tilde{g}_7) \\ \tilde{g}_9 &= \tfrac{1+3v}{6(1-3v)}(4\tilde{g}_3 + \tilde{g}_6 + \tilde{g}_7) \end{aligned}\right\} \text{ on } \Gamma_{\mathrm{A}}. \tag{4.33}$$

$$\left.\begin{aligned} \tilde{g}_5 &= -\tfrac{1}{6}(4\tilde{g}_3 + \tilde{g}_6 + \tilde{g}_7) \\ \tilde{g}_8 &= -\tfrac{1}{6}(4\tilde{g}_3 + \tilde{g}_6 + \tilde{g}_7) \\ \tilde{g}_9 &= -\tfrac{1}{6}(4\tilde{g}_3 + \tilde{g}_6 + \tilde{g}_7) \end{aligned}\right\} \text{ on } \Gamma_{\mathrm{T}}. \tag{4.34}$$

As a result, the design sensitivity for this optimization problem is defined as follows:

$$\langle \bar{J}_2', \delta\gamma \rangle = \int_I \int_D \left\{ 3\alpha_\gamma' \boldsymbol{u} \cdot \tilde{\boldsymbol{m}} + \beta_\gamma'(1-T)(1+\tilde{T}) \right\} \delta\gamma \mathrm{d}\Omega \mathrm{d}t, \tag{4.35}$$

with

$$\beta' = (\beta_{\min} - \beta_{\max})\left(1 - \frac{\gamma}{\gamma + q}\right)\frac{1+q}{\gamma+q}, \tag{4.36}$$

where J_2' is therefore given by $\int_I \left\{3\alpha_\gamma' \boldsymbol{u}\cdot\tilde{\boldsymbol{m}} + \beta_\gamma'(1-T)(1+\tilde{T})\right\}\mathrm{d}t$.

4.4 Numerical implementation

4.4.1 Optimization algorithm

The optimization algorithm of the proposed method is now described.

Step 1. The initial design variable is set in the fixed design domain D.

Step 2. The LBE for the heat exchange maximization problem, is calculated until a steady-state condition is satisfied.

Step 3. If the criteria of the objective functional and inequality constraint are satisfied, an optimal configuration is obtained and the optimization is finished, otherwise the adjoint equations are calculated and the procedure advances to Step 4.

Step 4. The design sensitivity $\bar{J}_2'$ is calculated using the current state and adjoint variables.

Step 5. The design variable is updated using the MMA, after which the optimization procedure returns to Step 2 of the iterative loop.

The following criteria is employed for judging the steady-state condition:

$$\left\| \frac{\boldsymbol{u}^N - \boldsymbol{u}^{N-1}}{\boldsymbol{u}^N} \right\|_{L^2(D)} < \epsilon_u, \tag{4.37}$$

$$\left\| \frac{\boldsymbol{q}_T^N - \boldsymbol{q}_T^{N-1}}{\boldsymbol{q}_T^N} \right\|_{L^2(D)} < \epsilon_q, \tag{4.38}$$

where ϵ_u and ϵ_q represent the judgment criteria for the steady-state condition of fluid velocity and heat flux, respectively. The values of these criteria are set so that $\epsilon_u = \epsilon_q = 1.0 \times 10^{-4}$. Note that the criteria represented in Eqs. (4.37) and (4.38) must be simultaneously satisfied to obtain an optimal configuration in the heat exchange maximization problem, whereas only the criterion represented in Eq. (4.37) is considered in the pressure drop minimization problem.

4.4.2 Adjoint lattice Boltzmann equation for a thermal-fluid flow

The adjoint problem based on the LBM in the heat exchange maximization problem can be formulated as follows:

$$\begin{cases} \tilde{f}_i^*(\boldsymbol{x}-\boldsymbol{c}_i\Delta x, t-\Delta t) = \tilde{f}_i(\boldsymbol{x},t) - \frac{1}{\tau_f}\{\tilde{f}_i(\boldsymbol{x},t) - \tilde{f}_i^{\mathrm{eq}}(\boldsymbol{x},t)\} + \frac{3T}{\rho\tau_g}(\boldsymbol{c}_i - \boldsymbol{u})\cdot\tilde{\boldsymbol{q}} \\ \tilde{f}_i(\boldsymbol{x}, t-\Delta t) = \tilde{f}_i^*(\boldsymbol{x}, t-\Delta t) - 3\Delta x\alpha_\gamma(\boldsymbol{x})\boldsymbol{E}_i\boldsymbol{c}_i\cdot\tilde{\boldsymbol{m}}(\boldsymbol{x}, t-\Delta t) \\ \tilde{f}_i(\boldsymbol{x}, t_{\mathrm{f}}) = 0 \qquad \text{(Initial condition)} \\ \tilde{f}_i(\boldsymbol{x}, t) = \tilde{f}_i^{\mathrm{b}}(\boldsymbol{x}, t) \quad \text{(Boundary condition)}, \end{cases} \tag{4.39}$$

$$\begin{cases} \tilde{g}_i^*(\boldsymbol{x}-\boldsymbol{c}_i\Delta x, t-\Delta t) = \tilde{g}_i(\boldsymbol{x},t) - \frac{1}{\tau_g}\{\tilde{g}_i(\boldsymbol{x},t) - \tilde{g}_i^{\mathrm{eq}}(\boldsymbol{x},t)\} \\ \tilde{g}_i(\boldsymbol{x}, t-\Delta t) = \tilde{g}_i^*(\boldsymbol{x}, t-\Delta t) + \Delta x\beta_\gamma(\boldsymbol{x})\{1+\tilde{T}(\boldsymbol{x}, t-\Delta t)\} \\ \tilde{g}_i(\boldsymbol{x}, t_{\mathrm{f}}) = 0 \qquad \text{(Initial condition)} \\ \tilde{g}_i(\boldsymbol{x}, t) = \tilde{g}_i^{\mathrm{b}}(\boldsymbol{x}, t) \quad \text{(Boundary condition)}, \end{cases} \tag{4.40}$$

where

$$\tilde{f}_{5,8,9}^{\mathrm{b}} = \begin{cases} \tilde{f}_{3,6,7} & \text{on } \Gamma_{\mathrm{W}} \\ \tilde{f}_{3,6,7} - \frac{2(\max\{0,\mu+\sigma P\})}{3(1-v_0)} + \frac{v_0}{3(1-v_0)}\left(4\tilde{f}_3 + \tilde{f}_6 + \tilde{f}_7\right) & \text{on } \Gamma_{\mathrm{V}} \\ \tilde{f}_{3,6,7} - \frac{1}{3}(4\tilde{f}_3 + \tilde{f}_6 + \tilde{f}_7) - \frac{12T(1+3v)}{\rho_0(1-3v)}(4\tilde{g}_3 + \tilde{g}_6 + \tilde{g}_7) & \text{on } \Gamma_{\mathrm{P}}, \end{cases} \tag{4.41}$$

$$\tilde{g}_{5,8,9}^{\mathrm{b}} = \begin{cases} \frac{1+3v}{6(1-3v)}(4\tilde{g}_3 + \tilde{g}_6 + \tilde{g}_7) & \text{on } \Gamma_{\mathrm{W}} \cup \Gamma_{\mathrm{P}} \\ -\frac{1}{6}(4\tilde{g}_3 + \tilde{g}_6 + \tilde{g}_7) & \text{on } \Gamma_{\mathrm{V}}. \end{cases} \tag{4.42}$$

The detail derivation process of the above adjoint problem is described in Appendix C.

4.5 Numerical examples

Here, we confirm the utility of our proposed method. In all the numerical examples, the reference length and speed are defined as the inlet width and inlet mean velocity magnitude, respectively. Using the kinematic viscosity in Eq. (3.14), and the thermal diffusivity α_T in Eq. (4.14), the Prandtl number Pr is defined as

$$Pr = \frac{\nu}{\alpha_T}. \tag{4.43}$$

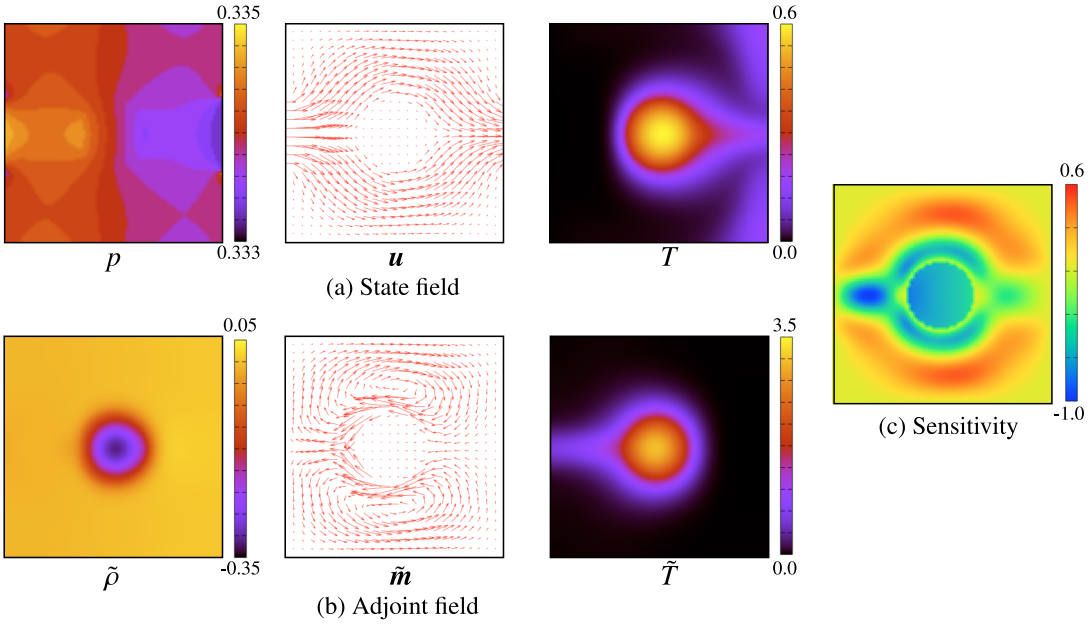

Fig. 4.1 State field (p, $\boldsymbol{u}$, T), adjoint field (ρ, $\tilde{\boldsymbol{m}}$, $\tilde{T}$), and the distribution of adjoint sensitivity in the heat exchange maximization problem using the LBM.

For all numerical examples, the initial conditions for the fluid velocity, density, and temperature are set so that $\boldsymbol{u}(\boldsymbol{x},0)=0$, $\rho(\boldsymbol{x},0)=1$ (corresponding to $p(\boldsymbol{x},0)=1/3$), and $T(\boldsymbol{x},0)=1$, respectively. Based on the initial conditions for f_i and g_i in Eqs. (3.17) and (4.17), the velocity distribution functions are $f_i(\boldsymbol{x},0)=g_i(\boldsymbol{x},0)=E_i$.

4.5.1 Validation of adjoint sensitivity

To confirm the validity of the proposed method, the design sensitivities computed using the proposed sensitivity analysis were compared with the outcome of finite differences using the same procedure as that of the previous Chapter.

At first, to confirm the relationship between the state and adjoint fields, Fig. 4.1 shows the sate field, the adjoint field, and the design sensitivity in the heat exchange maximization problem. It can be confirm that the adjoint variable $\tilde{\boldsymbol{m}}$ is circulated in the fixed design domain, and $\tilde{\rho}$ is totally different from the pressure (density). The adjoint sensitivity J_2' that is defined using $\boldsymbol{u}$, $\tilde{\boldsymbol{m}}$, T, and $\tilde{T}$ were obtained as shown in Fig. 4.1(c), in which it is indicated that the objective functional is improved by putting the heated structural domains at the positive value of the sensitivity.

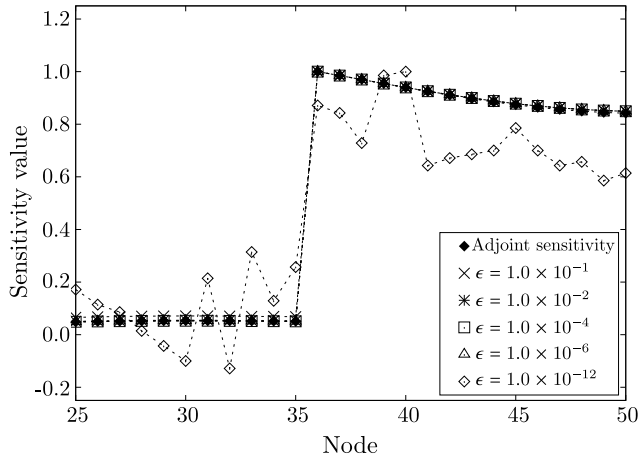

Fig. 4.2 Comparison of the adjoint sensitivity and finite difference approximation in the heat exchange maximization problem using the LBM.

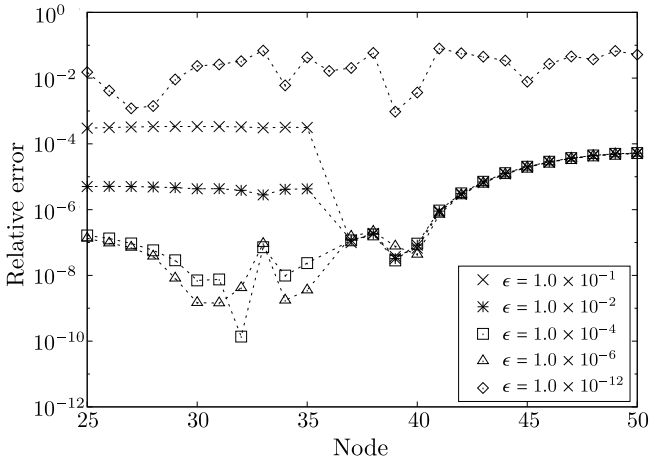

Fig. 4.3 Relative errors of the finite difference sensitivities with respect to the adjoint sensitivity in the heat exchange maximization problem using the LBM.

Next, we confirm the validity of the above adjoint sensitivity by comparing with the finite difference approximation. Here, certain nodes were selected in the design domain shown in Fig. 3.2, where the design domain is discretized using $100\Delta x \times 100\Delta x$ grids. As shown in Figs. 4.2 and 4.3, the proposed method computes sensitivities which are in agreement with the finite differences.

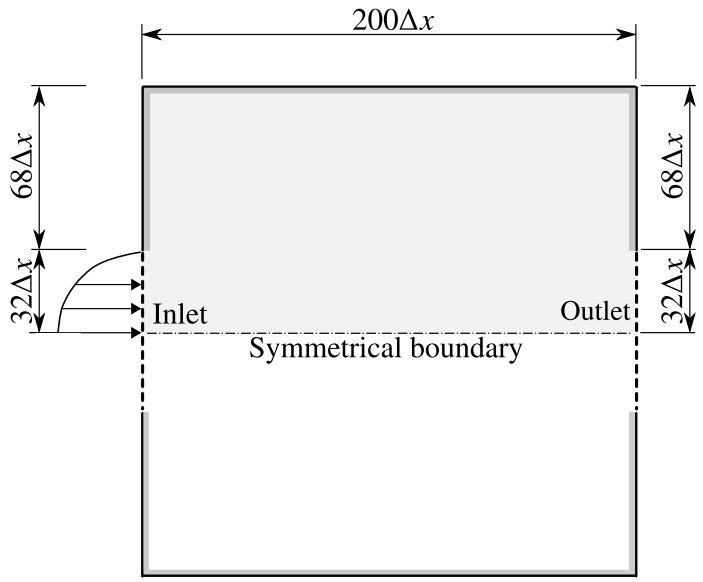

Fig. 4.4 Design settings in heat exchange maximization problem using the LBM. The analysis domain, where the symmetrical boundary condition is imposed, is discretized using $200\Delta x \times 100\Delta x$.

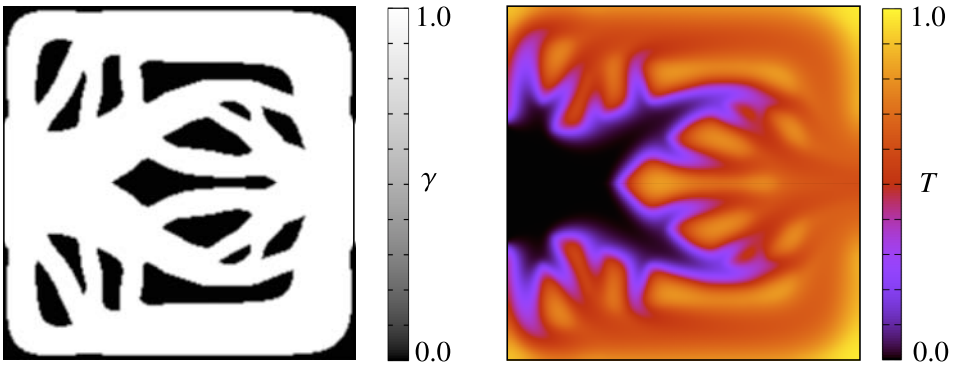

(a) Optimal configuration (b) Temperature distribution

Fig. 4.5 Heat exchange maximization problem: (a) design settings, (b) optimal configuration (black: solid, white: fluid), (c) temperature distribution.

4.5.2 Heat sink design

We now confirm the utility of the proposed method by applying it to a heat sink design problem, which is also treated in previous studies [75]. As shown in Fig. 4.4, the analysis domain is discretized using a $200\Delta x \times 100\Delta x$ grid, and a symmetrical boundary condition is

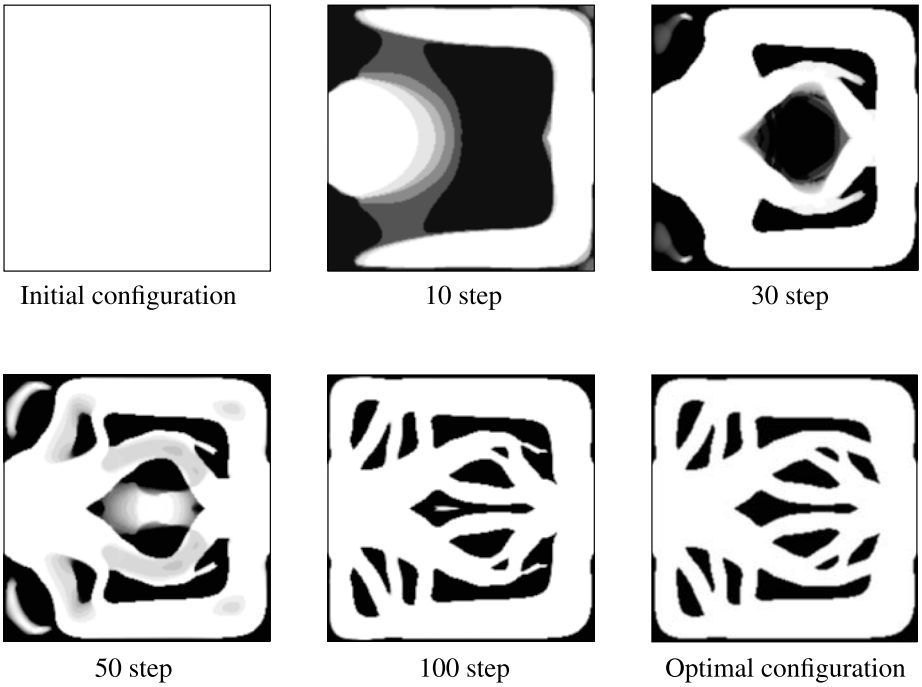

Fig. 4.6 Optimization history of design variable for the heat exchange maximization problem.

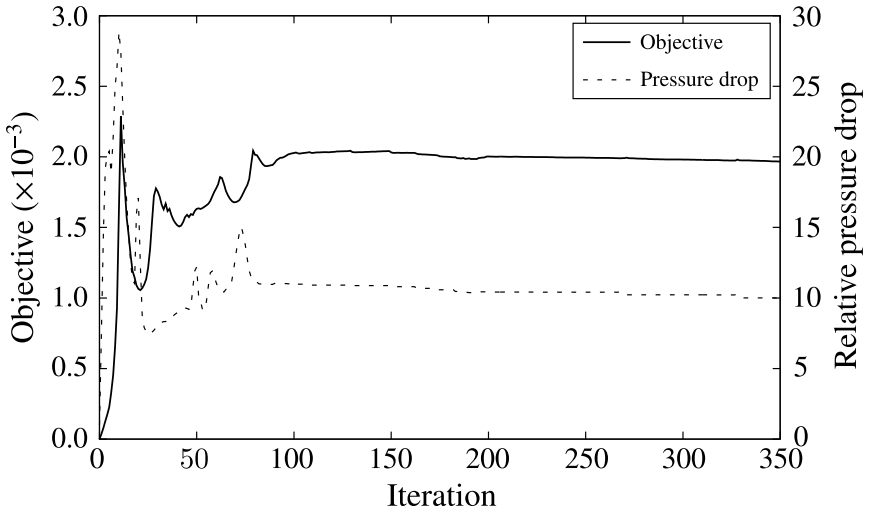

Fig. 4.7 Convergence histories of the objective functional J_2 and the relative pressure drop $\Delta p/\Delta p^{\text{init}}$, with Δp representing the current pressure drop.

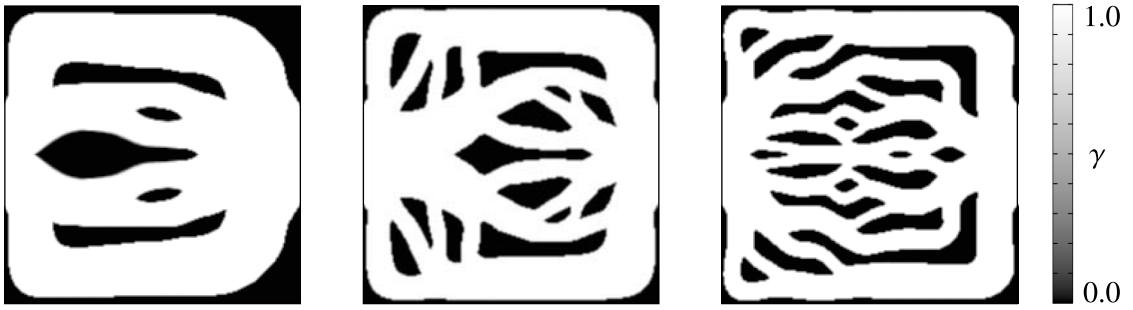

(a) $\eta_{\max} = 5$ (b) $\eta_{\max} = 10$ (c) $\eta_{\max} = 20$

Fig. 4.8 Effect of parameter $\eta_{\max}$ settings on optimal configurations: (a) $\eta_{\max} = 5$, (b) $\eta_{\max} = 10$, (c) $\eta_{\max} = 20$.

Table 4.1 Values of objective functional and relative pressure drop for different $\eta_{\max}$ settings in the heat exchange maximization problem.

$\eta_{\max}$	5	10	20
Objective ($\times 10^{-3}$)	1.41	1.96	2.34
Relative pressure drop	5.00	9.99	19.97

imposed. The initial design variable value is set to $\gamma = 1$ in the fixed design domain D. The inlet temperature is set to $T_0 = 0$ and the outlet pressure is set to $p_0 = \rho_0/3$, with $\rho_0 = 1.0$. The maximum value of inverse permeability was set to $\alpha_{\max} = 2.0 \times 10^2$.

Figures 4.5(a) and (b) show the optimal configuration and temperature distribution for parameter settings of $Re = 7$, $Pr = 6$, $\eta_{\max} = 10$, and $\beta_{\max} = 0.1$. The optimization history of the design variable γ is illustrated in Fig. 4.6, and the convergence histories of the objective functional and the pressure drop are shown in Fig. 4.7, in which both values are monotonically converged by approximately the 350th step. The optimal configuration is an appropriately complex channel that is suitable for efficient heat exchange between the fluid and solid domains. The complexity of the channel suggests that a large surface area between the fluid and solid domains is advantageous for heat exchange. This characteristic, of optimal configurations composed of geometrically complex channels, was also revealed in previous studies [75].

4.5.3 Effect of pressure drop coefficient

As described above, inequality constraint P is an essential constraint that prevents the optimal configuration from including channels with infinitesimal widths. For this reason, we investigated the effect of $\eta_{\max}$ settings on the optimal configuration.

Figure 4.8 shows the optimal results when parameter $\eta_{\max}$ is set to 5, 10, and 20. The different values of $\eta_{\max}$ result in dramatically different optimal configurations, and indicate that the allowable maximum value of the pressure drop greatly affects the geometrical complexity. That is, when the value of $\eta_{\max}$ is small, the result is a geometrically simple channel configuration, whereas a larger value of $\eta_{\max}$ produces a much more complex configuration. Table 4.1 shows the objective functional values for the three $\eta_{\max}$ settings at their respective final optimization steps. We can confirm that the proposed method enables a quantitative control of the maximum pressure drop in an optimal configuration, by setting an appropriate value of $\eta_{\max}$.

4.5.4 Effect of heat generation coefficient

Here, we investigate the effect of $\beta_{\max}$ settings on the optimal configuration. Figure 4.9(a) shows the optimal configurations for different $\beta_{\max}$ settings: $\beta_{\max} = 0.01, 0.1, 0.3$. Additionally, the temperature distributions for each $\beta_{\max}$ setting are shown in Figs. 4.9(b), (c), and (d).

Figure 4.9(a) clearly shows that the value of $\beta_{\max}$ greatly affects the geometrical complexity of the optimal configuration. Table 4.2 shows the crosscheck of objective functional values for the different optimal configurations and $\beta_{\max}$ settings. For the crosscheck, the optimal configurations were analyzed across the different $\beta_{\max}$ settings, and we can confirm that the configuration that is optimized for a certain flow condition is better than the others for its particular flow condition.

$\beta_{\max}$ is the coefficient that controls the heat generation according to the temperature difference. Thus, setting a large $\beta_{\max}$ value corresponds to the characteristic of a solid domain that is difficult to cool. In fact, as shown in Figs. 4.9(b), (c), and (d), we observe that temperatures in the solid domains tend to be high when $\beta_{\max}$ is set to a large value. Given high temperatures in the solid domains, the optimal configuration when $\beta_{\max} = 0.3$ is set to a large value is complex, with many small islands of solid distributed so that a large surface area is obtained under the prescribed maximum pressure drop. Although one might imagine that having more islands of solid in the optimal configuration to increase the

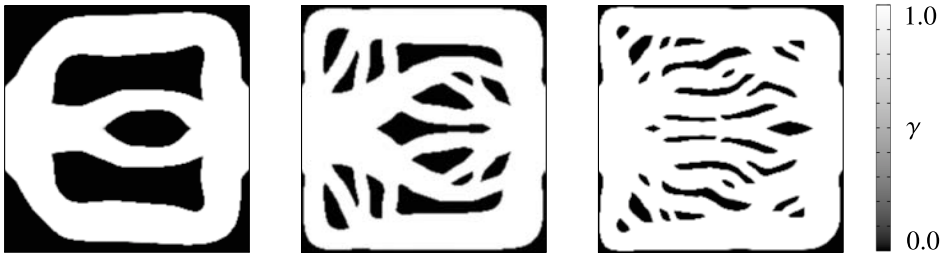

$\beta_{\max} = 0.01$ $\beta_{\max} = 0.1$ $\beta_{\max} = 0.3$

(a) Optimal configurations for different $\beta_{\max}$ values

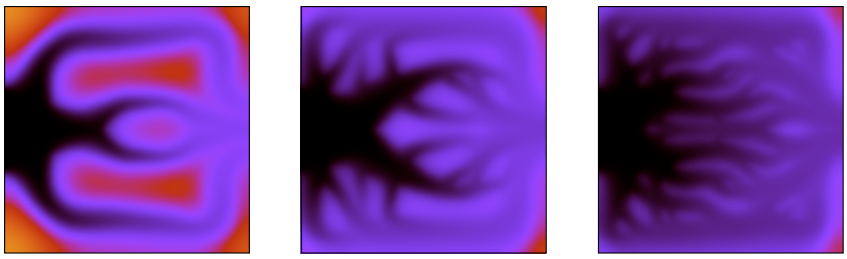

(b) Temperature distributions when $\beta_{\max} = 0.01$

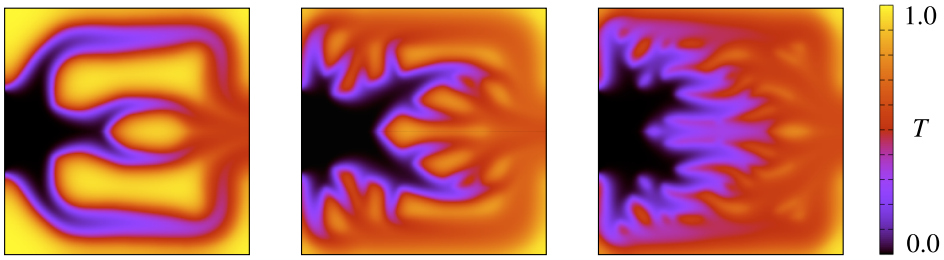

(c) Temperature distributions when $\beta_{\max} = 0.1$

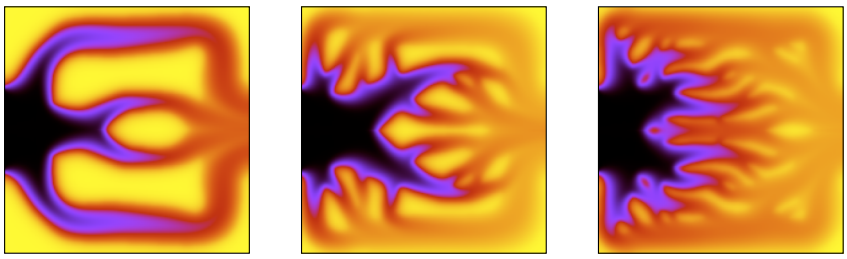

(d) Temperature distributions when $\beta_{\max} = 0.3$

Fig. 4.9 Effect of $\beta_{\max}$ settings on optimal configurations and the temperature distributions for different $\beta_{\max}$ settings: (a) Optimal configurations for different $\beta_{\max}$ values, (b) temperature distributions when $\beta_{\max} = 0.01$, (c) temperature distributions when $\beta_{\max} = 0.1$, and (d) temperature distributions when $\beta_{\max} = 0.3$.

Table 4.2 Crosscheck of objective functional values ($\times 10^{-3}$) for the heat exchange maximization problem shown in Fig. 4.9.

	Optimization $\beta_{\max}$		
Analysis $\beta_{\max}$	0.01	0.1	0.3
0.01	**0.63**	1.61	1.91
0.1	0.50	**1.96**	2.46
0.3	0.37	1.81	**2.50**

Table 4.3 Relative volume of fluid, defined as $\int_D \gamma \mathrm{d}\Omega / \int_D \mathrm{d}\Omega$, for the optimal configurations in Fig. 4.9(a), when different $\beta_{\max}$ settings in the heat exchange maximization problem.

$\beta_{\max}$	0.01	0.1	0.3
Relative volume of fluid	0.58	0.76	0.83

objective functional value would be an improvement, we note that this would violate the pressure drop constraint.

On the other hand, the optimal configuration when setting $\beta_{\max} = 0.01$ is geometrically simple, with only three large islands of solid. In this scenario, the total volume of solid domains takes precedence over the surface area, to increase the objective functional. Table 4.3 shows the fluid volume in the design domain for each optimal configuration shown in Fig. 4.9, and we observe that the fluid volume is increased as the value of $\beta_{\max}$ is increased. As shown in the left figure of 4.9(b), the interior of the solid domains are relatively cool due to the small value of $\beta_{\max}$, which corresponds to a small heat generation condition. On the other hand, when a larger value of $\beta_{\max}$ is set, as shown in the left figure in 4.9(d), the temperature distribution for the solid domains except in the vicinity of their boundaries is given as $T \approx 1$, which does not lead to improvement of the objective functional value. As a result, the optimal configurations shown in Fig. 4.9(a) can be viewed as being the most appropriate configurations for each flow condition.

4.6 Summary

This chapter presented a topology optimization method for thermal-fluid flow using the LBM incorporating the sensitivity analysis based on the discrete velocity Boltzmann equation.

The presented method was applied to the heat exchange minimization problem under the prescribed maximum pressure drop.

Optimal configurations for the heat exchange maximization problem were obtained, and the dependency of the optimal configurations with respect to settings of the pressure drop coefficient $\eta_{\max}$ was investigated. Based on the results, it was clarified the relationship between pressure drop coefficient settings and the geometrical complexity of the optimal configurations. That is, setting $\eta_{\max}$ to a relatively large value leads to an optimal configuration that has a complex channel configuration, whereas a relatively small value of this parameter results in a simpler geometry. In addition, the effects of $\beta_{\max}$was investigated. It was found that the optimal configurations strongly depend on the each parameter settings, and the proposed method can derive an appropriate result, which is composed of a complex channel that is a promising configuration to improve the objective functional with considering the prescribed pressure drop constraint.

Chapter 5

Two-phase fluid flow channel design

5.1 Introduction

The aim of this chapter is to construct a topology optimization method for the design of a flow channel considering two-phase fluid flows. Using this approach, fluidic devices such as two-phase microchannels can be designed so that they achieve a desired flow and accomplish maximal mixing and reaction, or extraction efficiencies.

These performances strongly depend on the design of the channel configuration, so that each process, such as mixing, reaction, or extraction, is finished as quickly as possible. In addition, to prevent damage to the microchannels, minimizing the pressure drop in the microchannel system is an important factor. Thus, to meet the most important design requirements of a two-phase microchannel, the maximization of the above efficiencies and the minimization of the pressure drop must be simultaneously considered. Designer intuition alone, however, seldom yields an optimal channel configuration that sufficiently satisfies these requirements. To overcome this problem, topology optimization is a particularly powerful approach for obtaining useful designs for the channel configuration of the devices under consideration here.

Based on this methodology, Okkels and Bruus [83] proposed a topology optimization method for the design of a micro reactor in which the reaction effect is mathematically modeled, and the aim was to achieve maximal reaction efficiency in the microchannel system given a uniform concentration of reactants. Andreasen et al. [7] proposed a topology optimization method for the design of a micro mixer in which maximization of mixing performance was the aim. And Makhija et al. [74] applied the LBM in mixing performance

maximization problem and investigated the relationship between the mixing performance and the pressure drop.

The basic idea of the above optimization methodologies for multi-component fluid flows is the introduction of concentration, governed by a convective-diffusion equation, into the formulation of the optimization problem. That is, since the fluid flow is not affected by concentration (one-way coupling), the above research cannot treat fluid flows of immiscible fluids in which the interface effect between the different phases must be considered. In particular, since the extraction process strongly depends on the difference between mass diffusivities in two-phase fluid flows [135], the conventional approach must be extended so that flows can be treated in extraction efficiency maximization problems.

Here, a new topology optimization method for an extraction efficiency maximization problem is constructed. In this method, two-phase fluid flows with the same density are analyzed based on the two-phase LBM proposed by Inamuro et al. [49]. In the LBM, mass and momentum are preserved even if a special treatment for tracking an interface is not conducted. It is well-known that the LBM is therefore suitable for the computation of multiphase fluid flows. In the following section, the basic concept of the two-phase LBM is discussed and the topology optimization problem is formulated for the extraction efficiency maximization problem. The numerical implementations and optimization algorithms are then explained and, finally, we provide a numerical example to validate the utility of the proposed method.

5.2 Two-phase lattice Boltzmann method with the same density

We now discuss the concept of the two-phase LBM [49] that will be applied here to incompressible fluids while considering two-phase fluid flows under identical density conditions. In the following, we use the non-dimensional variables shown in Appendix A. Here, we use the two-dimensional nine-velocity model, and two particle velocity distribution functions, f_{Ai}, and f_{Bi}. The function f_{Ai} is used for obtaining an index function that represents an interface profile between the phase X and phase Y, and f_{Bi} is used for computing the pressure and velocity of the two-phase fluid flows.

The evolution of the particle distribution functions $f_{Ai}(\boldsymbol{x},t)$ and $f_{Bi}(\boldsymbol{x},t)$ with velocity $\boldsymbol{c}_i$ at point $\boldsymbol{x}$ and at time t are computed with the following equations:

$$f_{Ai}(\boldsymbol{x}+\boldsymbol{c}_i\Delta x)-f_{Ai}(\boldsymbol{x},t)=\frac{1}{\tau_A}\left\{f_{Ai}(\boldsymbol{x},t)-f_{Ai}^{\mathrm{eq}}(\boldsymbol{x},t)\right\}, \tag{5.1}$$

$$f_{Bi}(\boldsymbol{x}+\boldsymbol{c}_i\Delta x)-f_{Bi}(\boldsymbol{x},t)=\frac{1}{\tau_B}\left\{f_{Bi}(\boldsymbol{x},t)-f_{Bi}^{\mathrm{eq}}(\boldsymbol{x},t)\right\}, \tag{5.2}$$

where f_{Ai}^{eq} and f_{Bi}^{eq} are equilibrium distribution functions, τ_A and τ_B represents non-dimensional single relaxation times.

The index function $\psi(\boldsymbol{x},t)$, pressure $p(\boldsymbol{x},t)$, and velocity $\boldsymbol{u}(\boldsymbol{x},t)$ are defined as follows:

$$\psi=\sum_{i=1}^{9}f_{Ai}\,, \tag{5.3}$$

$$p=\frac{1}{3}\sum_{i=1}^{9}f_{Bi}\,, \tag{5.4}$$

$$\boldsymbol{u}=\sum_{i=1}^{9}\boldsymbol{c}_i f_{Bi}\,. \tag{5.5}$$

Note that the definition of $\boldsymbol{u}$ is different from the standard one. The equilibrium distribution functions $f_{Ai}^{\mathrm{eq}}(\boldsymbol{x},t)$, and $f_{Bi}^{\mathrm{eq}}(\boldsymbol{x},t)$ are given by

$$f_{Ai}^{\mathrm{eq}}=H_i\psi+F_i\left(p_0-\kappa_f\psi\nabla^2\psi\right)+3E_i\psi\boldsymbol{c}_i\cdot\boldsymbol{u}+E_i\kappa_f\boldsymbol{G}:(\boldsymbol{c}_i\otimes\boldsymbol{c}_i), \tag{5.6}$$

$$f_{Bi}^{\mathrm{eq}}=E_i\left\{3p+3\boldsymbol{c}_i\cdot\boldsymbol{u}-\frac{3}{2}|\boldsymbol{u}|^2+\frac{9}{2}(\boldsymbol{c}_i\cdot\boldsymbol{u})^2\right\}+E_i\kappa_g\boldsymbol{G}:(\boldsymbol{c}_i\otimes\boldsymbol{c}_i), \tag{5.7}$$

where parameters E_i, H_i, and F_i are defined so that $E_1=4/9$, $E_2=E_3=E_4=E_5=1/9$, $E_6=E_6=E_8=E_9=1/36$, $H_1=1$, $H_2=H_3=\cdots=H_9=0$, $F_1=-7/3$, and $F_i=3E_i$ ($i=2,3,\cdots,9$). κ_f and κ_g are parameters with constant values that determine the width of the interface and the strength of the interfacial tension, respectively. The tensor $\boldsymbol{G}(\psi)$ is defined as follows:

$$\boldsymbol{G}=\frac{9}{2}\nabla\psi\otimes\nabla\psi-\frac{3}{2}|\nabla\psi|^2\boldsymbol{\delta}, \tag{5.8}$$

where $\boldsymbol{\delta}$ represents the Kronecker delta. In addition, $p_0(\psi)$ is given by

$$p_0=\psi\bar{T}\frac{1}{1-b\psi}-a\psi^2, \tag{5.9}$$

where a, b, and $\bar{T}$ are parameters for determining the profile of index function ψ.

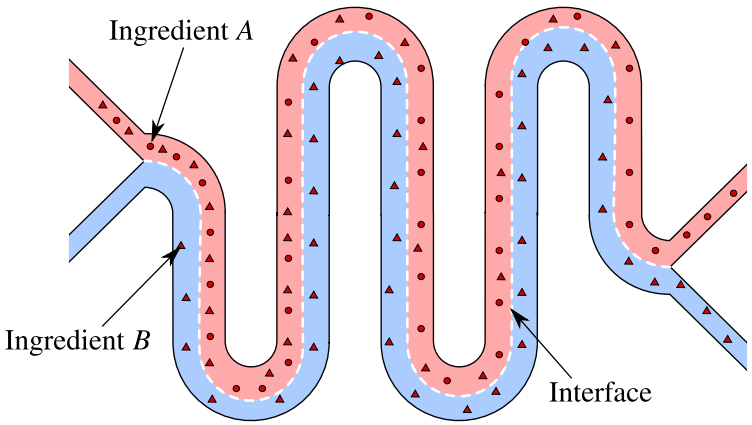

Fig. 5.1 Schematic diagram of liquid-liquid extraction in microchannel device.

Applying the asymptotic theory to Eqs. (5.1)–(5.9), we find that the macroscopic variables, ψ, and p and $\boldsymbol{u}$, respectively satisfy the Cahn-Hilliard equation including the advection term, and the Navier-Stokes equations (NSE). Note that the pressure is given by $p + (2/3)\kappa_g \nabla|\psi|^2$ in the interface [49].

5.3 Model of the liquid-liquid extraction

The extraction is the one of separation operation for extracting ingredients from a solvent by using two kind of solvents that have different molecular diffusive coefficients each other.

Among them, the liquid-liquid extraction that uses two immiscible solvents is often utilized in chemical analysis dealing with microchannel devices. As shown in Fig. 5.1, the basic principal of liquid-liquid extraction is that the ingredient B is only to be moved from the red phase composed by the mixture of ingredients A and B.Žnidarši č-Plazl and Plazl [135] proposed a mathematical model for simulating this extraction phenomenon by using a convective-diffusion equation for a passive scalar.

Based on this model and the two-phase LBM, a topology optimization method for the design of extraction microchannel is constructed. Although the convective-diffusion equation can be solved using a general numerical scheme such as the finite difference method, the LBM to solve the scalar transport problem is employed for the simplicity of numerical algorithm. That is, based on the previous chapter for the thermal-fluid problems, the lattice

Boltzmann equation (LBE) is introduced as follows:

$$f_{Ci}(\boldsymbol{x}+\boldsymbol{c}_i\Delta x)-f_{Ci}(\boldsymbol{x},t)=\frac{1}{\tau_C}\left\{f_{Ci}(\boldsymbol{x},t)-f_{Ci}^{\mathrm{eq}}(\boldsymbol{x},t)\right\}, \tag{5.10}$$

where f_{Ci}^{eq} is the equilibrium distribution functions for the scalar field T, and is given by

$$f_{Ci}^{\mathrm{eq}}=E_iT(1+3\boldsymbol{c}_i\cdot\boldsymbol{u}). \tag{5.11}$$

The scalar field $T(\boldsymbol{x},t)$ is defined as

$$T=\sum_{i=1}^{9}f_{Ci}\,. \tag{5.12}$$

In addition, the mass diffusivity κ is given by

$$\kappa=\frac{1}{3}\left(\tau_C-\frac{1}{2}\right)\Delta x. \tag{5.13}$$

As previously mentioned, since the liquid-liquid extraction is conducted by using two solvents that have different molecular diffusive coefficients each other, the relaxation time τ_C is expanded as follows:

$$\tau_C(\psi)=\frac{\psi_0^Y-\psi}{\psi_0^Y-\psi_0^X}\tau_C^X+\frac{\psi-\psi_0^X}{\psi_0^Y-\psi_0^X}\tau_C^Y, \tag{5.14}$$

where τ_C^X and τ_C^Y presents each relaxation time parameter for the phase X and Y, ψ_0^X, and ψ_0^Y are a reference value of order parameter. Note that the extraction is sufficiently completed when the scalar field T achieves the equilibrium state. And, the optimization problem should be formulated so that this equilibrium state is observed at the outlet of fluidic system defined as the fixed design domain.

5.4 Formulation of a topology optimization problem

The topology optimization problem for the design of a flow channel dealing with two-phase fluid flows is formulated. A schematic diagram of this problem is shown in Fig. 5.2, with fixed domain D composed of the fluid domain Ω and the solid domain $D\setminus\Omega$. The inlet boundary condition includes a prescribed velocity, $\boldsymbol{u}=\boldsymbol{u}_{\mathrm{in}}$ at Γ_{in}, and the outlet boundary

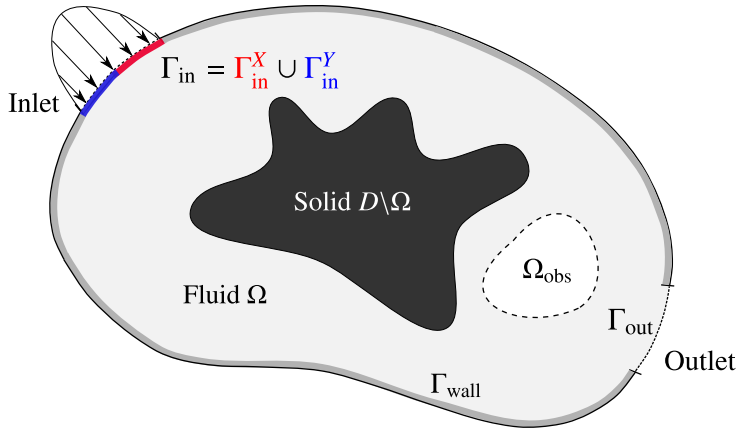

Fig. 5.2 Schematic figure of fixed design domain D composed of the fluid domain Ω, solid domain $D \setminus \Omega$ and observation domain Ω_{obs}. The boundary of fixed design domain is defined as $\Gamma = \Gamma_{\text{in}} \cup \Gamma_{\text{out}} \cup \Gamma_{\text{wall}}$ with $\Gamma_{\text{in}} \cap \Gamma_{\text{out}} \cap \Gamma_{\text{wall}} = \emptyset$.

condition includes a prescribed pressure, $p = p_{\text{out}}$ at Γ_{out}. At the inlet boundary Γ_{in}, the order parameters ψ and concentrations T are respectively set to $\psi = \psi_{\text{in}}^X$ at Γ_{in}^X, $\psi = \psi_{\text{in}}^Y$ at Γ_{in}^Y, $T = T_{\text{in}}^X$ at Γ_{in}^X, and $T = T_{\text{in}}^Y$ at Γ_{in}^Y, where $\Gamma_{\text{in}} = \Gamma_{\text{in}}^X \cup \Gamma_{\text{in}}^Y$ and $\Gamma_{\text{in}}^X \cap \Gamma_{\text{in}}^Y = \emptyset$. In addition, the boundary condition for ψ and T at $\Gamma_{\text{out}} \cup \Gamma_{\text{wall}}$ is set to a Neumann condition, with $\partial\psi/\partial\boldsymbol{n} = \boldsymbol{0}$ and $\partial T/\partial\boldsymbol{n} = \boldsymbol{0}$.

The important requirements in the design of extraction channel are shown as follows:

- The extraction is sufficiently completed at the outlet of channel;
- The pressure drop in the fluidic system is small as much as possible.

The first requirement can be satisfied by using a long channel, but such channel commonly occurs the large pressure drop between the inlet and outlet. In particular, since the large pressure drop can lead the damage to microchannel devices, the reduction of pressure drop is important element.

To simultaneously evaluate the extraction efficiency and pressure drop, we consider the following optimization problem:

$$\begin{cases} \inf\limits_{\gamma} \quad J_3 = \int_I \int_{\Omega_{\text{obs}}} \frac{(T - \langle T \rangle_{\text{in}})^2}{2\langle T \rangle_{\text{in}}^2} \mathrm{d}\Omega \mathrm{d}t \\ \text{s.t.} \quad P = \int_I \int_{\Gamma_{\text{in}}} p \, \mathrm{d}\Gamma \mathrm{d}t - \int_I \int_{\Gamma_{\text{out}}} p \, \mathrm{d}\Gamma \mathrm{d}t - \eta_{\max} \Delta p^{\text{init}} \leqslant 0 \\ \gamma \in \mathfrak{X}_{\text{ad}}, \end{cases} \tag{5.15}$$

where $\langle T \rangle_{\text{in}}$ is the average value of T at the inlet boundary. In the above optimization problem, the objective functional J_3 represents the relative error of T with respect to $\langle T \rangle_{\text{in}}$ in the observation domain, $\Omega_{\text{obs}} \subset D$. The phase X and phase Y concentrations are set to different values, i.e., $T_{\text{in}}^X \neq T_{\text{in}}^Y$. Thus, J_3 seldom becomes equal to zero during the optimization process. It is assumed that the extraction process is completely finished when the value of J_3 does become equal to zero.

In addition, the KKT conditions as the first order optimality condition are give by

$$\begin{aligned} &\bar{J}_3' = 0, \quad \mu P = 0 \quad \mu \geqslant 0, \quad \lambda V = 0, \quad \lambda \geqslant 0, \\ &l_0 \gamma(\boldsymbol{x}) = 0, \quad l_0 \geqslant 0, \quad l_1(\gamma - 1) = 0, \quad l_1 \geqslant 0, \end{aligned} \tag{5.16}$$

where $\mu \in \mathbb{R}$, $\lambda \in \mathbb{R}$, $l_0(\boldsymbol{x}) \in L^\infty(D)$, and $l_1(\boldsymbol{x}) \in L^\infty(D)$ represent the Lagrange multiplier for each inequality constraint, and $\bar{J}_3'(\boldsymbol{x})$ is the design sensitivity defined as the Gâteaux derivative in Eq. (3.25) with respect to the Lagrangian $\bar{J}_3 = J + \mu P + \lambda V + l_0 \gamma + l_1(\gamma - 1)$. Note that the design sensitivity $\bar{J}_3'$ is derived based on the adjoint LBM described in previous Chapters 3 and 4.

5.5 Numerical implementation

The optimization algorithm of the proposed method is now described.

Step 1. The initial design variable is set in the fixed design domain D.

Step 2. The LBE for the extraction maximization problem, are calculated until a steady-state condition is satisfied.

Step 3. If the criteria of the objective functional and inequality constraint are satisfied, an optimal configuration is obtained and the optimization is finished, otherwise the adjoint equations are calculated and the procedure advances to Step 4.

Step 4. The design sensitivity $\bar{J}_3'$ is calculated using the current state and adjoint variables.

Step 5. The design variable is updated using the MMA, after which the optimization procedure returns to Step 2 of the iterative loop.

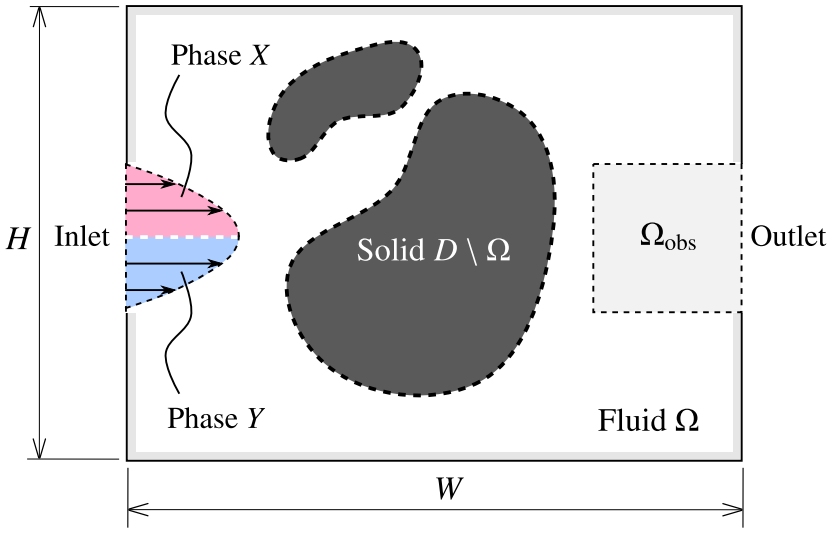

Fig. 5.3 Design domain is composed of the fluid domain Ω and the solid domain $D \setminus \Omega$. The objective functional J_3 is evaluated in the observation domain Ω_{obs}. The two-phase fluid flows are composed of the phase X and Y that are prescribed on the inlet boundary.

5.6 Numerical examples

Here, numerical examples using the proposed method are provided. Figure 5.3 shows the design settings in the extraction efficiency maximization problem. The analysis domain is discretized using a $W \times H$ grid, and the volume constraint is set with $V_{\max} = 0.6$. The main parameters for the two-phase LBM are shown in Table 5.1. The other parameters for the LBM were set to same values in the previous study [49].

Table 5.1 Setting parameters for the two-phase LBM with the same density in the extraction efficiency maximization problem.

Parameters	Values
U_{in}	5.3×10^{-2}
p_{out}	0.33
Re	10
$(\psi^X_{\mathrm{in}}, \psi^Y_{\mathrm{in}})$	$(0.40, 0.26)$
$(T^X_{\mathrm{in}}, T^Y_{\mathrm{in}})$	$(1.0 \times 10^{-2}, 1.0)$
(κ^X, κ^Y)	$(1.0 \times 10^{-3}\Delta x, 1.8 \times 10^{-2}\Delta x)$

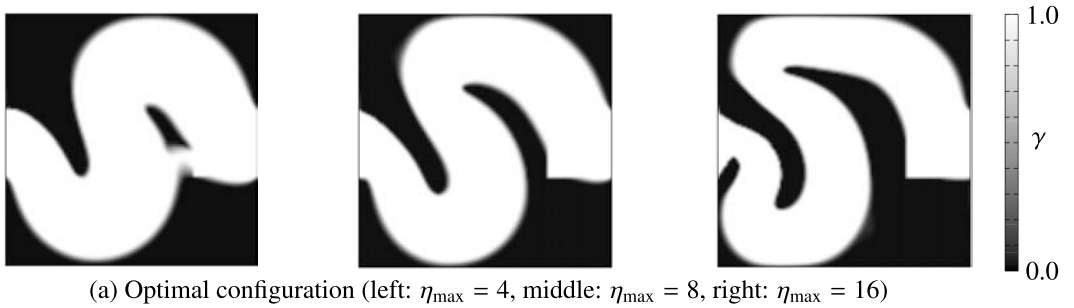

(a) Optimal configuration (left: $\eta_{\max} = 4$, middle: $\eta_{\max} = 8$, right: $\eta_{\max} = 16$)

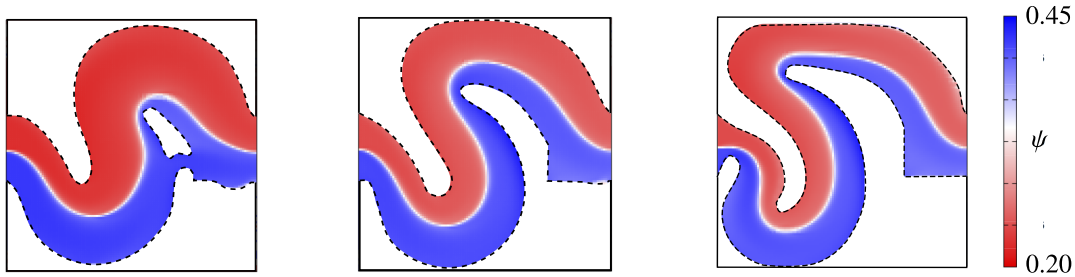

(b) Order parameter ψ

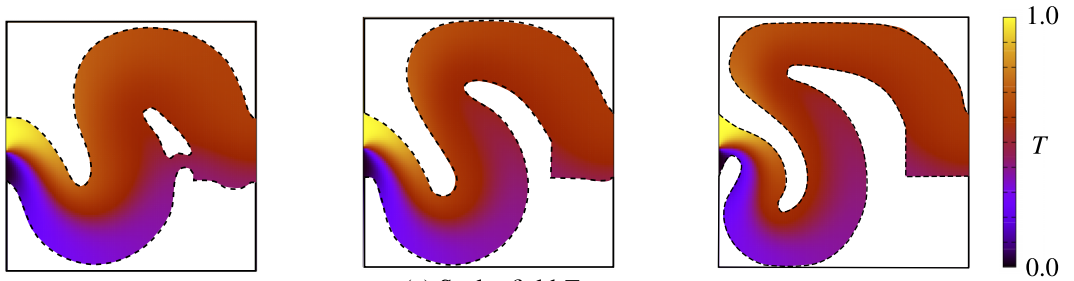

(c) Scalar field T

Fig. 5.4 Optimal configurations in the extraction efficiency maximization problem, with the distributions of order parameter ψ and scalar field T in the different settings of pressure drop coefficient: $\eta_{\max} = 4$ (left side figures); $\eta_{\max} = 8$ (middle figures); $\eta_{\max} = 16$ (right side figures).

5.6.1 Effect of pressure drop coefficient

Figure 5.4 shows the optimal configurations in different $\eta_{\max}$ settings: $\eta_{\max} = 4, 8, 16$. The analysis domain is discretized using $W \times H = 120\Delta x \times 120\Delta x$. As shown in Fig. 5.4, a sinuous channel is obtained as an optimal channel, which is a suitable shape that sufficiently diffuses the concentration so that the extraction is sufficiently completed. The distribution of concentration T is shown in Fig. 5.4(c). It can be confirmed that the interface between phase X and phase Y is expressed by the order parameter value, whose distribution is shown

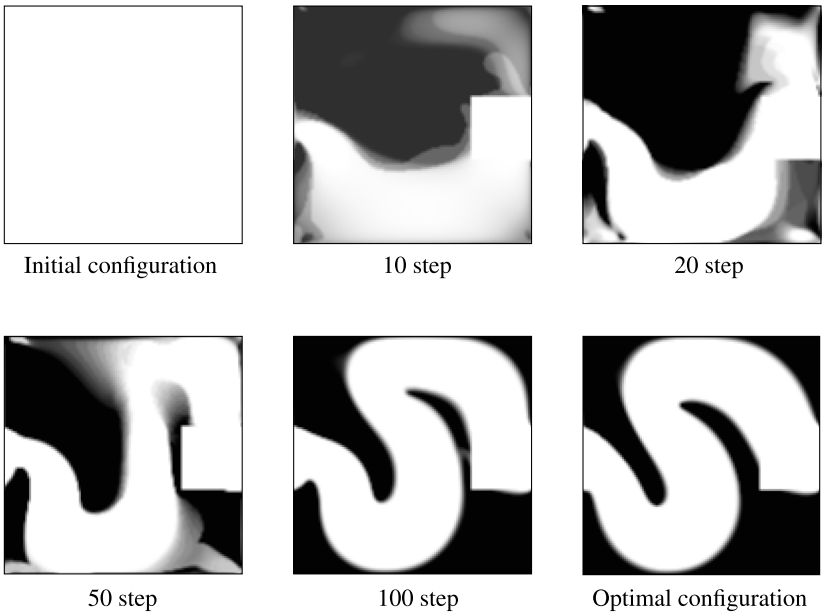

Fig. 5.5 Optimization history of design variable for the extraction efficiency maximization problem.

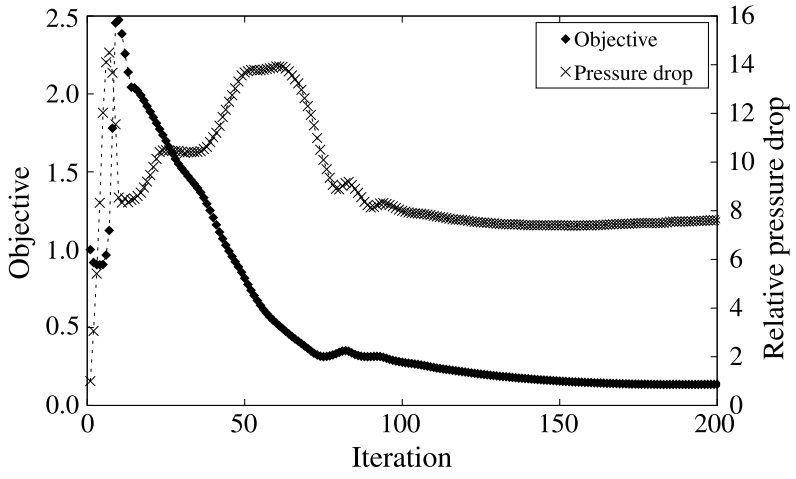

Fig. 5.6 Convergence histories of the relative objective functional $\hat{J}_3 = J_3/J_3^{\text{init}}$, with J_3^{init} representing the initial value of the objective functional, and the relative pressure drop $\Delta p/\Delta p^{\text{init}}$, with Δp representing the current pressure drop in the extraction efficiency maximization problem.

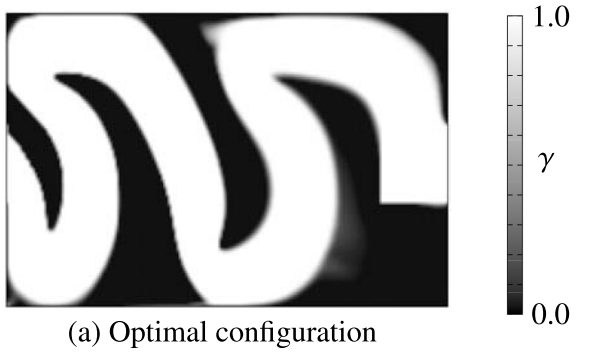

(a) Optimal configuration

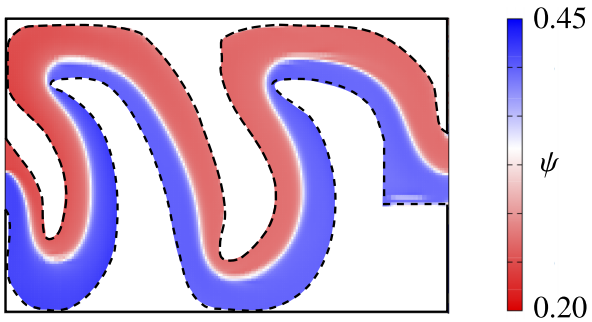

(b) Order parameter ψ

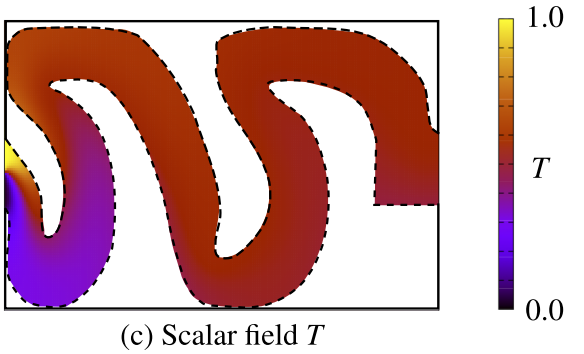

(c) Scalar field T

Fig. 5.7 Optimal configuration for the extraction efficiency maximization problem when setting $\eta_{\max} = 25$, with the distributions of order parameter ψ and scalar field T.

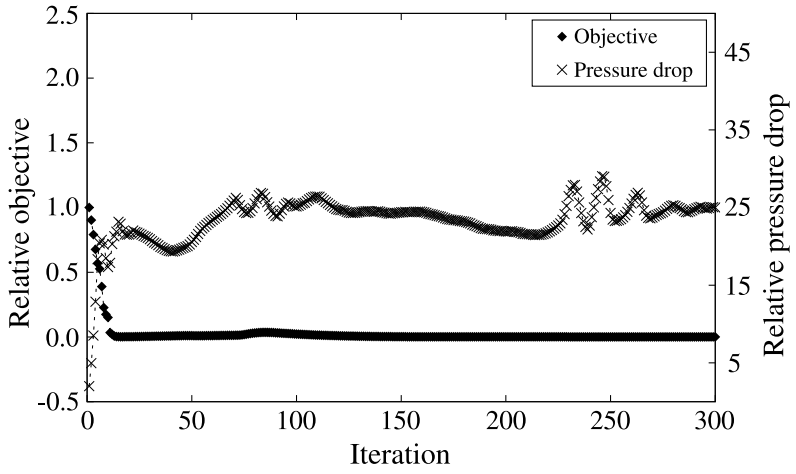

Fig. 5.8 Convergence histories for the extraction efficiency minimization problem in the case of $200\Delta x \times 120\Delta x$ grids with $\eta_{\max} = 25$. Normalized values of objective functional $\hat{J}_3 = J_3/J_3^{\text{init}}$, with J_3^{init} representing the initial value of the objective functional. Pressure drop fraction $\Delta p/\Delta p^{\text{init}}$, with Δp representing the current pressure drop.

Table 5.2 Values of objective functional J_3 and relative pressure drop for different $\eta_{\max}$ settings in the extraction efficiency maximization problem.

$\eta_{\max}$	4	8	16
Objective	0.30	0.17	0.14

in Fig. 5.4(b). The optimization history is shown in Fig. 5.5, the convergence histories of objective functional and pressure drop in the case of $\eta_{\max} = 8$ are shown in Fig. 5.6, and the final values of objective functional in each optimal configuration in Fig, 5.4 are shown in Table 5.2. As shown in Fig. 5.6, the pressure drop constraint is appropriately satisfied and the value of J_3 is sufficiently converged.

Note that the obtained optimal configuration is similar to the results of previous study [74, 73], in which the fluid flows are treated as miscible fluids that are governed by the NSE and the convective-diffusion equation.

5.6.2 Effect of aspect ratio of the analysis domain

Next, a numerical example where the design domain was discretized using a $W \times H = 200\Delta x \times 120\Delta x$ grid is provided. The numerical parameters were set as the same in Section 5.6.1, while the pressure drop coefficient was set to $\eta_{\max} = 25$. As shown in Fig. 5.7, it can be confirmed that the optimal configuration is to be more sinusoidal channel than the examples in Fig. 5.4 where the design domain is discretized using a $W \times H = 120\Delta x \times 120\Delta x$ grid. The value of objective functional J_3 in Fig. 5.7 is shown in Fig. 5.8, in which the pressure drop constraint is appropriately satisfied and the value of J_3 is sufficiently converged to zero that means the extraction process is sufficiently finished. Note that it is necessary to set a lager number of $\eta_{\max}$ in order to obtain such complex flow channel, since the complex channel causes the large pressure drop between the inlet and outlet of the design domain.

5.7 Summary

This chapter proposed a topology optimization method using a two-phase LBM with the same density for the design of a liquid-liquid extraction microchannel. The extraction process was modeled using concentration values governed by a convective-diffusion equation that is solved using the LBM. The optimization problem was formulated as an extraction efficiency maximization problem in which the uniform concentration is aimed so that the extraction process is sufficiently completed in the vicinity of outlet. In addition, the inequality constraint for the pressure drop was imposed to restrict the maximum pressure drop that can be controlled using a parameter called the pressure drop coefficient. The presented method was applied to an extraction efficiency maximization problem and several numerical examples demonstrated the utility of the proposed method. it was found that the optimal configuration depends on the pressure drop coefficient and the size of design domain, and there is a trade-off relationship between the extraction efficiency and the pressure drop in the fluidic system.

Chapter 6

General conclusions

This thesis focused on topology optimization for the design of flow channel, in which the fluid flow is calculated using the LBM. The following is a summary of achievements.

In Chapter 2, the basic idea of topology optimization was introduced, and the two popular approaches, i.e., the density and level set-based approaches, were presented. As an application of topology optimization for fluid dynamics problems, the heat exchange maximization problem was formulated on the basis of NSE. A level set-based topology optimization method was employed to derive an optimal configuration that has clear boundaries without grayscales. A non-dimensional parameter θ was defined for formulating the optimization problem, in which a Dirichlet boundary condition was imposed based on the prescribed pressure difference between the inlet and outlet. Based on the proposed formulation, several numerical examples for the design of heat sink device were obtained. Four different optimal configurations obtained for each numerical example allowed us to confirm the dependency of optimal configurations on the parameter θ, with higher θ resulting in more complex configurations. It was confirmed that the geometric complexity of optimal configuration can be qualitatively controlled by setting a regularization parameter to an appropriate value. A design engineer can therefore obtain flow channel designs for thermal device problems such as heat sinks that have a geometric layout that corresponds to a desired level of performance and manufacturability.

In Chapter 3, A topology optimization using the LBM was offered. The proposed method was applied to the flow resistance minimization problems for incompressible viscous flow. The optimization problem was formulated using the discrete Boltzmann equation, so that the accurate boundary conditions generally used in the LBM could be incorporated in the optimization problem formulation, and to enable a derivation of adjoint system in which the

boundary conditions for the adjoint equation reflect the boundary conditions of the LBM. It was demonstrated that the adjoint discrete Boltzmann equation can be discretized using the LBM, in contrast to previous research in which the use of the LBM required large-scale matrix operations due to the use of a typical strategy of sensitivity analysis based on the discrete formulation. That is, the proposed method enables the design sensitivity to be completely derived without matrix operations. In addition, due to the characteristics of explicit scheme, the converged state variable values and adjoint variable values at each optimization step were used as initial values when calculating the time evolution equation in the next optimization step, which greatly reduced computational cost. Based on the proposed formulation, several numerical examples for both two- and three-dimensional optimization problems were provided to confirm the validity and utility of the presented method for the flow resistance minimization problem. For the validation of proposed method, the design sensitivity that is derived using the sensitivity analysis based on the discrete Boltzmann equation was compared with the numerical result of direct method based on the finite different approximation. The result showed that the adjoint sensitivity is in good agreement with the finite difference approximation, confirming that the proposed sensitivity analysis yields an appropriate and useful solution. The diffuser and pipe bend problems were treated for bench mark problems, and it was found that the presented method obtains an optimal configuration similar to that when using an FEM-based method. In addition, it was also found that the presented method obtains optimal configurations that show minimal dependency upon the mesh size and dependency with respect to Reynolds number settings.

In Chapter 4, the topology optimization method using the LBM constructed in Chapter 3 was applied to a thermal-fluid coupling optimization problem. The heat exchange maximization problem that is also treated in Chapter 2 was formulated using the discrete Boltzmann equations, which corresponds to the NSE and the convective-diffusion equations as the macroscopic equations, respectively. An inequality constraint for restricting the maximum pressure drop was newly introduced, to quantitatively evaluate the pressure drop between the inlet and outlet in the design domain. The design sensitivity was derived using the adjoint variable method in which the adjoint equations were solved using the LBM, and the adjoint sensitivity was compared with the numerical result of direct method based on the finite difference approximation for the validation of proposed method. Numerical results showed that the proposed method successfully found optimal configurations for the design of heat sink. In addition, it was found that the maximum pressure drop in the fluidic system

can be appropriately controlled by setting the pressure drop coefficient parameter, and the geometrical complexity of optimal configuration is dependent on the value of pressure drop coefficient and the other parameters.

In Chapter 5, a topology optimization method for two-phase fluid problem was constructed based on the methods constructed in Chapter 3 and 4, in which the discrete Boltzmann equations are employed to formulate the optimization problems as the continuous formulation, whereas the particle velocity space is only discretized for incorporating the accurate boundary conditions in the LBM. To improve the performance of liquid-liquid extraction that is often utilized as the separation operation, the extraction efficiency maximization problem was formulated for the design of microchannel. Since the basic principal of the extraction is to use two kind of solvents that have different mass diffusivities each other, the two-phase LBM with the same density was used for computing the immiscible fluid flows. Additionally, based on a mathematical model for the liquid-liquid extraction, a passive scalar field, which represents the extraction phenomenon and is governed by the convective-diffusion equation, were introduced. The objective functional was defined as the error norm for the uniform concentration that corresponds to be finished the extraction process in the microchannel. In addition, the pressure drop constraint used in Chapter 4 was also imposed, to appropriately evaluate the pressure drop between the inlet and outlet in the extraction channel. Numerical results showed that the proposed method found optimal configurations that enables the concentration to be uniformed for achieving high-performance extraction channel, under the prescribed maximum pressure drop. It was found that the optimal configuration depends on the setting of pressure drop coefficient and the aspect ratio of the design domain.

Concluding, this thesis developed the topology optimization for fluid dynamics problems using the LBM, whereas typical topology optimization approaches for fluid flow problems were constructed based on the NSE in which the FEM is generally employed, due to its simple formulation based on the conventional framework for deriving the design sensitivity. Since the LBM is accompanied by several advantages including simplicity, parallelism, scalability and applicability to complex flow problems such as porous and immiscible fluids. It is my hope that this thesis will be useful to the design of flow channels that provide enhanced performances in a variety of practical applications.

Appendix A

Non-dimensional variables

The non-dimensional variables in this thesis are defined in the following, using a reference length L, a reference particle speed c, a reference time $t_{\text{ref}} = L/U$, where U is a reference flow speed, a reference density ρ_{ref}, a reference temperature T_{ref}, a reference order parameter ψ_{ref}, a reference diffusive coefficient of fluid k_{f}, and the specific heat at constant pressure c_p. Note that the asterisk of the non-dimensional variables are dropped for brevity in this thesis.

For Chapter 2

$$\begin{cases} \boldsymbol{x}^* = \boldsymbol{x}/L & t^* = t/t_{\text{ref}} \\ \boldsymbol{u}^* = \boldsymbol{u}/U & p^* = p/(\rho_{\text{ref}}U^2) \quad T^* = T/T_{\text{ref}} \\ \alpha_\gamma^* = L\alpha_\gamma/(\rho_{\text{ref}}U) & \beta_\gamma^* = L\beta_\gamma/k_{\text{f}} \end{cases} \tag{A.1}$$

For Chapter 3

$$\begin{cases} \boldsymbol{x}^* = \boldsymbol{x}/L & t^* = t/t_{\text{ref}} & \Delta x^* = \Delta x/L & \Delta t^* = \Delta t/t_{\text{ref}} \\ \boldsymbol{c}_i^* = \boldsymbol{c}_i/c & f_i^* = f_i/\rho_{\text{ref}} & & \\ \rho^* = \rho/\rho_{\text{ref}} & \boldsymbol{u}^* = \boldsymbol{u}/c & p^* = p/(\rho_{\text{ref}}c^2) & \\ \nu^* = \nu/(cL) & \alpha_\gamma^* = L\alpha_\gamma/(\rho_{\text{ref}}c) & & \end{cases} \tag{A.2}$$

For Chapter 4

$$\begin{cases} \boldsymbol{x}^* = \boldsymbol{x}/L & t^* = t/t_{\text{ref}} & \Delta x^* = \Delta x/L & \Delta t^* = \Delta t/t_{\text{ref}} \\ \boldsymbol{c}_i^* = \boldsymbol{c}_i/c & f_i^* = f_i/\rho_{\text{ref}} & g_i^* = g_i/T_{\text{ref}} & \rho^* = \rho/\rho_{\text{ref}} \\ T^* = T/T_{\text{ref}} & \boldsymbol{u}^* = \boldsymbol{u}/c & p^* = p/(\rho_{\text{ref}}c^2) & \boldsymbol{q}_T^* = \boldsymbol{q}_T/(\rho_{\text{ref}}c_p c T_{\text{ref}}) \\ \nu^* = \nu/(cL) & \alpha_T^* = \alpha_T/(cL) & \alpha_\gamma^* = L\alpha_\gamma/(\rho_{\text{ref}}c) & \beta_\gamma^* = L\beta_\gamma/c. \end{cases} \tag{A.3}$$

For Chapter 5

$$\begin{cases} \boldsymbol{x}^* = \boldsymbol{x}/L & t^* = t/t_{\text{ref}} & \Delta x^* = \Delta x/L & \Delta t^* = \Delta t/t_{\text{ref}} \\ \boldsymbol{c}_i^* = \boldsymbol{c}_i/c & f_{Ai}^* = f_{Ai}/\psi_{\text{ref}} & f_{Bi}^* = f_{Bi}/\rho_{\text{ref}} & f_{Ci}^* = f_{Ci}/T_{\text{ref}} \\ \rho^* = \rho/\rho_{\text{ref}} & \boldsymbol{u}^* = \boldsymbol{u}/c & p^* = p/(\rho_{\text{ref}} c^2) & \psi^* = \psi/\psi_{\text{ref}} \\ T^* = T/T_{\text{ref}} & \nu^* = \nu/(cL) & \alpha_\gamma^* = L\alpha_\gamma/(\rho_{\text{ref}} c) & \end{cases} \tag{A.4}$$

Appendix B

Adjoint lattice Boltzmann method

Here, we discuss the details concerning the derivation of the continuos adjoint equation, the so-called adjoint BGK-Boltzmann equation in [62, 63].

First, the specific formulation of $\delta_f J[f]$, which is represented as the variation of the objective functional, is derived as follows:

$$\delta_f J[f] := \langle J', \delta\gamma \rangle = \frac{\mathrm{d}}{\mathrm{d}\varrho} J(f + \varrho\eta)\bigg|_{\varrho=0} = \lim_{\varrho \to 0} \frac{J[f + \varrho\eta] - J[f]}{\varrho}, \tag{B.1}$$

which is based on the Gâtaux derivative. We consider an objective functional $J := J_D + J_\Gamma$, where $J_D = \int_D A(\rho, \boldsymbol{u})\mathrm{d}\Omega$, and $J_\Gamma = \int_{\Gamma_{\mathrm{in}} \cup \Gamma_{\mathrm{out}}} a(\rho, \boldsymbol{u})\mathrm{d}\Gamma$. Based on Eq. (B.1), $J_D[f + \varrho\eta]$ is derived as follows:

$$J_D[f + \varrho\eta] = J_D[A(\rho[f + \varrho\eta], \boldsymbol{u}[f + \varrho\eta])] = J_D[A\{\rho[f + \varrho\eta], \boldsymbol{u}(\rho[f + \varrho\eta], \boldsymbol{v}[f + \varrho\eta])\}], \tag{B.2}$$

and we $\boldsymbol{u}$ is defined as

$$\boldsymbol{u} = \frac{\boldsymbol{v}}{\rho}, \tag{B.3}$$

$$\boldsymbol{v} = \int_\Xi \boldsymbol{\xi} f \mathrm{d}\boldsymbol{\xi}. \tag{B.4}$$

Since ρ and $\boldsymbol{v}$ are linear functionals, the integrand A in Eq. (B.2) can be rewritten as

$$A\{\rho[f + \varrho\eta], \boldsymbol{u}(\rho[f + \varrho\eta], \boldsymbol{v}[f + \varrho\eta])\} = A\{\rho[f] + \varrho\rho[\eta], \boldsymbol{u}(\rho[f] + \varrho\rho[\eta], \boldsymbol{v}[f] + \varrho\boldsymbol{v}[\eta])\}, \tag{B.5}$$

where $\boldsymbol{u}(\rho[f]+\varrho\rho[\eta],\boldsymbol{v}[f]+\varrho\boldsymbol{v}[\eta])$ is expanded as follows, using the Taylor expansion:

$$\boldsymbol{u}(\rho[f]+\varrho\rho[\eta],\boldsymbol{v}[f]+\varrho\boldsymbol{v}[\eta])=\boldsymbol{u}(\rho[f],\boldsymbol{v}[f])+\varrho\left\{\frac{\partial\boldsymbol{u}}{\partial\rho}\rho[\eta]+\frac{\partial\boldsymbol{u}}{\partial\boldsymbol{v}}\boldsymbol{v}[\eta]\right\}+o(\varrho). \tag{B.6}$$

Furthermore, using Eq. (B.6), Eq. (B.5) can also be expanded as follows, using the Taylor expansion:

$$A\{\rho[f]+\varrho\rho[\eta],\boldsymbol{u}(\rho[f]+\varrho\rho[\eta],\boldsymbol{v}[f]+\varrho\boldsymbol{v}[\eta])\} \tag{B.7}$$

$$=A\{\rho[f],\boldsymbol{u}(\rho[f],\boldsymbol{v}[f])\}+\varrho\left\{\frac{\partial A}{\partial\rho}\rho[\eta]+\frac{\partial A}{\partial\boldsymbol{v}}\cdot\left(\frac{\partial\boldsymbol{u}}{\partial\rho}\rho[\eta]+\frac{\partial\boldsymbol{u}}{\partial\boldsymbol{v}}\boldsymbol{v}[\eta]\right)\right\}+o(\varrho), \tag{B.8}$$

where

$$\frac{\partial\boldsymbol{u}}{\partial\rho}=-\frac{\boldsymbol{v}}{\rho^2}, \tag{B.9}$$

$$\frac{\partial\boldsymbol{u}}{\partial\boldsymbol{v}}=\frac{1}{\rho}. \tag{B.10}$$

Hence, based on Eq. (B.1), the variation $\delta_f J_D$ is obtained as follows:

$$\begin{aligned}
\delta_f J_D&=\lim_{\varrho\to0}\frac{J_D[f+\varrho\eta]-J_D[f]}{\varrho}\\
&=\int_D\left\{\frac{\partial A}{\partial\rho}\rho[\eta]+\frac{\partial A}{\partial\boldsymbol{v}}\cdot\left(\frac{\partial\boldsymbol{u}(\rho[f],\boldsymbol{v}[f])}{\partial\rho}\rho[\eta]+\frac{\partial\boldsymbol{u}(\rho[f],\boldsymbol{v}[f])}{\partial\boldsymbol{v}}\boldsymbol{v}[\eta]\right)\right\}\mathrm{d}\Omega\\
&=\int_D\left\{\frac{\partial A}{\partial\rho}\rho[\eta]+\frac{\partial A}{\partial\boldsymbol{v}}\cdot\left(-\frac{\boldsymbol{v}[f]}{(\rho[f])^2}\rho[\eta]+\frac{1}{\rho[f]}\boldsymbol{v}[\eta]\right)\right\}\mathrm{d}\Omega\\
&=\int_D\left\{\frac{\partial A}{\partial\rho}\rho[\eta]+\frac{\partial A}{\partial\boldsymbol{v}}\cdot\left(-\frac{\boldsymbol{u}(\rho[f],\boldsymbol{v}[f])}{\rho[f]}\rho[\eta]+\frac{\boldsymbol{u}(\rho[\eta],\boldsymbol{v}[\eta])}{\rho[f]}\rho[\eta]\right)\right\}\mathrm{d}\Omega\\
&=\int_D\frac{1}{\rho[f]}\left\{\frac{\partial A}{\partial\rho}\rho[f]+\frac{\partial A}{\partial\boldsymbol{v}}\cdot\{\boldsymbol{u}(\rho[\eta],\boldsymbol{v}[\eta])-\boldsymbol{u}(\rho[f],\boldsymbol{v}[f])\}\right\}\rho[\eta]\mathrm{d}\Omega\\
&=\int_D\int_\Xi\frac{1}{\rho[f]}\left\{\frac{\partial A}{\partial\rho}\rho[f]+\frac{\partial A}{\partial\boldsymbol{v}}\cdot\{\boldsymbol{\xi}-\boldsymbol{u}(\rho[f],\boldsymbol{v}[f])\}\right\}\eta\mathrm{d}\boldsymbol{\xi}\mathrm{d}\Omega,
\end{aligned} \tag{B.11}$$

with the following functional used with respect to the arbitrary function η:

$$\rho[\eta] = \int_{\Xi} \eta \mathrm{d}\boldsymbol{\xi}, \tag{B.12}$$

$$\boldsymbol{u}(\rho[\eta], \boldsymbol{v}[\eta]) = \frac{1}{\rho[\eta]} \int_{\Xi} \boldsymbol{\xi} \eta \mathrm{d}\boldsymbol{\xi}. \tag{B.13}$$

Similarly, $\delta_f J_\Gamma$ can be derived as follows:

$$\begin{aligned}\delta_f J_\Gamma &= \lim_{\varrho \to 0} \frac{J_\Gamma[f + \varrho\eta] - J_\Gamma[f]}{\varrho} \\ &= \int_{\Gamma_{\mathrm{in}} \cup \Gamma_{\mathrm{out}}} \int_{\Xi} \frac{1}{\rho[f]} \left\{ \frac{\partial a}{\partial \rho} \rho[f] + \frac{\partial a}{\partial \boldsymbol{v}} \cdot \{\boldsymbol{\xi} - \boldsymbol{u}(\rho[f], \boldsymbol{v}[f])\} \right\} \eta \mathrm{d}\boldsymbol{\xi} \mathrm{d}\Gamma.\end{aligned} \tag{B.14}$$

Consequently, we obtain the following variation, $\delta_f J = \delta_f J_D + \delta_f J_\Gamma$, as

$$\begin{aligned}\delta_f J = &\int_D \int_{\Xi} \frac{1}{\rho[f]} \left\{ \frac{\partial A}{\partial \rho} \rho[f] + \frac{\partial A}{\partial \boldsymbol{v}} \cdot \{\boldsymbol{\xi} - \boldsymbol{u}(\rho[f], \boldsymbol{v}[f])\} \right\} \eta \mathrm{d}\boldsymbol{\xi} \mathrm{d}\Omega \\ &+ \int_{\Gamma_{\mathrm{in}} \cup \Gamma_{\mathrm{out}}} \int_{\Xi} \frac{1}{\rho[f]} \left\{ \frac{\partial a}{\partial \rho} \rho[f] + \frac{\partial a}{\partial \boldsymbol{v}} \cdot \{\boldsymbol{\xi} - \boldsymbol{u}(\rho[f], \boldsymbol{v}[f])\} \right\} \eta \mathrm{d}\boldsymbol{\xi} \mathrm{d}\Gamma.\end{aligned} \tag{B.15}$$

Next, we consider the derivation of $\delta_f E[f, g, \phi]$ that represents the functional for the BGK-Boltzmann equation. We now consider the variation of $\delta_f G$, $\delta_f I$, and $\delta_f B_n$ individually, since $E = G + I + B_n$. Therefore, using the above derivation of $\delta_f J$ as a basis, we obtain the following variations:

$$\begin{aligned}\delta_f G = &\left[\int_D \int_{\Xi} g \eta \mathrm{d}\boldsymbol{\xi} \mathrm{d}\Omega \right]_{t_0}^{t_1} - \int_I \int_D \int_{\Xi} \frac{\partial g}{\partial t} \eta \mathrm{d}\boldsymbol{\xi} \mathrm{d}\Omega \mathrm{d}t + \int_I \int_{\Gamma} \int_{\Xi} g \boldsymbol{\xi} \cdot \boldsymbol{n} \eta \mathrm{d}\boldsymbol{\xi} \mathrm{d}\Gamma \mathrm{d}t \\ &- \int_I \int_D \int_{\Xi} \boldsymbol{\xi} \cdot \nabla g \eta \mathrm{d}\boldsymbol{\xi} \mathrm{d}\Omega \mathrm{d}t + \int_I \int_D \int_{\Xi} \frac{1}{\tau_f \epsilon_K} (g - g^{\mathrm{eq}}) \eta \mathrm{d}\boldsymbol{\xi} \mathrm{d}\Omega \mathrm{d}t,\end{aligned} \tag{B.16}$$

$$\delta_f I = \int_D \int_{\Xi} g|_{t=t_0} \eta \mathrm{d}\boldsymbol{\xi} \mathrm{d}\Omega, \tag{B.17}$$

$$\delta_f B_1 = \int_I \int_{\Gamma_{\mathrm{w}}} \int_{\Xi_{\boldsymbol{n} \cdot \boldsymbol{\xi} < 0}} g\{\eta(\boldsymbol{\xi}) - \eta(-\boldsymbol{\xi})\} \mathrm{d}\boldsymbol{\xi} \mathrm{d}\Gamma \mathrm{d}t, \tag{B.18}$$

$$\delta_f B_2 = \int_I \int_{\Gamma_{\mathrm{in}}} \int_{\Xi} \left(g - g_{\mathrm{in}}^{\mathrm{eq}}\right) \eta \mathrm{d}\boldsymbol{\xi} \mathrm{d}\Gamma \mathrm{d}t, \tag{B.19}$$

$$\delta_f B_3 = \int_I \int_{\Gamma_{\mathrm{out}}} \int_{\Xi} \left(g - g_{\mathrm{out}}^{\mathrm{eq}}\right) \eta \mathrm{d}\boldsymbol{\xi} \mathrm{d}\Gamma \mathrm{d}t, \tag{B.20}$$

where g^{eq} is the variation of $\int_I \int_D \int_\Xi f^{\mathrm{eq}} g \mathrm{d}\boldsymbol{\xi}\mathrm{d}\Omega\mathrm{d}t$ with respect to f, and can be obtained as follows:

$$\begin{aligned}
&\int_I \int_D \int_\Xi f^{\mathrm{eq}}[f+\varrho\eta] g \mathrm{d}\boldsymbol{\xi}\mathrm{d}\Omega\mathrm{d}t \\
&\quad= \int_I \int_D \int_\Xi f^{\mathrm{eq}}\{\rho[f+\varrho\eta], \boldsymbol{u}(\rho[f+\varrho\eta], \boldsymbol{v}[f+\varrho\eta])\} g \mathrm{d}\boldsymbol{\xi}\mathrm{d}\Omega\mathrm{d}t \\
&\quad= \int_I \int_D \int_\Xi f^{\mathrm{eq}}\{\rho[f]+\varrho\rho[\eta], \boldsymbol{u}(\rho[f]+\varrho\rho[\eta], \boldsymbol{v}[f]+\varrho\boldsymbol{v}[\eta])\} g \mathrm{d}\boldsymbol{\xi}\mathrm{d}\Omega\mathrm{d}t \\
&\quad= \int_I \int_D \int_\Xi f^{\mathrm{eq}}\{\rho[f]+\varrho\rho[\eta], \boldsymbol{u}(\rho[f], \boldsymbol{v}[f]) + \varrho\frac{\partial \boldsymbol{u}}{\partial \rho}\rho[\eta] + \varrho\frac{\partial \boldsymbol{u}}{\partial \boldsymbol{v}}\boldsymbol{v}[\eta]\} g \mathrm{d}\boldsymbol{\xi}\mathrm{d}\Omega\mathrm{d}t + o(\varrho) \\
&\quad= \int_I \int_D \int_\Xi \Big\{ f^{\mathrm{eq}}\{\rho[f], \boldsymbol{u}(\rho[f], \boldsymbol{v}[f])\} \\
&\qquad\qquad + \varrho\frac{\partial f^{\mathrm{eq}}}{\partial \rho}\rho[\eta] + \frac{\partial f^{\mathrm{eq}}}{\partial \boldsymbol{u}} \cdot \left(\varrho\frac{\partial \boldsymbol{u}}{\partial \rho}\rho[\eta] + \varrho\frac{\partial \boldsymbol{u}}{\partial \boldsymbol{v}}\boldsymbol{v}[\eta] \right) \Big\} g \mathrm{d}\boldsymbol{\xi}\mathrm{d}\Omega\mathrm{d}t + o(\varrho),
\end{aligned} \tag{B.21}$$

thus,

$$\begin{aligned}
\int_I \int_D \int_\Xi g^{\mathrm{eq}} \eta \mathrm{d}\boldsymbol{\xi}\mathrm{d}\Omega\mathrm{d}t &= \int_I \int_D \int_\Xi \left\{ \frac{\partial f^{\mathrm{eq}}}{\partial \rho}\rho[\eta] + \frac{\partial f^{\mathrm{eq}}}{\partial \boldsymbol{u}} \cdot \left(\frac{\partial \boldsymbol{u}}{\partial \rho}\rho[\eta] + \frac{\partial \boldsymbol{u}}{\partial \boldsymbol{v}}\boldsymbol{v}[\eta] \right) \right\} g \mathrm{d}\hat{\boldsymbol{\xi}}\mathrm{d}\boldsymbol{\xi}\mathrm{d}\Omega\mathrm{d}t \\
&= \int_I \int_D \int_\Xi \int_\Xi \left\{ \frac{\partial f^{\mathrm{eq}}}{\partial \rho} + \frac{\partial f^{\mathrm{eq}}}{\partial \boldsymbol{u}} \cdot \left(\frac{\partial \boldsymbol{u}}{\partial \rho} + \frac{\partial \boldsymbol{u}}{\partial \boldsymbol{v}}\hat{\boldsymbol{\xi}} \right) \right\} g\eta(\hat{\boldsymbol{\xi}}) \mathrm{d}\hat{\boldsymbol{\xi}}\mathrm{d}\boldsymbol{\xi}\mathrm{d}\Omega\mathrm{d}t \\
&= \int_I \int_D \int_\Xi \int_\Xi \left\{ \frac{1}{\rho} f^{\mathrm{eq}} + \frac{\boldsymbol{\xi}-\boldsymbol{u}}{2RT} f^{\mathrm{eq}} \cdot \left(-\frac{\boldsymbol{v}}{\rho^2} + \frac{1}{\rho}\hat{\boldsymbol{\xi}} \right) \right\} g\eta(\hat{\boldsymbol{\xi}}) \mathrm{d}\hat{\boldsymbol{\xi}}\mathrm{d}\boldsymbol{\xi}\mathrm{d}\Omega\mathrm{d}t \\
&= \int_I \int_D \int_\Xi \int_\Xi \frac{g f^{\mathrm{eq}}}{2RT\rho} \left\{ 2RT + (\boldsymbol{\xi}-\boldsymbol{u}) \cdot (\hat{\boldsymbol{\xi}}-\boldsymbol{u}) \right\} \eta(\hat{\boldsymbol{\xi}}) \mathrm{d}\hat{\boldsymbol{\xi}}\mathrm{d}\boldsymbol{\xi}\mathrm{d}\Omega\mathrm{d}t.
\end{aligned} \tag{B.22}$$

In addition, $g_{\mathrm{in}}^{\mathrm{eq}}$ and $g_{\mathrm{out}}^{\mathrm{eq}}$ can be also obtained using the above formulation. Thus, we have

$$g^{\mathrm{eq}} = \int_\Xi \frac{g(\hat{\boldsymbol{\xi}}) f^{\mathrm{eq}}}{2RT\rho} \left\{ 2RT + (\hat{\boldsymbol{\xi}}-\boldsymbol{u}) \cdot (\boldsymbol{\xi}-\boldsymbol{u}) \right\} \mathrm{d}\hat{\boldsymbol{\xi}}, \tag{B.23}$$

$$g_{\mathrm{in}}^{\mathrm{eq}} = \int_\Xi \frac{g(\hat{\boldsymbol{\xi}}) f^{\mathrm{eq}}}{\rho} \mathrm{d}\hat{\boldsymbol{\xi}}, \tag{B.24}$$

$$g_{\mathrm{out}}^{\mathrm{eq}} = \int_\Xi \frac{g(\hat{\boldsymbol{\xi}}) f^{\mathrm{eq}}}{2RT\rho} (\hat{\boldsymbol{\xi}}-\boldsymbol{u}) \cdot (\boldsymbol{\xi}-\boldsymbol{u}) \mathrm{d}\hat{\boldsymbol{\xi}}. \tag{B.25}$$

The adjoint equation and its boundary and initial conditions are derived, using the Eqs. (B.15)–(B.20). First, the adjoint equation is obtained from Eq. (B.16), ignoring first and third

terms, as

$$\int_I \int_D \int_\Xi \left\{ -\frac{\partial g}{\partial t} - \boldsymbol{\xi} \cdot \nabla g + \frac{1}{\tau_c}(g - g^{\mathrm{eq}}) \right\} \eta \mathrm{d}\boldsymbol{\xi} \mathrm{d}\Omega \mathrm{d}t = 0. \tag{B.26}$$

Since η represents any function, the adjoint equation is defined as the integrand of Eq. (B.26):

$$-\frac{\partial g}{\partial t} - \boldsymbol{\xi} \cdot \nabla g + \frac{1}{\tau_c}(g - g^{\mathrm{eq}}) = 0 \quad \text{in } I \times D \times \Xi. \tag{B.27}$$

Next, we consider the initial condition of the adjoint equation. From Eqs. (B.15), (B.16) and (B.17), we obtain the following equation:

$$\begin{aligned} &\int_D \int_\Xi A' \eta(t_1) \mathrm{d}\boldsymbol{\xi} \mathrm{d}\Omega + \int_{\Gamma_{\mathrm{in}} \cup \Gamma_{\mathrm{out}}} \int_\Xi a' \eta(t_1) \mathrm{d}\boldsymbol{\xi} \mathrm{d}\Omega \\ &\quad + \int_D \int_\Xi \{ g(t_1)\eta(t_1) - g(t_0)\eta(t_0) \} \mathrm{d}\boldsymbol{\xi} \mathrm{d}\Omega + \int_D \int_\Xi g(t_0)\eta(t_0) \mathrm{d}\boldsymbol{\xi} \mathrm{d}\Omega = 0, \end{aligned} \tag{B.28}$$

where

$$A' = \frac{1}{\rho} \left\{ \frac{\partial A}{\partial \rho} \rho + \frac{\partial A}{\partial \boldsymbol{u}} \cdot (\boldsymbol{\xi} - \boldsymbol{u}) \right\}, \tag{B.29}$$

$$a' = \frac{1}{\rho} \left\{ \frac{\partial a}{\partial \rho} \rho + \frac{\partial a}{\partial \boldsymbol{u}} \cdot (\boldsymbol{\xi} - \boldsymbol{u}) \right\}. \tag{B.30}$$

Therefore, the initial condition of the adjoint equation is the following,

$$g(t_1) + A' = 0 \quad \text{in } D \times \Xi. \tag{B.31}$$

We note that the second term of Eq. (B.28) affects the initial boundary conditions for the adjoint BGK-Boltzmann equation.

Finally, we consider the boundary conditions of the adjoint equation. From the third term of Eq. (B.15), and Eqs. (B.18)–(B.20), we obtain the following:

$$\begin{aligned} &\int_I \int_\Gamma \int_\Xi g \boldsymbol{\xi} \cdot \boldsymbol{n} \eta \mathrm{d}\boldsymbol{\xi} \mathrm{d}\Gamma \mathrm{d}t + \int_I \int_{\Gamma_{\mathrm{w}}} \int_{\Xi_{\boldsymbol{n} \cdot \boldsymbol{\xi} < 0}} g \{ \eta(\boldsymbol{\xi}) - \eta(-\boldsymbol{\xi}) \} \mathrm{d}\boldsymbol{\xi} \mathrm{d}\Gamma \mathrm{d}t \\ &\quad + \int_I \int_{\Gamma_{\mathrm{in}}} \int_\Xi \left(g - g_{\mathrm{in}}^{\mathrm{eq}} \right) \eta \mathrm{d}\boldsymbol{\xi} \mathrm{d}\Gamma \mathrm{d}t + \int_I \int_{\Gamma_{\mathrm{out}}} \int_\Xi \left(g - g_{\mathrm{out}}^{\mathrm{eq}} \right) \eta \mathrm{d}\boldsymbol{\xi} \mathrm{d}\Gamma \mathrm{d}t = 0. \end{aligned} \tag{B.32}$$

The second term of the above equation can be eliminated. Therefore, the above equation is rewritten as

$$\int_I\int_{\Gamma_\mathrm{w}}\int_\Xi g\boldsymbol{\xi}\cdot\boldsymbol{n}\eta\mathrm{d}\boldsymbol{\xi}\mathrm{d}\Gamma\mathrm{d}t+\int_I\int_{\Gamma_\mathrm{in}}\int_\Xi g\boldsymbol{\xi}\cdot\boldsymbol{n}\eta\mathrm{d}\boldsymbol{\xi}\mathrm{d}\Gamma\mathrm{d}t+\int_I\int_{\Gamma_\mathrm{out}}\int_\Xi g\boldsymbol{\xi}\cdot\boldsymbol{n}\eta\mathrm{d}\boldsymbol{\xi}\mathrm{d}\Gamma\mathrm{d}t$$
$$+\int_I\int_{\Gamma_\mathrm{in}}\int_\Xi\left(g-g_\mathrm{in}^\mathrm{eq}\right)\eta\mathrm{d}\boldsymbol{\xi}\mathrm{d}\Gamma\mathrm{d}t+\int_I\int_{\Gamma_\mathrm{out}}\int_\Xi\left(g-g_\mathrm{out}^\mathrm{eq}\right)\eta\mathrm{d}\boldsymbol{\xi}\mathrm{d}\Gamma\mathrm{d}t=0. \tag{B.33}$$

Here, using the first term of the above equation, the boundary condition of Γ_w is obtained as follows:

$$\begin{aligned}\int_I\int_{\Gamma_\mathrm{w}}\int_\Xi g\boldsymbol{\xi}\cdot\boldsymbol{n}\eta\mathrm{d}\boldsymbol{\xi}\mathrm{d}\Gamma\mathrm{d}t&=\int_I\int_{\Gamma_\mathrm{w}}\int_{\Xi_{\boldsymbol{n}\cdot\boldsymbol{\xi}\geqslant0}}g(\boldsymbol{\xi})\boldsymbol{\xi}\cdot\boldsymbol{n}\eta\mathrm{d}\boldsymbol{\xi}\mathrm{d}\Gamma\mathrm{d}t\\&\quad+\int_I\int_{\Gamma_\mathrm{w}}\int_{\Xi_{\boldsymbol{n}\cdot\boldsymbol{\xi}<0}}g(\boldsymbol{\xi})\boldsymbol{\xi}\cdot\boldsymbol{n}\eta\mathrm{d}\boldsymbol{\xi}\mathrm{d}\Gamma\mathrm{d}t\\&=\int_I\int_{\Gamma_\mathrm{w}}\int_{\Xi_{\boldsymbol{n}\cdot\boldsymbol{\xi}\geqslant0}}g(\boldsymbol{\xi})\boldsymbol{\xi}\cdot\boldsymbol{n}\eta\mathrm{d}\boldsymbol{\xi}\mathrm{d}\Gamma\mathrm{d}t\\&\quad-\int_I\int_{\Gamma_\mathrm{w}}\int_{\Xi_{\boldsymbol{n}\cdot\boldsymbol{\xi}\geqslant0}}g(-\boldsymbol{\xi})\boldsymbol{\xi}\cdot\boldsymbol{n}\eta\mathrm{d}\boldsymbol{\xi}\mathrm{d}\Gamma\mathrm{d}t\\&=\int_I\int_{\Gamma_\mathrm{w}}\int_{\Xi_{\boldsymbol{n}\cdot\boldsymbol{\xi}\geqslant0}}\boldsymbol{\xi}\cdot\boldsymbol{n}\{g(\boldsymbol{\xi})-g(-\boldsymbol{\xi})\}\eta\mathrm{d}\boldsymbol{\xi}\mathrm{d}\Gamma\mathrm{d}t\\&=\int_I\int_{\Gamma_\mathrm{w}}\int_{\Xi_{\boldsymbol{n}\cdot\boldsymbol{\xi}>0}}\boldsymbol{\xi}\cdot\boldsymbol{n}\{g(\boldsymbol{\xi})-g(-\boldsymbol{\xi})\}\eta\mathrm{d}\boldsymbol{\xi}\mathrm{d}\Gamma\mathrm{d}t,\end{aligned} \tag{B.34}$$

where $\Xi_{\boldsymbol{n}\cdot\boldsymbol{\xi}>0}$ is the velocity space of $\boldsymbol{\xi}$ that satisfies $\boldsymbol{n}\cdot\boldsymbol{\xi}>0$. Note that the boundary condition of Γ_w for the adjoint equation has to be set in $\boldsymbol{n}\cdot\boldsymbol{\xi}>0$, while the boundary condition of Boltzmann equation has to be set so that $\boldsymbol{n}\cdot\boldsymbol{\xi}<0$. The reason why different settings are required for the Boltzmann equation and the adjoint equation is that both the propagation and time evolution directions of adjoint equation are opposite those of the Boltzmann equation. Consequently, from the above equation, the following boundary conditions are obtained:

$$g(\boldsymbol{\xi})-g(-\boldsymbol{\xi})=0\quad\text{in}\ \ I\times\Gamma_\mathrm{w}\times\Xi_{\boldsymbol{n}\cdot\boldsymbol{\xi}>0}. \tag{B.35}$$

Similarly, the boundary conditions for Γ_in and Γ_out can be described as follows:

$$g-g_\mathrm{in}^\mathrm{eq}=0\quad\text{in}\ \ I\times\Gamma_\mathrm{in}\times\Xi, \tag{B.36}$$

$$g-g_\mathrm{out}^\mathrm{eq}=0\quad\text{in}\ \ I\times\Gamma_\mathrm{out}\times\Xi. \tag{B.37}$$

Appendix C

Adjoint boundary conditions

C.1 Prescribed pressure and velocity boundary conditions

First, the boundary condition for the no-slip boundary, Γ_{W}, in Eq. (3.18) for the adjoint equation can be derived as follows:

$$\begin{aligned}
\Theta_{\mathrm{W}} &= \int_I \int_{\Gamma_{\mathrm{W}}} \sum_{i=1}^{9} (\boldsymbol{c}_i \cdot \boldsymbol{n}) \delta f_i^{\mathrm{b}} \tilde{f}_i \mathrm{d}\Gamma \mathrm{d}t \\
&= \int_I \int_{\Gamma_{\mathrm{W}}} \left(-\tilde{f}_3 \delta f_3 + \tilde{f}_5 \delta f_5 - \tilde{f}_6 \delta f_6 - \tilde{f}_7 \delta f_7 + \tilde{f}_8 \delta f_8 + \tilde{f}_9 \delta f_9 \right) \mathrm{d}\Gamma \mathrm{d}t \\
&= \int_I \int_{\Gamma_{\mathrm{W}}} \left(-\tilde{f}_3 \delta f_5 + \tilde{f}_5 \delta f_5 - \tilde{f}_6 \delta f_8 - \tilde{f}_7 \delta f_9 + \tilde{f}_8 \delta f_8 + \tilde{f}_9 \delta f_9 \right) \mathrm{d}\Gamma \mathrm{d}t \\
&= \int_I \int_{\Gamma_{\mathrm{W}}} \left\{ (\tilde{f}_5 - \tilde{f}_3) \delta f_5 + (\tilde{f}_8 - \tilde{f}_6) \delta f_8 + (\tilde{f}_9 - \tilde{f}_7) \delta f_9 \right\} \mathrm{d}\Gamma \mathrm{d}t,
\end{aligned} \tag{C.1}$$

where, since the boundary condition is defined so that Eq. (C.1) equals zero under $\delta f_{5,8,9} \neq 0$, the boundary condition is obtained as follows:

$$\left.\begin{aligned}
\tilde{f}_5 &= \tilde{f}_3 \\
\tilde{f}_8 &= \tilde{f}_6 \\
\tilde{f}_9 &= \tilde{f}_7
\end{aligned}\right\} \text{ on } \Gamma_{\mathrm{W}}. \tag{C.2}$$

This is same result as that of the previous research in which the Boltzmann equation was used to formulate the optimization problem, and is used here for the bounce back boundary condition expressed in Eq. (3.18).

Next, the boundary condition corresponding to the prescribed velocity boundary condition in Eq. (3.19) is derived as

$$\begin{aligned}\Theta_{\mathrm{V}} &= \int_I \int_{\Gamma_{\mathrm{V}}} \frac{1}{3} \sum_{i=1}^{9} \delta f_i \mathrm{d}\Gamma \mathrm{d}t + \int_I \int_{\Gamma_{\mathrm{V}}} \sum_{i=1}^{9} (\boldsymbol{c}_i \cdot \boldsymbol{n}) \delta f_i^{\mathrm{b}} \tilde{f}_i \mathrm{d}\Gamma \mathrm{d}t \\ &= \int_I \int_{\Gamma_{\mathrm{V}}} \left(\frac{1}{3} \sum_{i=1}^{9} \delta f_i - \tilde{f}_3 \delta f_3 + \tilde{f}_5 \delta f_5 - \tilde{f}_6 \delta f_6 - \tilde{f}_7 \delta f_7 + \tilde{f}_8 \delta f_8 + \tilde{f}_9 \delta f_9 \right) \mathrm{d}\Gamma \mathrm{d}t, \end{aligned} \tag{C.3}$$

where, based on Eq. (3.19), δf_3, δf_6, and δf_7 are represented as follows:

$$\begin{cases} \delta f_3 = \delta f_5 + \frac{2}{3} \rho' v^0 \\ \delta f_6 = \delta f_8 + \frac{1}{6} \rho' v^0 - \frac{1}{2} (\delta f_2 - \delta f_4) \\ \delta f_7 = \delta f_9 + \frac{1}{6} \rho' v^0 + \frac{1}{2} (\delta f_2 - \delta f_4), \end{cases} \tag{C.4}$$

where

$$\rho' = \frac{\delta f_1 + \delta f_2 + \delta f_4 + 2(\delta f_5 + \delta f_8 + \delta f_9)}{1 - v^0}. \tag{C.5}$$

Equation (C.3) can be rewritten as

$$\begin{aligned}\Theta_{\mathrm{V}} = \int_I \int_{\Gamma_{\mathrm{V}}} \Bigg\{ & \frac{1}{3} \sum_{i=1}^{9} \delta f_i - \tilde{f}_3 \left(\delta f_5 + \frac{2}{3} \rho' v^0 \right) + \tilde{f}_5 \delta f_5 \\ & - \tilde{f}_6 \left(\delta f_8 + \frac{1}{6} \rho' v^0 - \frac{1}{2} (\delta f_2 - \delta f_4) \right) \\ & - \tilde{f}_7 \left(\delta f_9 + \frac{1}{6} \rho' v^0 + \frac{1}{2} (\delta f_2 - \delta f_4) \right) + \tilde{f}_8 \delta f_8 + \tilde{f}_9 \delta f_9 \Bigg\} \mathrm{d}\Gamma \mathrm{d}t, \end{aligned} \tag{C.6}$$

in which it is assumed that $\delta f_{1,2,4} = 0$ is naturally satisfied when the velocity at Γ_{V} is orthogonal to this boundary. Thus, we obtain the following equation,

$$\begin{aligned}\Theta_{\mathrm{V}} = \int_I \int_{\Gamma_{\mathrm{V}}} \Bigg\{ & \delta f_5 \left(\frac{2}{3(1-v^0)} - \tilde{f}_3 + \tilde{f}_5 - \frac{v^0}{1-v^0} \left(\frac{4}{3} \tilde{f}_3 + \frac{1}{3} \tilde{f}_6 + \frac{1}{3} \tilde{f}_7 \right) \right) \\ & + \delta f_8 \left(\frac{2}{3(1-v^0)} - \tilde{f}_6 + \tilde{f}_8 - \frac{v^0}{1-v^0} \left(\frac{4}{3} \tilde{f}_3 + \frac{1}{3} \tilde{f}_6 + \frac{1}{3} \tilde{f}_7 \right) \right) \\ & + \delta f_9 \left(\frac{2}{3(1-v^0)} - \tilde{f}_7 + \tilde{f}_9 - \frac{v^0}{1-v^0} \left(\frac{4}{3} \tilde{f}_3 + \frac{1}{3} \tilde{f}_6 + \frac{1}{3} \tilde{f}_7 \right) \right) \Bigg\} \mathrm{d}\Gamma \mathrm{d}t. \end{aligned} \tag{C.7}$$

As a result, the boundary condition on Γ_{V} for the adjoint equation is defined as follows:

$$\left.\begin{aligned}
\tilde{f}_5 &= -\tfrac{2}{3(1-v^0)} + \tilde{f}_3 + \tfrac{v^0}{3(1-v^0)}\left(4\tilde{f}_3 + \tilde{f}_6 + \tilde{f}_7\right)\\
\tilde{f}_8 &= -\tfrac{2}{3(1-v^0)} + \tilde{f}_6 + \tfrac{v^0}{3(1-v^0)}\left(4\tilde{f}_3 + \tilde{f}_6 + \tilde{f}_7\right)\\
\tilde{f}_9 &= -\tfrac{2}{3(1-v^0)} + \tilde{f}_7 + \tfrac{v^0}{3(1-v^0)}\left(4\tilde{f}_3 + \tilde{f}_6 + \tilde{f}_7\right)
\end{aligned}\right\} \text{ on } \Gamma_{\mathrm{V}}. \tag{C.8}$$

The boundary condition corresponding to the prescribed pressure boundary condition expressed in Eq. (3.20) is derived as

$$\begin{aligned}
\Theta_{\mathrm{P}} &= -\int_I\int_{\Gamma_{\mathrm{P}}} \frac{1}{3}\sum_{i=1}^{9}\delta f_i \mathrm{d}\Gamma\mathrm{d}t + \int_I\int_{\Gamma_{\mathrm{P}}}\sum_{i=1}^{9}(\boldsymbol{c}_i\cdot\boldsymbol{n})\delta f_i^{\mathrm{b}}\tilde{f}_i\mathrm{d}\Gamma\mathrm{d}t\\
&= \int_I\int_{\Gamma_{\mathrm{P}}}\left(-\frac{1}{3}\sum_{i=1}^{9}\delta f_i - \tilde{f}_3\delta f_3 + \tilde{f}_5\delta f_5 - \tilde{f}_6\delta f_6 - \tilde{f}_7\delta f_7 + \tilde{f}_8\delta f_8 + \tilde{f}_9\delta f_9\right)\mathrm{d}\Gamma\mathrm{d}t,
\end{aligned} \tag{C.9}$$

where, based on Eq. (3.20), δf_3, δf_6, and δf_7 are represented as

$$\begin{cases}
\delta f_3 = \delta f_5 + \frac{2}{3}\rho^0 v'\\
\delta f_6 = \delta f_8 + \frac{1}{6}\rho^0 v' - \frac{1}{2}(\delta f_2 - \delta f_4)\\
\delta f_7 = \delta f_9 + \frac{1}{6}\rho^0 v' + \frac{1}{2}(\delta f_2 - \delta f_4),
\end{cases} \tag{C.10}$$

where

$$v' = -\frac{\delta f_1 + \delta f_2 + \delta f_4 + 2(\delta f_5 + \delta f_8 + \delta f_9)}{\rho^0}. \tag{C.11}$$

Equation (C.9) can be rewritten as

$$\begin{aligned}
\Theta_{\mathrm{P}} = \int_I\int_{\Gamma_{\mathrm{P}}}\Bigg\{&-\frac{1}{3}\sum_{i=1}^{9}\delta f_i - \tilde{f}_3\left(\delta f_5 + \frac{2}{3}\rho^0 v'\right) + \tilde{f}_5\delta f_5\\
&-\tilde{f}_6\left(\delta f_8 + \frac{1}{6}\rho^0 v' - \frac{1}{2}(\delta f_2 - \delta f_4)\right)\\
&-\tilde{f}_7\left(\delta f_9 + \frac{1}{6}\rho^0 v' + \frac{1}{2}(\delta f_2 - \delta f_4)\right) + \tilde{f}_8\delta f_8 + \tilde{f}_9\delta f_9\Bigg\}\mathrm{d}\Gamma\mathrm{d}t,
\end{aligned} \tag{C.12}$$

in which it is assumed that $\delta f_{1,2,4} = 0$ is naturally satisfied when the velocity at Γ_P is orthogonal to this boundary. Thus, we obtain the following:

$$\begin{aligned}\Theta_\mathrm{P} = \int_I \int_{\Gamma_\mathrm{P}} \Big\{ & \delta f_5 \left(-\frac{1}{3}\tilde{f}_3 + \frac{4}{3}\tilde{f}_3 + \tilde{f}_5 + \frac{1}{3}\tilde{f}_6 + \frac{1}{3}\tilde{f}_7 \right) \\ & + \delta f_8 \left(\frac{4}{3}\tilde{f}_3 + \tilde{f}_8 - \tilde{f}_6 + \frac{1}{3}\tilde{f}_6 + \frac{1}{3}\tilde{f}_7 \right) \\ & + \delta f_9 \left(\frac{4}{3}\tilde{f}_3 + \tilde{f}_9 + \frac{1}{3}\tilde{f}_6 - \tilde{f}_7 + \frac{1}{3}\tilde{f}_7 \right) \Big\} \mathrm{d}\Gamma \mathrm{d}t. \end{aligned} \tag{C.13}$$

Consequently, the boundary condition on Γ_P for the adjoint equation is defined as follows:

$$\left.\begin{aligned} \tilde{f}_5 &= \tilde{f}_3 - \tfrac{1}{3}\left(4\tilde{f}_3 + \tilde{f}_6 + \tilde{f}_7\right) \\ \tilde{f}_8 &= \tilde{f}_6 - \tfrac{1}{3}\left(4\tilde{f}_3 + \tilde{f}_6 + \tilde{f}_7\right) \\ \tilde{f}_9 &= \tilde{f}_7 - \tfrac{1}{3}\left(4\tilde{f}_3 + \tilde{f}_6 + \tilde{f}_7\right) \end{aligned}\right\} \text{ on } \Gamma_\mathrm{P}. \tag{C.14}$$

In the pressure drop minimization problem based on the proposed method, the adjoint equation in Eq. (3.39) is solved using the initial condition expressed in Eq. (3.40), and the boundary conditions expressed in Eqs. (C.8) and (C.14). In addition, it is noted that boundary conditions other than those presented above can be used, including a higher accuracy method (e.g., [72, 21]), in fluid flow optimization problems using the LBM.

C.2 Adiabatic and prescribed temperature boundary conditions

We first consider the adjoint boundary condition for the adiabatic boundary, $\Gamma_\mathrm{W} \cup \Gamma_\mathrm{P}$. In the following, only Γ_P is treated, since Γ_W is the specific case when $\boldsymbol{u} = \boldsymbol{0}$. The adjoint boundary condition for Γ_P can be derived as follows:

$$\begin{aligned}\Theta_\mathrm{A} &= \int_I \int_{\Gamma_\mathrm{P}} \sum_{i=1}^{9} (\boldsymbol{c}_i \cdot \boldsymbol{n}) \delta g_i^\mathrm{b} \tilde{g}_i \mathrm{d}\Gamma \mathrm{d}t \\ &= \int_I \int_{\Gamma_\mathrm{P}} (-\tilde{g}_3 \delta g_3 + \tilde{g}_5 \delta g_5 - \tilde{g}_6 \delta g_6 - \tilde{g}_7 \delta g_7 + \tilde{g}_8 \delta g_8 + \tilde{g}_9 \delta g_9) \mathrm{d}\Gamma \mathrm{d}t, \end{aligned} \tag{C.15}$$

where, based on Eq. (4.18), δg_3, δg_6, and δg_7 are represented as follows:

$$\begin{cases} \delta g_3 = \frac{1}{9}T'(1+3v) + \frac{1}{3}Tv' \\ \delta g_6 = \frac{1}{36}T'(1+3v) + \frac{1}{12}Tv' \\ \delta g_7 = \frac{1}{36}T'(1+3v) + \frac{1}{12}Tv', \end{cases} \tag{C.16}$$

where

$$T' = \frac{6(\delta g_5 + \delta g_8 + \delta g_9)}{1-3v} + \frac{18(g_5 + g_8 + g_9)}{(1-3v)^2}v', \tag{C.17}$$

and v' is given by Eq. (C.11). Equation (C.15) can be rewritten as

$$\begin{aligned} \Theta_{\mathrm{A}} = \int_I \int_{\Gamma_{\mathrm{P}}} \Bigg\{ & -\tilde{g}_3 \left(\frac{1}{9}T'(1+3v) + \frac{1}{3}Tv' \right) + \tilde{g}_5 \delta g_5 \\ & -\tilde{g}_6 \left(\frac{1}{36}T'(1+3v) + \frac{1}{12}Tv' \right) \\ & -\tilde{g}_7 \left(\frac{1}{36}T'(1+3v) + \frac{1}{12}Tv' \right) + \tilde{g}_8 \delta g_8 + \tilde{g}_9 \delta g_9 \Bigg\} \mathrm{d}\Gamma \mathrm{d}t \\ = \int_I \int_{\Gamma_{\mathrm{P}}} \Bigg\{ & \delta g_5 \left(\frac{1+3v}{1-3v} \left(-\frac{2}{3}\tilde{g}_3 - \frac{1}{6}\tilde{g}_6 - \frac{1}{6}\tilde{g}_7 \right) + \tilde{g}_5 \right) \\ & + \delta g_8 \left(\frac{1+3v}{1-3v} \left(-\frac{2}{3}\tilde{g}_3 - \frac{1}{6}\tilde{g}_6 - \frac{1}{6}\tilde{g}_7 \right) + \tilde{g}_8 \right) \\ & + \delta g_9 \left(\frac{1+3v}{1-3v} \left(-\frac{2}{3}\tilde{g}_3 - \frac{1}{6}\tilde{g}_6 - \frac{1}{6}\tilde{g}_7 \right) + \tilde{g}_9 \right) \\ & + v' \left(\frac{T(1+3v)}{1-3v} \left(-\frac{2}{3}\tilde{g}_3 - \frac{1}{6}\tilde{g}_6 - \frac{1}{6}\tilde{g}_7 \right) \right) \Bigg\} \mathrm{d}\Gamma \mathrm{d}t. \end{aligned} \tag{C.18}$$

Consequently, the boundary condition on Γ_{P} for the adjoint equation is defined as

$$\left.\begin{aligned} \tilde{g}_5 &= \tfrac{1+3v}{6(1-3v)}(4\tilde{g}_3 + \tilde{g}_6 + \tilde{g}_7) \\ \tilde{g}_8 &= \tfrac{1+3v}{6(1-3v)}(4\tilde{g}_3 + \tilde{g}_6 + \tilde{g}_7) \\ \tilde{g}_9 &= \tfrac{1+3v}{6(1-3v)}(4\tilde{g}_3 + \tilde{g}_6 + \tilde{g}_7) \end{aligned}\right\} \text{ on } \Gamma_{\mathrm{P}}. \tag{C.19}$$

Due to $v' \neq 0$ on Γ_{P}, the adjoint boundary condition for $\tilde{f}_i$ is defined as

$$\left.\begin{aligned} \tilde{f}_5 &= \tilde{f}_3 - \tfrac{1}{3}\left(4\tilde{f}_3 + \tilde{f}_6 + \tilde{f}_7\right) - \tfrac{12T(1+3v)}{\rho_0(1-3v)}(4\tilde{g}_3 + \tilde{g}_6 + \tilde{g}_7) \\ \tilde{f}_8 &= \tilde{f}_6 - \tfrac{1}{3}\left(4\tilde{f}_3 + \tilde{f}_6 + \tilde{f}_7\right) - \tfrac{12T(1+3v)}{\rho_0(1-3v)}(4\tilde{g}_3 + \tilde{g}_6 + \tilde{g}_7) \\ \tilde{f}_9 &= \tilde{f}_7 - \tfrac{1}{3}\left(4\tilde{f}_3 + \tilde{f}_6 + \tilde{f}_7\right) - \tfrac{12T(1+3v)}{\rho_0(1-3v)}(4\tilde{g}_3 + \tilde{g}_6 + \tilde{g}_7) \end{aligned}\right\} \text{ on } \Gamma_{\mathrm{P}}. \tag{C.20}$$

Next, the boundary condition corresponding to the prescribed temperature condition, expressed in Eq. (4.19) is derived as

$$\begin{aligned}\Theta_{\mathrm{T}} &= \int_I \int_{\Gamma_{\mathrm{V}}} \sum_{i=1}^{9} (\boldsymbol{c}_i \cdot \boldsymbol{n}) \delta g_i^{\mathrm{b}} \tilde{g}_i \mathrm{d}\Gamma \mathrm{d}t \\ &= \int_I \int_{\Gamma_{\mathrm{V}}} (-\tilde{g}_3 \delta g_3 + \tilde{g}_5 \delta g_5 - \tilde{g}_6 \delta g_6 - \tilde{g}_7 \delta g_7 + \tilde{g}_8 \delta g_8 + \tilde{g}_9 \delta g_9) \mathrm{d}\Gamma \mathrm{d}t, \end{aligned} \tag{C.21}$$

where, based on Eq. (4.19), δg_3, δg_6, and δg_7 are represented as follows:

$$\begin{cases} \delta g_3 = \frac{1}{9} T'(1+3v) \\ \delta g_6 = \frac{1}{36} T'(1+3v) \\ \delta g_7 = \frac{1}{36} T'(1+3v), \end{cases} \tag{C.22}$$

where

$$T' = -\frac{6(\delta g_1 + \delta g_2 + \delta g_4 + \delta g_5 + \delta g_8 + \delta g_9)}{1+3v}. \tag{C.23}$$

Thus, Eq. (C.21) can be rewritten as

$$\begin{aligned}\Theta_{\mathrm{T}} = \int_I \int_{\Gamma_{\mathrm{V}}} \Bigg\{ &-\tilde{g}_3 \left(\frac{1}{9} T'(1+3v)\right) + \tilde{g}_5 \delta g_5 - \tilde{g}_6 \left(\frac{1}{36} T'(1+3v)\right) \\ &-\tilde{g}_7 \left(\frac{1}{36} T'(1+3v)\right) + \tilde{g}_8 \delta g_8 + \tilde{g}_9 \delta g_9 \Bigg\} \mathrm{d}\Gamma \mathrm{d}t \\ = \int_I \int_{\Gamma_{\mathrm{V}}} \Bigg\{ &\delta g_5 \left(\frac{2}{3}\tilde{g}_3 + \frac{1}{6}\tilde{g}_6 + \frac{1}{6}\tilde{g}_7 + \tilde{g}_5\right) + \delta g_8 \left(\frac{2}{3}\tilde{g}_3 + \frac{1}{6}\tilde{g}_6 + \frac{1}{6}\tilde{g}_7 + \tilde{g}_8\right) \\ &+\delta g_9 \left(\frac{2}{3}\tilde{g}_3 + \frac{1}{6}\tilde{g}_6 + \frac{1}{6}\tilde{g}_7 + \tilde{g}_9\right) \Bigg\} \mathrm{d}\Gamma \mathrm{d}t. \end{aligned} \tag{C.24}$$

Consequently, the boundary condition on Γ_{V} for the adjoint equation is defined as

$$\left.\begin{aligned} \tilde{g}_5 &= -\tfrac{1}{6}(4\tilde{g}_3 + \tilde{g}_6 + \tilde{g}_7) \\ \tilde{g}_8 &= -\tfrac{1}{6}(4\tilde{g}_3 + \tilde{g}_6 + \tilde{g}_7) \\ \tilde{g}_9 &= -\tfrac{1}{6}(4\tilde{g}_3 + \tilde{g}_6 + \tilde{g}_7) \end{aligned}\right\} \text{ on } \Gamma_{\mathrm{V}}. \tag{C.25}$$

References

[1] Aage, N., Poulsen, T. H., Gersborg-Hansen, A., and Sigmund, O. (2008). Topology optimization of large scale Stokes flow problems. *Structural and Multidisciplinary Optimization*, 35(2):175–180.

[2] Aidun, C. K. and Clausen, J. R. (2010). Lattice-Boltzmann method for complex flows. *Annual Review of Fluid Mechanics*, 42(1):439–472.

[3] Allaire, G., Dapogny, C., and Frey, P. (2014). Shape optimization with a level set based mesh evolution method. *Computer Methods in Applied Mechanics and Engineering*, 282:22–53.

[4] Allaire, G., Jouve, F., and Toader, A.-M. (2004). Structural optimization using sensitivity analysis and a level-set method. *Journal of Computational Physics*, 194(1):363–393.

[5] Allen, S. M. and Cahn, J. W. (1979). A microscopic theory for antiphase boundary motion and its application to antiphase domain coarsening. *Acta Metall*, 27(6):1085–1095.

[6] Amstutz, S. (2005). The topological asymptotic for the Navier-Stokes equations. *ESAIM: Control, Optimisation and Calculus of Variations*, 11(3):401–425.

[7] Andreasen, C. S., Gersborg, A. R., and Sigmund, O. (2009). Topology optimization of microfluidic mixers. *International Journal for Numerical Methods in Fluids*, 61(5):498–513.

[8] Andreassen, E., Clausen, A., Schevenels, M., Lazarov, B. S., and Sigmund, O. (2011). Efficient topology optimization in MATLAB using 88 lines of code. *Structural and Multidisciplinary Optimization*, 43(1):1–16.

[9] Bendsøe, M. P. (1989). Optimal shape design as a material distribution problem. *Structural Optimization*, 1(4):193–202.

[10] Bendsøe, M. P. and Kikuchi, N. (1988). Generating optimal topologies in structural design using a homogenization method. *Computer Methods in Applied Mechanics and Engineering*, 71(2):197–224.

[11] Bendsøe, M. P. and Sigmund, O. (2003). *Topology optimization: theory, methods and applications*. Springer, New York.

[12] Benzi, R., Succi, S., and Vergassola, M. (1992). The lattice Boltzmann equation: theory and applications. *Physics Reports*, 222(3):145–197.

[13] Bhatnagar, P. L., Gross, E. P., and Krook, M. (1954). A model for collision processes in gases. I. Small amplitude processes in charged and neutral one-component systems. *Physical Review*, 94(3):511–525.

[14] Borrvall, T. and Petersson, J. (2003). Topology optimization of fluids in Stokes flow. *International Journal for Numerical Methods in Fluids*, 41(1):77–107.

[15] Bourdin, B. and Chambolle, A. (2003). Topology optimization approaches. *ESAIM: Control, Optimisation and Calculus of Variations*, 9:19–48.

[16] Briscolini, M., Santangelo, P., Succi, S., and Benzi, R. (1994). Extended self-similarity in the numerical simulation of three-dimensional homogeneous flows. *Physical Review E*, 50(3):R1745–R1747.

[17] Cahn, J. W. and Hilliard, J. E. (1958). Free energy of a nonuniform system. I. Interfacial free energy. *J Chem Phys*, 28(2):258–267.

[18] Challis, V. J. and Guest, J. K. (2009). Level set topology optimization of fluids in Stokes flow. *International Journal for Numerical Methods in Engineering*, 79(10):1284–1308.

[19] Chen, H., Kandasamy, S., Orszag, S., Shock, R., Succi, S., and Yakhot, V. (2003). Extended Boltzmann kinetic equation for turbulent flows. *Science*, 301(5633):633–636.

[20] Chen, S. and Doolen, G. D. (1998). Lattice Boltzmann method for fluid flows. *Annual Review of Fluid Mechanics*, 30(1):329–364.

[21] Chen, S., Martinez, D., and Mei, R. (1996). On boundary conditions in lattice Boltzmann methods. *Physics of Fluids*, 8(9):2527–2536.

[22] Chikatamarla, S. S. and Karlin, I. V. (2013). Entropic lattice Boltzmann method for turbulent flow simulations: Boundary conditions. *Physica A: Statistical Mechanics and its Applications*, 392(9):1925–1930.

[23] Choi, K. K. and Kim, N.-H. (2006). *Structural sensitivity analysis and optimization 1: linear systems*. Springer Science & Business Media.

[24] Deaton, J. D. and Grandhi, R. V. (2014). A survey of structural and multidisciplinary continuum topology optimization: post 2000. *Structural and Multidisciplinary Optimization*, 49(1):1–38.

[25] Dede, E. M. (2012). Optimization and design of a multipass branching microchannel heat sink for electronics cooling. *Journal of Electronic Packaging*, 134(4):041001.

[26] Deng, Y., Liu, Z., Wu, J., and Wu, Y. (2013a). Topology optimization of steady Navier–Stokes flow with body force. *Computer Methods in Applied Mechanics and Engineering*, 255:306–321.

[27] Deng, Y., Liu, Z., Zhang, P., Liu, Y., and Wu, Y. (2011). Topology optimization of unsteady incompressible Navier-Stokes flows. *Journal of Computational Physics*, 230(17):6688–6708.

[28] Deng, Y., Zhang, P., Liu, Y., Wu, Y., and Liu, Z. (2013b). Optimization of unsteady incompressible Navier-Stokes flows using variational level set method. *International Journal for Numerical Methods in Fluids*, 71(12):1475–1493.

[29] Duan, X., Ma, Y., and Zhang, R. (2008a). Optimal shape control of fluid flow using variational level set method. *Physics Letters A*, 372(9):1374–1379.

[30] Duan, X.-B., Ma, Y.-C., and Zhang, R. (2008b). Shape-topology optimization for Navier-Stokes problem using variational level set method. *Journal of Computational and Applied Mathematics*, 222(2):487–499.

[31] Errico, R. M. (1997). What is an adjoint model? *Bulletin of the American Meteorological Society*, 78(11):2577–2592.

[32] Eschenauer, H. A., Kobelev, V. V., and Schumacher, A. (1994). Bubble method for topology and shape optimization of structures. *Structural Optimization*, 8(1):42–51.

[33] Feng, Z.-G. and Michaelides, E. E. (2004). The immersed boundary-lattice Boltzmann method for solving fluid-particles interaction problems. *Journal of Computational Physics*, 195(2):602–628.

[34] Fleury, C. (1989). CONLIN: an efficient dual optimizer based on convex approximation concepts. *Structural Optimization*, 1(2):81–89.

[35] Gersborg-Hansen, A., Sigmund, O., and Haber, R. B. (2005). Topology optimization of channel flow problems. *Structural and Multidisciplinary Optimization*, 30(3):181–192.

[36] Gill, P. E., Murray, W., and Saunders, M. A. (2002). SNOPT: An SQP algorithm for large-scale constrained optimization. *SIAM Journal on Optimization*, 12(4):979–1006.

[37] Gregersen, M. M., Okkels, F., Bazant, M. Z., and Bruus, H. (2009). Topology and shape optimization of induced-charge electro-osmotic micropumps. *New Journal of Physics*, 11(7):075019.

[38] Guest, J. K., Prévost, J., and Belytschko, T. (2004). Achieving minimum length scale in topology optimization using nodal design variables and projection functions. *International Journal for Numerical Methods in Engineering*, 61(2):238–254.

[39] Guest, J. K. and Prévost, J. H. (2006). Topology optimization of creeping fluid flows using a Darcy-Stokes finite element. *International Journal for Numerical Methods in Engineering*, 66(3):461–484.

[40] Guo, Z. and Zhao, T. (2002). Lattice Boltzmann model for incompressible flows through porous media. *Physical Review E*, 66(3):036304.

[41] Hassine, M. and Masmoudi, M. (2004). The topological asymptotic expansion for the quasi-Stokes problem. *ESAIM: Control, Optimisation and Calculus of Variations*, 10(4):478–504.

[42] He, X. and Luo, L.-S. (1997). A priori derivation of the lattice Boltzmann equation. *Physical Review E*, 55(6):R6333–R6336.

[43] Higuera, F. and Jimenez, J. (1989). Boltzmann approach to lattice gas simulations. *Europhysics Letters*, 9(7):663–668.

[44] Higuera, F., Succi, S., and Benzi, R. (1989). Lattice gas dynamics with enhanced collisions. *Europhysics Letters*, 9(4):345–349.

[45] Hou, S., Zou, Q., Chen, S., Doolen, G., and Cogley, A. C. (1995). Simulation of cavity flow by the lattice Boltzmann method. *Journal of Computational Physics*, 118(2):329–347.

[46] Husain, A. and Kim, K.-Y. (2008). Optimization of a microchannel heat sink with temperature dependent fluid properties. *Applied Thermal Engineering*, 28(8-9):1101–1107.

[47] Inamuro, T. (2006). Lattice Boltzmann methods for viscous fluid flows and for two-phase fluid flows. *Fluid Dynamics Research*, 38(9):641–659.

[48] Inamuro, T., Ogata, T., Tajima, S., and Konishi, N. (2004). A lattice Boltzmann method for incompressible two-phase flows with large density differences. *Journal of Computational Physics*, 198(2):628–644.

[49] Inamuro, T., Tomita, R., and Ogino, F. (2003). Lattice Boltzmann simulations of drop deformation and breakup in shear flows. *International Journal of Modern Physics B*, 17(1-2):21–26.

[50] Inamuro, T., Yoshino, M., Inoue, H., Mizuno, R., and Ogino, F. (2002). A lattice Boltzmann method for a binary miscible fluid mixture and its application to a heat-transfer problem. *Journal of Computational Physics*, 179(1):201–215.

[51] Inamuro, T., Yoshino, M., and Ogino, F. (1995). A non-slip boundary condition for lattice Boltzmann simulations. *Physics of Fluids*, 7(12):2928–2930; Erratum: 8 (4) (1996) 1124.

[52] Inamuro, T., Yoshino, M., and Ogino, F. (1997). Accuracy of the lattice Boltzmann method for small Knudsen number with finite Reynolds number. *Physics of Fluids*, 9(11):3535–3542.

[53] Ito, K. and Kunisch, K. (2008). *Lagrange multiplier approach to variational problems and applications*, volume 15. SIAM.

[54] Iwata, Y., Azegami, H., Aoyama, T., and Katamine, E. (2010). Numerical solution to shape optimization problems for non-stationary Navier-Stokes problems. *JSIAM Letters*, 2:733–740.

[55] Junk, M., Klar, A., and Luo, L.-S. (2005). Asymptotic analysis of the lattice Boltzmann equation. *Journal of Computational Physics*, 210(2):676–704.

[56] Katamine, E., Tsubata, T., and Azegami, H. (2003). Solution to shape optimization problem of viscous flow fields considering convection term. *Inverse Problems in Engineering Mechanics*, 4:401–408.

[57] Kim, S., Kim, D., and Lee, D. (2000). On the local thermal equilibrium in microchannel heat sinks. *International Journal of Heat and Mass Transfer*, 43(10):1735–1748.

[58] Kim, S. J. (2004). Methods for thermal optimization of microchannel heat sinks. *Heat transfer engineering*, 25(1):37–49.

[59] Koga, A. A., Lopes, E. C. C., Villa Nova, H. F., Lima, C. R. d., and Silva, E. C. N. (2013). Development of heat sink device by using topology optimization. *International Journal of Heat and Mass Transfer*, 64:759–772.

[60] Kondoh, T., Matsumori, T., and Kawamoto, A. (2011). Drag minimization and lift maximization in laminar flows via topology optimization employing simple objective function expressions based on body force integration. *Structural and Multidisciplinary Optimization*, 45(5):693–701.

[61] Koo, J. and Kleinstreuer, C. (2005). Laminar nanofluid flow in microheat-sinks. *International Journal of Heat and Mass Transfer*, 48(13):2652–2661.

[62] Krause, M. J. (2010). Fluid flow simulation and optimisation with lattice Boltzmann methods on high performance computers: application to the human respiratory system. *Karlsruhe Institute of Technology, KIT*.

[63] Krause, M. J., Thäter, G., and Heuveline, V. (2013). Adjoint-based fluid flow control and optimisation with lattice Boltzmann methods. *Computers and Mathematics with Applications*, 65(6):945–960.

[64] Kreissl, S. and Maute, K. (2012). Levelset based fluid topology optimization using the extended finite element method. *Structural and Multidisciplinary Optimization*, 46(3):311–326.

[65] Kreissl, S., Pingen, G., Evgrafov, A., and Maute, K. (2010). Topology optimization of flexible micro-fluidic devices. *Structural and Multidisciplinary Optimization*, 42(4):495–516.

[66] Kreissl, S., Pingen, G., and Maute, K. (2011). An explicit level set approach for generalized shape optimization of fluids with the lattice Boltzmann method. *International Journal for Numerical Methods in Fluids*, 65(5):496–519.

[67] Lin, L.-S., Chen, Y.-C., and Lin, C.-A. (2011). Multi relaxation time lattice boltzmann simulations of deep lid driven cavity flows at different aspect ratios. *Computers & Fluids*, 45(1):233–240.

[68] Lin, S., Zhao, L., Guest, J. K., Weihs, T. P., and Liu, Z. (2015). Topology optimization of fixed-geometry fluid diodes. *Journal of Mechanical Design*, 137(8):081402.

[69] Liu, G., Geier, M., Liu, Z., Krafczyk, M., and Chen, T. (2014). Discrete adjoint sensitivity analysis for fluid flow topology optimization based on the generalized lattice Boltzmann method. *Computers and Mathematics with Applications*, 68(10):1374–1392.

[70] Liu, Z., Gao, Q., Zhang, P., Xuan, M., and Wu, Y. (2010). Topology optimization of fluid channels with flow rate equality constraints. *Structural and Multidisciplinary Optimization*, 44(1):31–37.

[71] Lyness, J. N. and Moler, C. B. (1967). Numerical differentiation of analytic functions. *SIAM Journal on Numerical Analysis*, 4(2):202–210.

[72] Maier, R. S., Bernard, R. S., and Grunau, D. W. (1996). Boundary conditions for the lattice Boltzmann method. *Physics of Fluids*, 8(7):1788–1801.

[73] Makhija, D. and Maute, K. (2015). Level set topology optimization of scalar transport problems. *Structural and Multidisciplinary Optimization*, 51(2):267–285.

[74] Makhija, D., Pingen, G., Yang, R., and Maute, K. (2012). Topology optimization of multi-component flows using a multi-relaxation time lattice Boltzmann method. *Computers & Fluids*, 67:104–114.

[75] Matsumori, T., Kondoh, T., Kawamoto, A., and Nomura, T. (2013). Topology optimization for fluid-thermal interaction problems under constant input power. *Structural and Multidisciplinary Optimization*, 47(4):571–581.

[76] McNamura, G. R. and Zanetti, G. (1988). Use of the Boltzmann equation to simulate lattice-gas automata. *Physical Review Letters*, 61(20):2332–2335.

[77] Mei, R., Shyy, W., Yu, D., and Luo, L.-S. (2000). Lattice Boltzmann method for 3-D flows with curved boundary. *Journal of Computational Physics*, 161(2):680–699.

[78] Missaggia, L., Walpole, J., Liau, Z., and Phillips, R. (1989). Microchannel heat sinks for two-dimensional high-power-density diode laser arrays. *Quantum Electronics, IEEE Journal of*, 25(9):1988–1992.

[79] Mohammadi, B. and Pironneau, O. (2001). *Applied shape optimization for fluid*. Oxford University Press, Oxford.

[80] Mohammadi, B. and Pironneau, O. (2004). Shape optimization in fluid mechanics. *Annual Review of Fluid Mechanics*, 36:255–279.

[81] Morini, G. L. (2004). Single-phase convective heat transfer in microchannels: a review of experimental results. *International Journal of Thermal Sciences*, 43(7):631–651.

[82] Murat, F. and Tartar, L. (1985). Optimality conditions and homogenization. *Research Notes in Mathematics*, 127:1–8.

[83] Okkels, F. and Bruus, H. (2007). Scaling behavior of optimally structured catalytic microfluidic reactors. *Physical Review E*, 75(1):016301.

[84] Olesen, L. H., Okkels, F., and Bruus, H. (2006). A high-level programming-language implementation of topology optimization applied to steady-state Navier-Stokes flow. *International Journal for Numerical Methods in Engineering*, 65(7):975–1001.

[85] Osher, S. and Fedkiw, R. (2006). *Level set methods and dynamic implicit surfaces*, volume 153. Springer Science & Business Media.

[86] Osher, S. and Sethian, J. A. (1988). Fronts propagating with curvature-dependent speed: Algorithms based on Hamilton-Jacobi formulations. *Journal of computational physics*, 79(1):12–49.

[87] Otomori, M., Yamada, T., Izui, K., and Nishiwaki, S. (2011). Level set-based topology optimisation of a compliant mechanism design using mathematical programming. *Mechanical Sciences*, 2(1):91–98.

[88] Otomori, M., Yamada, T., Izui, K., and Nishiwaki, S. (2014). Matlab code for a level set-based topology optimization method using a reaction diffusion equation. *Structural and Multidisciplinary Optimization*, pages 1–14.

[89] Papoutsis-Kiachagias, E., Kontoleontos, E., Zymaris, A., Papadimitriou, D., and Giannakoglou, K. (2011). Constrained topology optimization for laminar and turbulent flows, including heat transfer. *CIRA, editor, EUROGEN, Evolutionary and Deterministic Methods for Design, Optimization and Control, Capua, Italy, 2011*.

[90] Pingen, G., Evgrafov, A., and Maute, K. (2007). Topology optimization of flow domains using the lattice Boltzmann method. *Structural and Multidisciplinary Optimization*, 34(6):507–524.

[91] Pingen, G., Evgrafov, A., and Maute, K. (2008). A parallel Schur complement solver for the solution of the adjoint steady-state lattice Boltzmann equations: application to design optimisation. *International Journal of Computational Fluid Dynamics*, 22(7):457–464.

[92] Pingen, G., Evgrafov, A., and Maute, K. (2009a). Adjoint parameter sensitivity analysis for the hydrodynamic lattice Boltzmann method with applications to design optimization. *Computers & Fluids*, 38(4):910–923.

[93] Pingen, G. and Maute, K. (2010). Optimal design for non-Newtonian flows using a topology optimization approach. *Computers and Mathematics with Applications*, 59(7):2340–2350.

[94] Pingen, G., Waidmann, M., Evgrafov, A., and Maute, K. (2009b). A parametric level-set approach for topology optimization of flow domains. *Structural and Multidisciplinary Optimization*, 41(1):117–131.

[95] Pironneau, O. (1973). On optimum profiles in Stokes flow. *Journal of Fluid Mechanics*, 59(1):117–128.

[96] Pironneau, O. (1974). On optimum design in fluid mechanics. *Journal of Fluid Mechanics*, 64(1):97–110.

[97] Qu, W. and Mudawar, I. (2002). Analysis of three-dimensional heat transfer in micro-channel heat sinks. *International Journal of heat and mass transfer*, 45(19):3973–3985.

[98] Schmit, L. A. (1960). Structural design by systematic synthesis. In *Proc. of the Second ASCE Conference on Electronic Computation*, pages 105–122.

[99] Sethian, J. A. (1999). *Level set methods and fast marching methods: evolving interfaces in computational geometry, fluid mechanics, computer vision, and materials science*, volume 3. Cambridge University Press.

[100] Sethian, J. A. and Wiegmann, A. (2000). Structural boundary design via level set and immersed interface methods. *Journal of Computational Physics*, 163(2):489–528.

[101] Shan, X. and Chen, H. (1993). Lattice Boltzmann model for simulating flows with multiple phases and components. *Physical Review E*, 47(3):1815–1819.

[102] Shu, C., Liu, N., and Chew, Y. (2007). A novel immersed boundary velocity correction-lattice Boltzmann method and its application to simulate flow past a circular cylinder. *Journal of Computational Physics*, 226(2):1607–1622.

[103] Sigmund, O. (2001). A 99 line topology optimization code written in matlab. *Structural and Multidisciplinary Optimization*, 21(2):120–127.

[104] Sigmund, O. (2007). Morphology-based black and white filters for topology optimization. *Structural and Multidisciplinary Optimization*, 33(4-5):401–424.

[105] Sigmund, O. and Maute, K. (2013). Topology optimization approaches. *Structural and Multidisciplinary Optimization*, 48(6):1031–1055.

[106] Sigmund, O. and Petersson, J. (1998). Numerical instabilities in topology optimization: a survey on procedures dealing with checkerboards, mesh-dependencies and local minima. *Structural Optimization*, 16(1):68–75.

[107] Sone, Y. (1971). Asymptotic theory of flow of rarefied gas over a smooth boundary II. *in: Rarefied Gas Dynamics, edited by, D. Dini, Editrice Tecnico Scientifica, Pisa*, pages 737–749.

[108] Spaid, M. A. A. and Phelan, F. R. (1997). Lattice Boltzmann methods for modeling microscale flow in fibrous porous media. *Physics of Fluids*, 9(9):2468–2474.

[109] Srinath, D. N. and Mittal, S. (2010). An adjoint method for shape optimization in unsteady viscous flows. *Journal of Computational Physics*, 229(6):1994–2008.

[110] Succi, S. (2001). *Lattice Boltzmann equation for fluid dynamics and beyond*. Oxford University Press, New York.

[111] Succi, S., Foti, E., and Higuera, F. (1989). Three-dimensional flows in complex geometries with the lattice Boltzmann method. *Europhysics Letters*, 10(5):433–438.

[112] Suzuki, K. and Inamuro, T. (2011). Effect of internal mass in the simulation of a moving body by the immersed boundary method. *Computers & Fluids*, 49(1):173–187.

[113] Suzuki, K. and Inamuro, T. (2013). A higher-order immersed boundary-lattice Boltzmann method using a smooth velocity field near boundaries. *Computers & Fluids*, 76:105–115.

[114] Suzuki, K. and Kikuchi, N. (1991). A homogenization method for shape and topology optimization. *Computer Methods in Applied Mechanics and Engineering*, 93(3):291–318.

[115] Svanberg, K. (1987). The method of moving asymptotes–a new method for structural optimization. *International Journal for Numerical Methods in Engineering*, 24(2):359–373.

[116] Takezawa, A., Nishiwaki, S., and Kitamura, M. (2010). Shape and topology optimization based on the phase field method and sensitivity analysis. *Journal of Computational Physics*, 229(7):2697–2718.

[117] Tekitek, M., Bouzidi, M., Dubois, F., and Lallemand, P. (2006). Adjoint lattice Boltzmann equation for parameter identification. *Computers & Fluids*, 35(8):805–813.

[118] Tuckerman, D. B. and Pease, R. F. W. (1981). High-performance heat sinking for vlsi. *Electron Device Letters, IEEE*, 2(5):126–129.

[119] van Dijk, N. P., Maute, K., Langelaar, M., and Van Keulen, F. (2013). Level-set methods for structural topology optimization: a review. *Structural and Multidisciplinary Optimization*, 48(3):437–472.

[120] Vergnault, E. and Sagaut, P. (2014). An adjoint-based lattice Boltzmann method for noise control problems. *Journal of Computational Physics*, 276:39–61.

[121] Wang, A., Ma, Y., and Gao, Z. (2009). Shape optimization of a body in the Oseen flow. *Numerical Methods for Partial Differential Equations*, 26(6):1642–1659.

[122] Wang, L., Fan, Y., and Luo, L. (2010). Heuristic optimality criterion algorithm for shape design of fluid flow. *Journal of Computational Physics*, 229(20):8031–8044.

[123] Wang, M. Y., Wang, X., and Guo, D. (2003). A level set method for structural topology optimization. *Computer Methods in Applied Mechanics and Engineering*, 192(1):227–246.

[124] Xie, Y. and Steven, G. P. (1993). A simple evolutionary procedure for structural optimization. *Computers and structures*, 49(5):885–896.

[125] Yamada, T., Izui, K., Nishiwaki, S., and Takezawa, A. (2010). A topology optimization method based on the level set method incorporating a fictitious interface energy. *Computer Methods in Applied Mechanics and Engineering*, 199(45-48):2876–2891.

[126] Yamasaki, S., Nomura, T., Kawamoto, A., Sato, K., and Nishiwaki, S. (2011). A level set-based topology optimization method targeting metallic waveguide design problems. *International Journal for Numerical Methods in Engineering*, 87(9):844–868.

[127] Yonekura, K. and Kanno, Y. (2014). A flow topology optimization method for steady state flow using transient information of flow field solved by lattice Boltzmann method. *Structural and Multidisciplinary Optimization*, 51(1):159—-172.

[128] Yoon, G. H. (2010). Topology optimization for stationary fluid-structure interaction problems using a new monolithic formulation. *International Journal for Numerical Methods in Engineering*, 82(5):591–616.

[129] Yoon, G. H. (2012). Topological layout design of electro-fluid-thermal-compliant actuator. *Computer Methods in Applied Mechanics and Engineering*, 209-212:28–44.

[130] Yoshino, M. and Inamuro, T. (2003). Lattice Boltzmann simulations for flow and heat/mass transfer problems in a three-dimensional porous structure. *International Journal for Numerical Methods in Fluids*, 43(2):183–198.

[131] Yoshino, M. and Mizutani, Y. (2006). Lattice Boltzmann simulation of liquid–gas flows through solid bodies in a square duct. *Mathematics and Computers in Simulation*, 72(2):264–269.

[132] Zabarankin, M. and Molyboha, A. (2011). 3D shape optimization in viscous incompressible fluid under Oseen approximation. *SIAM Journal on Control and Optimization*, 49(3):1358–1382.

[133] Zhou, S. and Li, Q. (2008). A variational level set method for the topology optimization of steady-state Navier-Stokes flow. *Journal of Computational Physics*, 227(24):10178–10195.

[134] Zienkiewicz, O. C. and Gallagher, R. H. (1973). *Optimum structural design: theory and applications*. Wiley.

[135] Žnidaršič-Plazl, P. and Plazl, I. (2007). Steroid extraction in a microchannel system-mathematical modeling and experiments. *Lab on a Chip*, 7(7):883–889.

[136] Zou, Q. and He, X. (1997). On pressure and velocity boundary conditions for the lattice Boltzmann BGK model. *Physics of Fluids*, 9(6):1591–1598.

[137] Zymaris, A. S., Papadimitriou, D. I., Giannakoglou, K. C., and Othmer, C. (2010). Adjoint wall functions: A new concept for use in aerodynamic shape optimization. *Journal of Computational Physics*, 229(13):5228–5245.

List of publications

International journal papers

(1) Yaji, K., Yamada, T., Yoshino, M., Matsumoto, T., Izui, K. and Nishiwaki, S. (2014). Topology optimization using the lattice Boltzmann method incorporating level set boundary expressions, *Journal of Computational Physics*, 274:158–181.

(2) Yaji, K., Yamada, T., Kubo, S., Izui, K. and Nishiwaki, S. (2015). A topology optimization method for a coupled thermal-fluid problem using level set boundary expressions, *International Journal of Heat and Mass Transfer*, 81:878–888.

(3) Yaji, K., Yamada, T., Yoshino, M., Matsumoto, T., Izui, K. and Nishiwaki, S. (2016) Topology optimization in thermal fluid flow using the lattice Boltzmann method, *Journal of Computational Physics*, 307:355–377.

(4) Yaji, K., Otomori, M., Yamada, T., Kubo, S., Izui, K., Nishiwaki, S. and Pironneau, O. Shape optimization based on the convected level set method, *submitted.*

(5) Kubo, S., Yaji, K., Yamada, T., Izui, K. and Nishiwaki, S. A level set-based topology optimization method for optimal manifold designs with flow uniformity in plate-type microchannel reactors, *submitted.*

Domestic journal papers (in Japanese)

(1) Yaji, K., Yamada, T., Kubo, S., Izui, K. and Nishiwaki, S. (2012). Topology optimization method based on level set method in Oseen flow, *Transactions of the Japan Society for Computational Methods in Engineering*, 12(02-121212):7–12.

(2) Yaji, K., Yamada, T., Yoshino, M., Matsumoto, T., Izui, K. and Nishiwaki, S. (2013). A level set-based topology optimization using the lattice Boltzmann method, *Transactions of the Japan Society of Mechanical Engineers*, 79(802):2152–2163.

(3) Yaji, K., Yamada, T., Yoshino, M., Matsumoto, T., Izui, K. and Nishiwaki, S. (2013). Level set-based topology optimization using lattice kinetic scheme, *Transactions of the Japan Society for Computational Methods in Engineering*, 13(18-131129):85–90.

(4) Kubo, S., Yaji, K., Yamada, T., Izui, K. and Nishiwaki, S. (2014). Level set-based topology optimization of steady state incompressible viscous flows under outflow rate inequality constraint, *Transactions of the Japan Society of Mechanical Engineers*, 80(815):DM023.

(5) Yaji, K., Kitamura, Y., Matsushima, T., Yamada, T., Izui, K. and Nishiwaki, S. (2014). Structural optimization of a brake disc—topology optimization to simultaneously improve cooling performance and reduce brake squeal—, *Journal of the Japan Society for Precision Engineering*, 80(8):763–770.

(6) Yaji, K., Yamada, T., Yoshino, M., Matsumoto, T., Izui, K. and Nishiwaki, S. (2014). Sensitivity analysis based on discrete Boltzmann equation in topology optimization for fluid problems, *Transactions of the Japan Society for Computational Methods in Engineering*, 14(16-141206):67–72.

(7) Koguchi, A., Yaji, K., Yamada, T., Izui, K. and Nishiwaki, S. (2015). Level set-based topology optimization in an incompressible viscous flow using the finite volume method, *Transactions of the Japan Society for Computational Engineering and Science*, 2015(20150002).

(8) Yaji, K., Yamada, T., Yoshino, M., Matsumoto, T., Izui, K. and Nishiwaki, S. (2015). Topology optimization using the lattice Boltzmann method for two-phase fluids with the same density, *Transactions of the Japan Society for Computational Methods in Engineering*, 15(09-151204):49–54.

(9) Tanaka, R., Yaji, K., Yamada, T., Izui, K. and Nishiwaki, S. Level set-based topology optimization targeting micropumps employing an induced-charge electro-osmosis flow, *submitted.*

Acknowledgments

I would like to express my gratitude to my supervisors, Professor Shinji Nishiwaki, Professor Kazuhiro Izui, and Professor Takayuki Yamada, for providing me the opportunity to treat the research topic described in this thesis, and for their continuous encouragement and patient guidance to accomplish my doctoral work.

I would also like to express my gratitude to Professor Takaji Inamuro in the Department of Aeronautics and Astronautics, Graduate School of Engineering, Kyoto University, and to Professor Atsushi Matsubara in the Department of Micro Engineering, Graduate School of Engineering, Kyoto University, for their invaluable advices and for serving on my dissertation committee.

I am grateful for the kind help and valuable suggestions provided to me by Professor Toshiro Matsumoto in the Department of Mechanical Engineering and Science, Graduate School of Engineering, Nagoya University, and Professor Masato Yoshino in the Institute of Engineering, Academic Assembly, Shinshu University. My doctoral work would not have been possible without their kind help and useful discussions about the topology optimization problems using the LBM. Also, I owe my deepest gratitude to Dr. Otomori at AISIN AW Co., Ltd, Mr. Seiji Kubo at IHI Corporation, Dr. Atsushi Koguchi at IDAJ Co., Ltd, Mr. Toru Matsushima at Toyota Motor Corporation, and Dr. Yuta Kitamura at IHI Corporation. Collaborative research with them led to a widening of viewpoint.

Part of this study was carried out during my visit to Laboratories in France, and I would like to express my special thanks to Professor Olivier Pironneau in the Laboratoire Jacques-Louis Lions (LJLL), Université Paris 6. He willingly accepted to be the host of my overseas research, and gave me great opportunities for learning not only cutting-edge studies of structural optimization but also the attitude as a researcher. I would also like to thank Professor Frédéric Hecht in the LJLL, Professor François Jouve in the LJLL, Université Paris 7, and Professor Thierry Coupez in the Ecole des Mines de Paris, Centre de Mise en Forme

des Matériaux. Thanks to their cooperation, the overseas research for three months was very fruitful.

I wish to express my thanks to my colleagues in the Manufacturing Systems Engineering Laboratory at Kyoto University for their warmth, kindness and tireless supports. They always cheer me up and lift my spirits. I would also like to thank Mr. John E. Goodman for his help in editing my papers in English over the years.

In addition, I would like to thank Dr. Tetsuo Higashihara, and Professor Kenji Nakamura in the Department of Mechanical Engineering, Kyushu Sangyo University. They had belonged to my old school (Matsue National College of Technology) and taught me interests of science. This is why I decided to be a researcher, and they are still my role model as ideal teachers.

I am extremely grateful to Dr. Goken Sakamoto who is a specialist of exercise physiology and my rowing coach. Rowing is an important part of my life as well as research, and it would had been impossible to compete in the All Japan Rowing Championship without his technical and psychological supports.

I would like to extend my sincere thanks to everyone who contributed to my doctoral work. In addition, I sincerely appreciate the financial supports: Grant-in-Aid for JSPS Fellows (No. 26·2008), and Kyoto University Foundation, Grants for Researchers Attending International Conferences.

Finally, I would like to offer my thanks to my family for their kind support in my long student life.

Kyoto, March, 2016

Kentaro Yaji